**Synthesis, evaluation, and applications of hydrogen sulfide-releasing supramolecular materials**

Kuljeet Kaur

Dissertation submitted to the faculty of the Virginia Polytechnic Institute and State University in partial fulfillment of the requirements for the degree of

Doctor of Philosophy

In

Chemistry

John B. Matson, Chair

Richard D. Gandour

Webster Santos

Judy Riffle

December 3, 2019

Blacksburg, Virginia

Keywords: Hydrogen sulfide ($H_2S$), Carbonyl sulfide (COS), Peptides, Materials, Drug-delivery, Intimal hyperplasia, Smooth muscle cells, Proliferation, Hydrogel

**Synthesis, evaluation, and applications of hydrogen sulfide-releasing supramolecular materials**

Kuljeet Kaur

ABSTRACT

$H_2S$ is a biologically relevant signaling gas that is endogenously produced throughout the body. The (patho)physiological roles of $H_2S$ have led researchers to develop various compounds that decompose to release $H_2S$ ($H_2S$ donors) for exogenous $H_2S$ administration. However, many small molecule $H_2S$ donors suffer from poor solubility, low stability, and lack of control over $H_2S$ release rates. As a result, there has been an increasing interest in utilizing supramolecular materials for exogenous $H_2S$ delivery.

With growing potential applications of supramolecular $H_2S$-releasing materials, it is important to explore their properties, e.g., solubility and stability under physiological conditions. We investigated the hydrolytic stability over a range of pH conditions of a series of peptides containing $H_2S$-releasing *S*-aroylthiooximes (SATOs). The SATO-peptides showed structure–reactivity relationships with SATO ring substituents playing a crucial role in hydrolysis rates. Electron-donating substituents accelerate the rate of hydrolysis while electron-withdrawing substituents slows it down. We also explored their hydrolysis mechanisms at different pH values. SATO-peptides were then used to form hydrogels at 1 wt.% triggered by $Ca^{2+}$. Hydrogels can be applied directly at a site of interest, potentially improving the efficacy of $H_2S$ compared with small molecule donors that diffuse away. We developed a $H_2S$-releasing hydrogel capable of slowly releasing $H_2S$ locally to test its efficacy on intimal hyperplasia. The hydrogel delivered $H_2S$ over the period of several hours and inhibited the proliferation of human vascular smooth

muscle cells (VSMCs) significantly better than fast-releasing NaSH salts. This study shows a promising application of supramolecular $H_2S$-releasing materials over widely used sulfide salts.

The macroscopic properties of peptide hydrogels could be further modulated to achieve additional control over the $H_2S$ release properties. We synthesized a series of peptide hydrogels incorporating different linker segments to study their effects on hydrogelation properties. Most peptides formed hydrogels but with significantly different rheological behavior. We found that peptides with flexible linkers such as ethyl, substituted O-methylene, and others, formed stronger hydrogels compared to those with more rigid linkers. Interestingly, we found that stiffer hydrogels released $H_2S$ over longer periods than softer ones by retarding the diffusion of a thiol trigger, likely due to bulk degradation of the soft gels but surface erosion of the stiff gels as they release $H_2S$.

**Synthesis, evaluation, and applications of hydrogen sulfide-releasing supramolecular materials**

Kuljeet Kaur

GENERAL AUDIENCE ABSTRACT

$H_2S$ has long been known as a foul smelling gas until it was discovered that it is endogenously produced throughout the body and plays many (patho)physiological roles. Therapeutic benefits of $H_2S$ have led researchers to develop various compounds that release $H_2S$ ($H_2S$ donors) for exogenous $H_2S$ administration. However, many small molecule $H_2S$ donors suffer from poor solubility, low stability, and unregulated $H_2S$ release. As a result, there has been an increasing interest in utilizing materials for exogenous $H_2S$ delivery.

With growing potential applications of $H_2S$-releasing materials, it is important to explore their properties, e.g., solubility and stability under physiological conditions. We investigated the stability of a series of peptides containing $H_2S$-releasing *S*-aroylthiooximes (SATOs) over a range of pH conditions. The stability of SATO-peptides was dependent on chemical makeup of the SATO part of the peptides. We also explored their hydrolysis mechanisms at different pH values.

SATO-peptides were then used to form hydrogels triggered by $Ca^{2+}$. Hydrogels can be applied directly at a site of interest, potentially improving the efficacy of $H_2S$ compared with small molecule donors that diffuse away. We developed a $H_2S$-releasing hydrogel capable of slowly releasing $H_2S$ locally to test its efficacy on intimal hyperplasia. The hydrogel delivered $H_2S$ over the period of several hours and inhibited the proliferation of human vascular smooth muscle cells (VSMCs) significantly better than fast-releasing NaSH salts. This study shows a promising application of supramolecular $H_2S$-releasing materials over widely used sulfide salts.

The macroscopic properties of peptide hydrogels could be further modulated to achieve additional control over the $H_2S$ release properties. We synthesized a series of peptide hydrogels incorporating different linker segments to study their effects on hydrogelation properties. Most peptides formed weak to strong hydrogels with calcium chloride.We found that peptides with flexible linkers formed stronger hydrogels compared to those with more rigid linkers. Interestingly, we found that stiffer hydrogels released $H_2S$ over longer periods than softer ones.

# *Acknowledgements*

There are many people I would like to thank, who have contributed to this journey in their own unique ways. But I would like to start by thanking my advisor, John B. Matson. He has been a constant source of inspiration and guidance. He never discouraged me from pursuing any idea, no matter how unrealistic it seemed. Secondly, I would like to thank my PhD advisory committee, Prof. Richard Gandour, Prof. Webster Santos and Prof. Judy Riffle for their constructive discussions throughout the course of my Ph.D.

I would like to extend a special thanks to Joli Huynh, Ken Knott, Geno Iannaccone, Dr. N. Murthy, Steve McCartney, Chris Winkler for their technical support and extreme patience. Thanks are also in order for Prof. Tijana Grove and Prof. Diego Troya for helpful discussions.

Further, I thank my friends and colleagues for making my time at Virginia Tech worthwhile. Especially, Jeff, Scott, Kyle, Chad, Ryan, Kearsley, Sam, Sarah B and S, Yin, Zhao, Jackie, Anastasia, Mohammed, Yun, and Ming and all the undergrads I worked with. Apart from science, I also learned a lot about different cultures (also learned a few words in different languages). I can say that you all will be missed deeply.

Finally, this journey could not have been completed without the support of my family, especially my husband. His constant encouragement and patience got me sailing smoothly throughout my graduate career.

**Table of Contents**

## Attributions

This dissertation consists of chapters that were written with help of several co-workers, colleagues, and collaborators. They are acknowledged below along with their affiliations.

Dr. Yun Qian (Macromolecules Innovation Institute, Virginia Tech)

Dr. Yin Wang (Department of Chemistry, Virginia Tech)

Dr. Richard Gandour (Department of Chemistry, Virginia Tech)

Dr. Florent Allagant (CHUV, Switzerland)

Dr. Chad Powel (Department of Chemistry, Virginia Tech)

Patrick Enders (M.S., Department of Chemistry, Johannes Gutenberg University, Mainz, Germany)

### Chapter 1

Kuljeet Kaur and Ryan Carrazone contributed equally to the writing of this chapter. John Matson is the advisor and committee chair and provided guidance and help with writing and editing.

### Chapter 2

Kuljeet Kaur provided majority of writing of the manuscript along with synthesis, characterization, hydrolysis studies and majority of data processing. Yun Qian helped with some characterization and helped with data processing. Dr. Richard Gandour is a senior author and provided guidance, helped in editing of the manuscript as well as in crucial calculations for Hammett sigma values. John Matson is the advisor and committee chair and provided guidance,

help with tabulating data, writing, editing, and setting up of excel formulas for hydrolysis rate calculation.

**Chapter 3**

Kuljeet Kaur provided majority of part of the writing of the manuscript along with synthesis and characterization of the peptides. Alban Longchamp, Diane Macabrey, Celine Dubuis, Jean-Marc Corpataux, Sébastien Déglise, are our Swiss collaborators who helped with the writing and editing the remining part of the manuscripts and *in vitro* studies. John Matson is the advisor and committee chair and provided guidance and help with writing and editing. Florent Allagnat is the corresponding author and provided help with writing and editing.

**Chapter 4**

Kuljeet Kaur provided primary writing of the manuscript along with synthesis and characterization of all peptides. Yin Wang provided useful discussions and helped with characterization. John Matson is the advisor and committee chair and provided guidance and help with writing and editing.

## Chapter 1. Introduction

### The Benefits of Macromolecular/Supramolecular Approaches in $H_2S$ Delivery: A Review of Polymeric and Self-Assembled $H_2S$ Donors

Reprinted with permissions from *The Benefits of Macromolecular/Supramolecular Approaches in $H_2S$ Delivery: A Review of Polymeric and Self-Assembled $H_2S$ Donors,* Antioxidants and Redox Signaling, 32, 2, **2019**, 79-95, published by Mary Ann Liebert Inc., New Rochelle, NY. The final publication is available online at: https://www.liebertpub.com/doi/10.1089/ars.2019.7864

### 1.1 Authors

Kuljeet Kaur, Ryan J. Carrazzone, John B. Matson

Next-generation approaches to disease treatment will rely on the precise and controlled delivery of active pharmaceutical ingredients (APIs) such as drugs, peptides, enzymes, and vaccines, among others. [1, 2, 3] To this end, drug delivery systems provide numerous benefits, including a wide range of administration techniques, increased efficacy and longer circulation times relative to pure APIs, and the potential for advanced delivery conditions (e.g., targeting, triggered response). Often researchers transport, contain, and/or protect therapeutic agents using synthetic polymers due to their ease of synthesis and wide versatility.[4] In fact, many pharmaceuticals on the market use macromolecular/supramolecular delivery approaches including microparticle depots (e.g., Lupron, Vivitrol), liposomal formulations (e.g., Doxil), nanoparticles (e.g., Abraxane), and implantable systems (e.g., Vitrasert). [5, 6, 7, 8, 9] The development of polymeric drug delivery systems is well studied, with

any thorough reviews existing in the literature. [10, 11, 12, 13, 14, 15] Despite several decades of work in this field, there remains a clinical need to continue to develop drug delivery systems.

Signaling gases, known as gasotransmitters,[16, 17, 18] stand to benefit from drug delivery approaches even more than conventional small molecule drugs, proteins, and other APIs due to their potency and fast action. There exist three known gasotransmitters: Nitric oxide (NO), carbon monoxide (CO), and hydrogen sulfide ($H_2S$). Each is produced and regulated endogenously, and each has specific physiological functions and targets. There exist therapeutics on the market and/or in clinical trials for formulations of each gasotransmitter, either in the form of the gas itself or as small molecules that release or generate the gas in vivo.[19,20,21] Unlike other chemical messengers, gasotransmitter signaling is not limited by exocytosis-mediated release, receptor-binding, vesicular storage, and/or elaborate removal processes from the site of action.[18] Instead, cells quickly turn on or off gasotransmitter production to regulate autocrine or paracrine signaling, and these gases diffuse rapidly through biological membranes. Their short *in vivo* half-lives match their rapid production, allowing NO, CO, and $H_2S$ to work together to regulate cell behavior nearly instantaneously.[22] Due to their gaseous nature, fast diffusivity, and high reactivity, gasotransmitters are challenging to administer therapeutically but may offer substantial benefits if delivered at a desired site of action in a controlled manner.

$H_2S$, the most recent addition to the list of gasotransmitters,[23,24,25] has attracted attention due to its various biological roles, including cardioprotection, [26,27,28] vasodilation,[29,30,31] angiogenesis,[32,33,34] anti-inflammation,[35,36] neurotransmission,[37,38,39] and others. It is produced endogenously by the enzymes CSE, CBS, and 3-MST, which are present in organs and systems throughout the body. Physiological concentrations of $H_2S$ are highly regulated by distinct biosynthetic processes, which contribute toward homeostasis of the organism. The appreciable

roles of $H_2S$ in physiological and pathophysiological processes have led researchers to develop methods to deliver $H_2S$ to study its physiological pathways and therapeutic potential.[40,41,42] Indeed, small molecules that release $H_2S$ *in vivo* (so-called $H_2S$ donors) provide evidence for the beneficial effects of exogenous delivery of $H_2S$. [43,44, 45,46] However, as is true for other gasotransmitters, $H_2S$ is toxic at high concentrations, it has a short half-life, and it has no specific receptor but many targets. Coupled with its propensity to oxidize, these factors make sustained release and precise dosage control vital for $H_2S$ delivery, even more so than in delivery of traditional therapeutics.[47]

Delivery of $H_2S$ can take several forms. Direct inhalation presents the most straightforward method for exogenous $H_2S$ administration, delivering the gas without any byproducts or carriers. The inhalation method can deliver the required $H_2S$ dosage by modulating gas partial pressure over time. Researchers have successfully employed inhalation to systemically deliver $H_2S$ in mice, initiating a state of suspended animation or slower metabolism.[48] Despite its advantages, inhaled delivery of $H_2S$ is not likely to reach a clinical setting due to the malodorous nature of the gas and its lack of targeting. Stringent safety regulations concerning storage of this flammable and corrosive gas also hinder inhaled delivery. Inorganic sulfide salts (NaHS, $Na_2S$, and CaS) are common alternatives to gaseous $H_2S$ delivery, providing instantaneous access to $H_2S$ in its pure form while avoiding the need to handle the gas directly. Sulfide salts are currently the most widely employed delivery strategy in biological and preclinical studies investigating the *in vitro* and *in vivo* role of $H_2S$. Despite their availability and easy administration, sulfide salts have several drawbacks. In particular, the burst $H_2S$ release profile from aqueous sulfide salt solutions stands in stark contrast to sustained, tightly regulated enzymatic $H_2S$ production. To

address these drawbacks, chemists and pharmacologists have designed synthetic $H_2S$ donors over the past decade with control over the release kinetics, dosage, and location of release. Recent reviews cover the many types of existing small molecule $H_2S$ donors.[49,50,51,52] However, designing a synthetic $H_2S$ donor is not trivial and requires careful consideration of stability, water solubility, $H_2S$ release rate, trigger specificity, and toxicity of the donor itself as well as any byproducts generated after $H_2S$ release. Thus, despite great progress in the development of $H_2S$ donors, advanced delivery methods are still needed.

Due to the benefits of drug delivery systems, and the inherent challenges in effectively delivering $H_2S$, there has been a strong interest in macromolecular and supramolecular $H_2S$ donors.[47,53,54] Here we provide an overview of the development and current state of macromolecular/supramolecular $H_2S$ donor systems. In particular, we focus on the distinct advantages that polymeric and self-assembled delivery systems provide over small molecule $H_2S$ donors, and we illustrate how these advantages may enable a greater understanding of $H_2S$ (patho)physiology and potentially translate to clinical applications of $H_2S$ therapy.

### 1.2 Advantages of macromolecular systems

Macromolecular/supramolecular drug delivery systems can modulate the chemical, physical, and pharmacokinetic properties of an API without drastically changing the chemical nature of the payload. Through this control over these key properties, many of the challenges associated with delivering therapeutics can be addressed. For example, a large number of potential therapeutic agents are inherently hydrophobic. This presents a problem with solubility in biological systems, ultimately leading to low bioavailability and drug efficacy. Incorporating the hydrophobic drug

into a water-soluble polymeric drug delivery system facilitates delivery in aqueous environments.[55,56] Furthermore, the incorporated hydrophobic drug adopts the pharmacokinetic properties of the polymer/supramolecular structure; therefore, changes that alter these properties (i.e., changes to polymer composition, morphology, or functionality) may enable sustained or timed release of the payload.[57,58] Additionally, the polymer/supramolecular scaffold shields the entrapped API from the surrounding environment, leading to reduced cytotoxicity in situations where a burst release of the drug might be hazardous or toxic.[59] The shielding structure also provides a large area for attachment of targeting functionalities, which may enable triggered or localized release of the payload.[60,61] Altogether, it is clear that integrating small molecule therapeutics into macromolecular/supramolecular systems provides advantages for biological delivery.

The two major strategies for preparing macromolecular drug delivery systems include covalent linkage and physical entrapment. In the covalent linkage approach, APIs are chemically linked to polymer scaffolds. The linkage method often depends on the specific chemical nature of the API, making this approach specific to a given drug. In the physical entrapment approach, APIs are sequestered in polymeric nanostructures without the formation of covalent bonds. While this approach often leads to lower loading rates than covalent linking, the lack of chemical modification enables its use with a wider range of APIs. For example, poly(lactide-*co*-glycolide) (PLGA) has been used to deliver a wide range of APIs by physical entrapment.[62,63,64,65] While these preparation methods differ in their implementation, they both succeed in changing the chemical, physical, and pharmacokinetic properties of small molecule drugs, proteins, and other APIs.

### 1.3 Macromolecular systems with covalently bound $H_2S$ donors

Chemically linking APIs to a polymer scaffold, despite the need for linker chemistry specific to each API, provides several advantages over physical entrapment. For example, a physically entrapped API is prone to leaching, a process in which the drug escapes from the polymer scaffold in an undesirable fashion (i.e., too quickly or before reaching the desired site of release).

*$H_2S$ releasing linear polymers*

Covalent linkage of drug to the polymer scaffold minimizes leeching and maintains the desired release profile and/or pharmacokinetics. Additionally, chemical incorporation of the API can be used to influence the physical properties of the polymer itself. For example, conjugation of a hydrophobic drug to a hydrophilic polymer can result in amphiphilic behavior, which provides a method for modifying the morphology of the system that is unique to covalently linked donors. Finally, covalent linkers can be designed to release the drugs under specific conditions, such as a change in pH or the presence of a particular enzyme. As a result of these advantages of covalently linked drug delivery systems over physically entrapped systems, a variety of chemically linked $H_2S$ releasing polymers have been developed.

Covalent attachment of an $H_2S$ donating motif to a linear polymer provides a simple strategy for design of a macromolecular donor. To this end, a variety of systems utilizing small molecule $H_2S$ donors attached to linear polymers have been developed. A popular $H_2S$ donor that can be easily attached to polymers is 5-(4-hydroxyphenyl)-3*H*-1,2-dithiole-3-thione (ADT-OH). ADT-OH is the active metabolite in a dry mouth drug and may have bioactivity aside from releasing $H_2S$;[66] beyond this, its mechanism of release is not clear, nor are the factors that affect its rate of release. Despite these issues, it has been conjugated onto several polymer systems, the first of which was reported by Hasegawa et al. in 2014 (Fig. 1.1A).[67] In this work, ADT-OH was conjugated to the

chain end of poly(ethylene glycol) (PEG), producing PEG-ADT. Conjugation to the polymer provided improved solubility of the drug, significantly reducing toxicity *in vitro* in RAW-Blue macrophages.

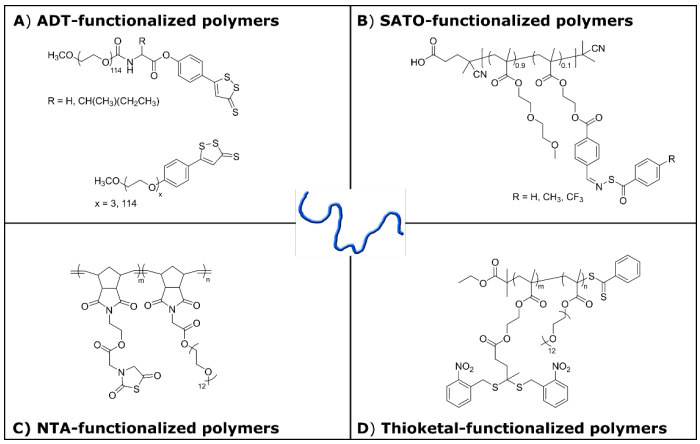


**Fig. 1.1. Chemical structures of $H_2S$-releasing linear polymers: A)** ADT-functionalized PEG-based polymers. **B)** SATO-functionalized copolymer. **C)** NTA-functionalized statistical copolymer. **D)** Thioketal-functionalized copolymer. PEG, poly(ethylene glycol); ADT, 5-(4-hydroxyphenyl)-3-H-1,2-dithiole-3-thione; SATO, *S*-aroylthiooxime; NTA, *N*-thiocarboxyanhydride.

Interestingly, the authors demonstrated that PEG-ADT conjugates became less cytotoxic with more hydrolytically stable linkages, underlining the importance of covalently attaching ADT-OH to the polymer. The PEG-ADT conjugates entered cells through endocytosis, while small molecule ADT-OH diffused across the cell membrane into the cytoplasm. The authors attribute the difference in cytotoxicity between small molecule and polymeric donors to a difference in intracellular distribution due to these unique pathways of cellular entry. Furthermore, the slower release of $H_2S$ from PEG-ADT relative to ADT-OH resulted in a significantly enhanced potentiating effect on lipopolysaccharide-induced inflammation.

Also in 2014, our group developed macromolecular $H_2S$-donating polymers with each repeating unit functionalized with *S*-aroylthiooximes (SATOs) through a post-polymerization modification of pendant aldehyde groups (Fig. 1.1B).[68] SATOs, reported by our group earlier in 2014, release $H_2S$ upon addition of a thiol. $H_2S$ release rate from SATOs could be tuned by changing substituents on the aroyl ring.[69] The SATO-conjugated polymers retained control of $H_2S$ release through electronics of the aroyl structure, allowing for the preparation of several polymers with varying $H_2S$ release kinetics. A statistical copolymer, in which polymer repeat units are randomly distributed, containing SATO pendant groups as well as oligo(ethylene glycol) (OEG) pendant groups enhanced the water solubility of these hydrophobic donors.

In 2016, we developed a different $H_2S$-donating polymer system using *N*-thiocarboxyanhydrides (NTAs) as the $H_2S$-releasing groups (Fig. 1.1C).[70] Nucleophilic addition of an amine to the carbonyl neighboring the unsubstituted $CH_2$ unit caused ring-opening of the NTA and released carbonyl sulfide, which is rapidly converted into $H_2S$ enzymatically by carbonic anhydrase.[71] We synthesized NTA-functionalized and OEG-functionalized norbornene derivatives for use in ring-opening metathesis polymerization (ROMP). ROMP provided a polymerization method devoid of nucleophiles potentially capable of opening the NTA ring, and copolymerization with the OEG-functionalized norbornene derivative imparted good water solubility to the copolymer. Conjugation of NTA motifs to the polymer resulted in prolonged $H_2S$ release, with a 3-fold increase in release half-life relative to the small molecule NTA. This change in release profile may be a result of steric crowding around the NTA, retarding nucleophilic addition, which again showcases the protective effect of polymer systems on sensitive prodrugs.

Recently Li et al. reported an $H_2S$-donating polymer system based on conjugation of 2-nitrobenzenemethanethiol to pendant ketones on a polymethacrylate backbone, creating a photodegradable thioketal linkage (Fig. 1.1D).[72] Upon UV irradiation, the thioketal linkage degraded to release $H_2S$ and 1,2-nitrobenzaldehyde, while also regenerating the parent polymer. Copolymerization of a ketone functionalized methacrylate with an OEG-functionalized methacrylate produced a highly water-soluble graft copolymer with a molecular weight close to the renal excretion threshold (40 kg/mol), the size below which clearance by the kidneys is rapid.[73] The rate of $H_2S$ release from the copolymer correlated positively with the intensity of UV irradiation, with no release observed in the absence of irradiation. Additionally, the gem-dithiol functionalized polymer and its byproducts showed no cytotoxicity below 25 μM in NIH3T3 cells.

*Polymeric micelles for $H_2S$ delivery*

Polymer micelles, a common drug delivery system made from amphiphilic block copolymers, are known for their drug loading capability and long circulation times in the bloodstream.[74] In such systems, amphiphilic block copolymers, polymers in which long runs of repeat units are discretely partitioned but chemically linked, self-assemble in water to form micelles due to the differential solubility of the component blocks. Polymer micelles form core-shell architectures in aqueous environments, with hydrophobic blocks forming the core and hydrophilic blocks composing the surrounding shell. As a result, micellar systems can carry various hydrophobic drug molecules within their cores, either through covalent attachment or via physical encapsulation, thereby behaving as efficient drug delivery vehicles. Furthermore, the size range

(typically 10–100 nm) of polymer micelles is critical in determining their biodistribution, as larger micelles may exceed the renal excretion threshold and accumulate in sites of interest through the enhanced permeability and retention (EPR) effect.[75] Additionally, micellar carriers improve aqueous solubility and prolong the circulation times of encapsulated hydrophobic small molecule APIs in the bloodstream.

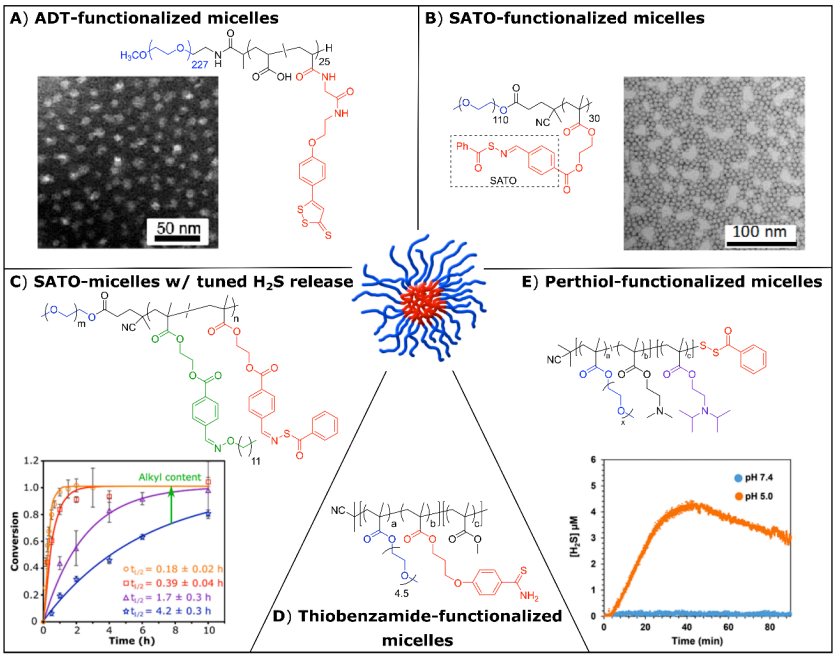


**Fig. 1.2. $H_2S$-releasing micelles from amphiphilic block copolymers. A)** PEG-*b*-PADT block copolymer consisting of PEG and ADT-functionalized blocks and TEM image of block copolymer micelles. **B)** SATO-functionalized block copolymer with PEG as a hydrophilic block and TEM image of block copolymer micelles. **C)** Structure of SATO-functionalized block copolymers consisting of a PEG hydrophilic block and alkyl-*co*-SATO-functionalized blocks as hydrophobic blocks. A graphical representation of $H_2S$ release kinetics of the micelles depicting decrease in $H_2S$ release half-lives with increasing amounts of alkyl component. **D)** Structure of thiobenzamide-functionalized block copolymer. **E)** Structure of PEG-based block copolymer with persulfide end group and a graph of $H_2S$ release at two pH values. TEM, transmission electron microscopy; PEG, polyethylene glycol; PADT, poly(5-(4-hydroxyphenyl)-3H-1,2-dithiole-3-thione); SATO, *S*-aroylthiooxime.

Among the earliest examples of $H_2S$ releasing polymer micelles, Hasegawa et al. expanded upon

their previous work with linear $H_2S$-donating polymers to create ADT-containing polymer micelles (Fig. 1.2A).[76] In this work, ADT was conjugated to poly(acrylic acid) that was polymerized through reversible addition-fragmentation chain-transfer (RAFT) polymerization, a radical polymerization technique capable of producing polymers with controllable molecular weights and end-group fidelity, using a PEGylated chain transfer agent (CTA) to yield an amphiphilic block copolymer. Here PEG was the hydrophilic block and ADT-functionalized poly(acrylic acid) (PADT) was the hydrophobic block. Analysis by dynamic light scattering (DLS) and transmission electron microscopy (TEM) revealed formation of spherical micelles in water, with an average hydrodynamic radius of 36 nm. Although only small amounts were released, the $H_2S$ release profiles observed for these PEG-*b*-PDAT polymer micelles were similar to those for linear PEG-ADT, indicating that micellization did not hinder $H_2S$ release from the encapsulated ADT-OH moieties. As reported for PEG-ADT linear polymers, PEG-*b*-PADT micelles showed less cytotoxicity than small molecule ADT-OH *in vitro*. Interestingly, PEG-*b*-PADT micelles enhanced the pro-inflammatory response in gardiquimode-stimulated murine macrophages, whereas ADT-OH slightly decreased the pro-inflammatory response under similar conditions. The observed difference is likely due to the altered cellular internalization of ADT micelles relative to ADT-OH, similar to that observed for ADT-PEG polymers. This study showed the ability of micellar systems to attenuate certain toxic effects of $H_2S$ donors by shielding them and controlling their entry into cells.

In 2017, we reported an $H_2S$-releasing polymer micelle system to address the rapid clearance rate associated with linear polymers and access better pharmacokinetics (Fig. 1.2B).[77] In this work, 2-(4-formylbenzoyloxy)ethyl methacrylate (FBEMA) monomer was polymerized via RAFT using

a PEGylated CTA to give an amphiphilic block copolymer bearing pendant SATO in the hydrophobic block. Uniform spherical micelles were then prepared with an average core diameter of 21 ± 2 nm as measured via TEM and hydrodynamic diameter of 38 ± 4 nm as measured by DLS. Confinement of SATO moieties in the hydrophobic core of micelles resulted in a significant increase in the $H_2S$ release half-life, with micelles releasing 9-fold more slowly than a small molecule analog. We attributed this drastic difference in release rate to restricted diffusion of the hydrophilic Cys trigger into the hydrophobic micelle cores, retarding $H_2S$ release compared with molecularly dissolved small molecules and linear polymers. This finding highlights the potential for tuned release rate of $H_2S$ through control of polymer properties. Furthermore, the polymer micelles were more effective relative to common small molecule $H_2S$ donors ($Na_2S$, a small molecule SATO, and GYY4137) in decreasing viability of HCT116 colon carcinoma cells. These results reveal the importance of $H_2S$ release rate on biological activity and further underline the potential of polymeric $H_2S$ donors.

Expanding upon the previous study, in 2019 we developed a method for systematically tuning $H_2S$ release rate from SATO-conjugated micelles (Fig. 1.2C).[78] PEG-*b*-pFBEMA block copolymers, prepared in a similar fashion to the previous work, were conjugated with functionalized SATO derivatives. We hypothesized that controlling the rate of Cys diffusion into the micelle core would control the $H_2S$ release rate. $H_2S$ release experiments on micelles swollen in water with varying amounts of ethanol provided evidence to support this claim, where the $H_2S$ release rate became increasingly faster with greater degrees of micelle swelling. We further hypothesized that $H_2S$ release from SATO-conjugated micelles could be systematically tuned by controlling the chain mobility of the micelle core. To this end, we co-functionalized PEG-*b*-

FBEMA block copolymers with varying amounts of SATO and an alkyl plasticizing agent, which we expected would increase the mobility of polymer chains. As expected, the resulting series of block copolymers showed a trend in hydrophobic block $T_g$, the temperature above which long-range polymer backbone movement can occur, correlating with the mass ratio of SATO versus alkyl group. Additionally, the $H_2S$ release rate varied over 20-fold throughout the series, with the lowest $T_g$ hydrophobic block resulting in a release half-life similar to that of small molecule SATOs. Overall, this work highlighted the structural tunability of polymeric micelles and demonstrated precise control over $H_2S$ release from a polymeric system without chemically modifying the donor.

Another thiobenzamide-functionalized macromolecular $H_2S$-releasing system was reported by Davis et al. in 2016 (Fig. 1.2D).[79] Two amphiphilic polymethacrylates were synthesized by co-polymerizing 3-(4-cyanophenoxy)propyl methacrylate (CPPMA), oligo(ethylene glycol) monomethyl ether methacrylate (OEGMA), and methyl methacrylate using RAFT polymerization. Pendant thioamides were generated in-situ via thionation of benzonitrile pendant groups present on the CPPMA block in a post-polymerization modification. The final polymers, [POEGMA-*co*-PTHA]-*b*-PMMA and POEGMA-*b*-[PTHA-*co*-PMMA] both formed micelles in aqueous buffered solutions. Faster $H_2S$ release from [POEGMA-*co*-PTHA]-*b*-PMMA versus POEGMA-*b*-[PTHA-*co*-PMMA] micelles was attributed to the placement of the $H_2S$-releasing thioamide units in the hydrophilic corona of the micelle in the former system versus within the hydrophobic core for the latter system. The differences observed in the $H_2S$ release profiles of the two micellar systems highlights the shielding effect of micellization in slowing down the hydrolysis of donors encapsulated within the core. Furthermore, the $H_2S$ delivered from slow-

releasing POEGMA-*b*-[PTHA-*co*-PMMA] polymer micelles gradually increased levels of cytosolic extracellular signal–regulated kinases and plasma membrane-localized protein kinase C activity in HEK293 cells.

In 2017, Quinn et al. reported on $H_2S$ releasing micelles from perthiol-containing polymer constructs synthesized via RAFT polymerization with facile end-group modification (Fig. 1.2E).[80] The benzyl dithioester chain end was first functionalized with pyridyl disulfide groups and subsequently reacted with thiobenzoic acid to yield polymers with benzoyl-capped perthiol ω-chain ends. The final persulfide polymer P[OEGMA]-S-S-(C=O)Ph underwent nucleophilic attack by cysteine to release a free perthiol, which subsequently liberated $H_2S$. The polymer remained stable in buffered aqueous solutions without thiol. As an extension of this concept, the authors prepared an amphiphilic block copolymer by polymerizing butyl methacrylate as a hydrophobic block to yield P[OEGMA-*b*-BMA]-S-S-(C=O)Ph. This polymer readily formed micelles when dispersed in PBS (pH = 7.4) and showed significantly slower $H_2S$ release relative to the homopolymers. The authors attributed the slower release from micelles to confinement of the $H_2$cysteine Furthermore, a pH-responsive amphiphilic block copolymer was synthesized by copolymerizing *N,N*-(dimethylamino) ethyl methacrylate (DMAEMA) and *N,N*-(diisopropylamino) ethyl methacrylate (DIPMA) to generate P[OEGMA-*co*-DMAEMA-*b*-DIPMA]-S-S-(C=O)Ph. Cys-triggered $H_2S$ release from these pH-responsive micelles significantly accelerated under acidic conditions. This phenomenon was attributed to increased hydrophilicity of the DIPMA block under acidic conditions, leading to micelle disassembly and increased exposure to cysteine; this work demonstrated the potential for triggered release of gasotransmitters through careful design of a polymeric drug delivery system.

*Polymeric Liposomes*

Related to micelles, liposomes represent another nanostructure accessible from surfactants or amphiphilic block copolymers. The structure of liposomes resembles that of a lipid bilayer as found in cell membranes—the amphiphilic constituents of liposomes arrange in parallel to form a bilayer with hydrophilic units forming the lining of the bilayer and hydrophobic tails forming the core. As a result, liposomes can encapsulate hydrophobic drugs in the bilayer core and hydrophilic drugs in the aqueous inner compartment. Additionally, manipulation of membrane properties allows for controlled release of bilayer-encapsulated drugs and/or penetration of triggering molecules into the hydrophilic core.

In 2017, Quinn et al. reported on a liposomal $H_2S$-donating macro- and supramolecular system utilizing PEG-cholesterol (PEG-Chol) conjugates with trisulfide linkages.[81] Organic polysulfides, which are biologically active components in various natural products, release $H_2S$ upon thiol exchange reactions.[82,83,84] The authors hypothesized that incorporation of the trisulfide linker into the PEG-Chol conjugate would allow for thiol-triggered $H_2S$ release, and the resultant disruption of the liposomal membrane might induce release of a hydrophilic payload trapped inside the liposome. Thiol-triggered release of $H_2S$ from micelles formed by the trisulfide-linked conjugates was confirmed using SF4, an $H_2S$ selective fluorescent probe. In contrast, no $H_2S$ release was observed from micelles that included disulfide or amide linkages in place of the trisulfide. The PEG-Chol conjugates were then incorporated into pre-formed liposomes using the cholesterol group to anchor the conjugates into the bilayer. $H_2S$ release from these liposomes was evaluated through amperometry using an $H_2S$-selective micro-sensor. Trisulfide conjugates

incorporated into liposomes showed a reduced peaking concentration of $H_2S$ relative to micelles. The authors attributed this decrease in total $H_2S$ release to partial inaccessibility of trisulfides in the bilayer membrane, which suggests a potential for tuning release from liposomes through control of membrane properties.

*Polymeric micro/nanoparticles*

Nanoparticles range in diameter from a few to a few hundred nanometers, making them suitable for injection directly into the bloodstream. This allows for free circulation throughout the vasculature, targeting to specific tissues, and long-term systemic release of APIs for long-circulating nanoparticles. Polymer nanoparticles differ from polymer micelles in that they are typically made using specific processing methods such as nanoprecipitation, a phase separation process rather than a self-assembly process. Conversely, microparticles range in diameter from 1–100 μm and are therefore restricted in migrating from their site of injection. As a result, microparticles are more useful for applications requiring long-term localized release through injection or implantation at a desired site (e.g., muscle tissue, peritoneum). Due to their much smaller surface area to volume ratio compared with nanoparticles, microparticles degrade more slowly and release their cargo more slowly. Combined with their retention in tissue, these features make microparticles suitable for long-term delivery of APIs.

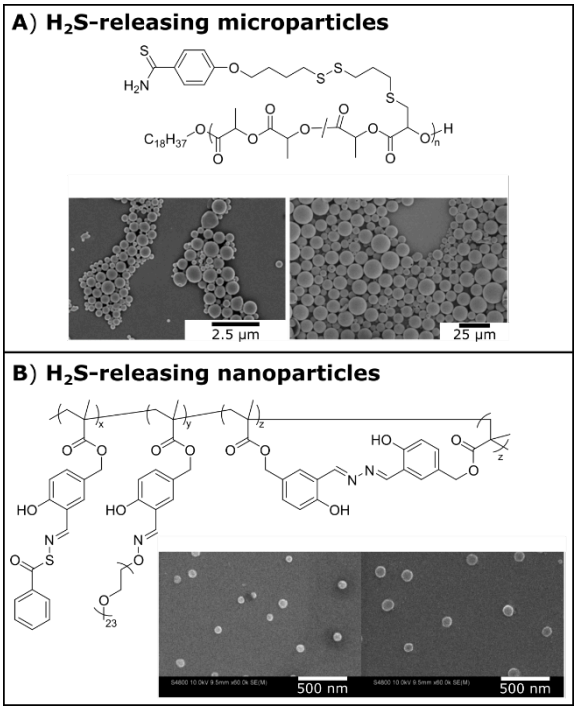


**Fig. 1.3. Chemical structure and TEM images of $H_2S$-releasing nano- and microparticles. A)** Structure of thiobenzamides-containing polylactide block copolymer and SEM images of polymer microparticles. **B)** Statistical copolymer consisting of SATO-, PEG-, and AIEgen-functionalized polymethacrylate and SEM images of polymer nanoparticles. SEM, scanning electron microscopy; SATO, *S*-aroylthiooxime; PEG, polyethylene glycol; AIEgen, aggregation induced emission fluorophore.

In 2015, Bowden et al. reported a polymeric $H_2S$-donating microparticle system consisting of a polylactide backbone decorated with thiobenzamide groups.[85] Ring-opening copolymerization of L-lactide and a 4-hydroxythiobenzamide-functionalized lactide monomer afforded polymers with varying thiobenzamide loading along the backbone. Two sets of spherical microparticles were generated with average diameters of 12 ± 4 and 0.5 ± 0.1 µm (Fig. 1.3A). Degradation studies of the microparticles revealed 10% weight loss after four weeks at pH 7.4, suggesting the potential for prolonged $H_2S$ delivery. However, the authors could not quantitatively measure $H_2S$ levels due to low thiobenzamide loadings in the microparticles, slow microparticle degradation, and

rapid loss of $H_2S$ from aqueous solutions. The need for better analytical methods to assess $H_2S$ delivery over sustained periods is addressed in the Key Challenges and Future Perspectives section below. Despite this limitation, microparticle systems offer the potential for localized $H_2S$ delivery in the range of weeks to months, which could be useful in a number of indications where low endogenous $H_2S$ levels need long-term supplementation.

In related work focusing on nanoparticles instead of microparticles, Lin and co-workers recently described self-fluorescing, $H_2S$-releasing nanoparticles containing SATOs and aggregation-induced emission fluorophores (AIEgens).[86] RAFT polymerization of 3-formyl-4-hydroxybenzyl methacrylate (FHMA) yielded poly(FHMA) or pFHMA decorated with salicylaldehyde (ortho-hydroxybenzaldehyde) units as reactive handles, which were functionalized in three different ways (Fig. 1.3B). A small percentage of aldehyde units were functionalized with aminooxy PEG to impart water solubility to the polymer, while others were crosslinked with hydrazine to form salicylalhydrazine as an AIEgen. Crosslinking with hydrazine was carried out at a high dilution to promote intra-chain crosslinking of aldehyde units, yielding a water-soluble, AIE-active polymer nanoparticle. Finally, the remaining salicylaldehyde units were converted into SATO groups, yielding $H_2S$-releasing, AIE-active nanoparticles. The crosslinked polymers were then dispersed in water with vigorous stirring, and nanoparticles were in the range of 100 nm, as confirmed by SEM and DLS. Cellular internalization of the polymeric nanoparticles was observed by confocal laser scanning microscopy, highlighting the self-fluorescence characteristics of the nanoparticles. This was the first example of $H_2S$ releasing nanoparticles that could also be traced within the living systems, exhibiting the superiority of this AIE-active, $H_2S$-releasing polymer over conventional fluorophores. This work provides insight into the

multi-functional capabilities of polymeric drug delivery systems and exhibits the potential for in vivo $H_2S$ quantification directly at the targeted sites.

*Complex self-assembled and crosslinked materials*

Hydrogels are three dimensional networks of entangled covalent or supramolecular polymers that trap a substantial amount of water. In the field of drug delivery, hydrogels are studied widely due to their resemblance to soft tissue in terms of morphology and mechanical properties combined with their ability to sequester and release APIs. Hydrogels can be broadly categorized as physically or chemically crosslinked gels depending on the type of network crosslinking. Physically crosslinked hydrogels retain their 3D structures through reversible, non-covalent supramolecular interactions, whereas covalent bonds link individual chains in chemically crosslinked hydrogels. Hydrogels can be particularly advantageous for delivering $H_2S$ in a localized manner. While macromolecular assemblies like micelles and nanoparticles may deliver $H_2S$ to the targeted tissues through systemic administration, hydrogels can be injected or implanted at the site of interest and deliver $H_2S$ locally.

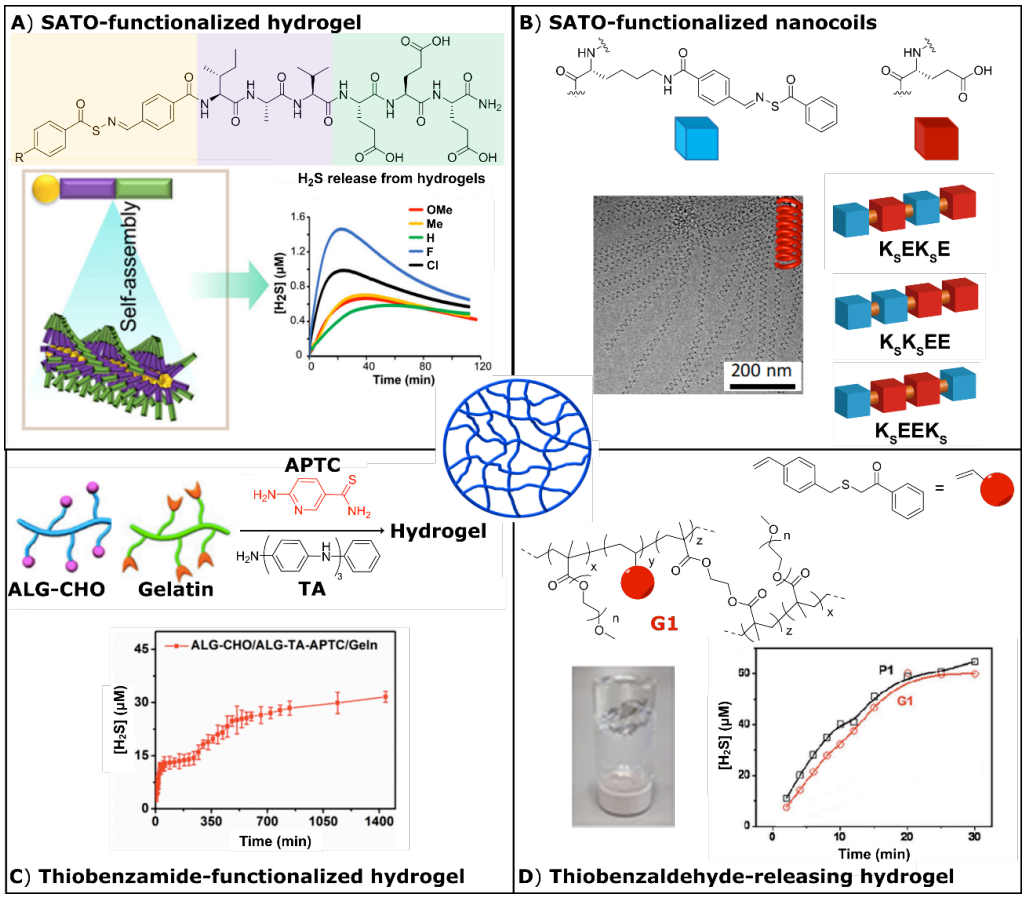


**Fig. 1.4. $H_2S$-releasing hydrogels with covalently bound $H_2S$ donors. A)** Structure of SATO-functionalized peptide with SATO unit screened in yellow, β-sheet region in purple, and charged region in green. Cartoon illustration shows self-assembly of SATO-peptide into one-dimensional nanostructures. $H_2S$ release profiles of SATO hydrogels with varying SATO substituents show that peaking times and concentrations depend on R group. **B)** Structure of SATO-modified lysine and glutamic acid is represented as blue and red cubes respectively. Three different sequences of constitutionally isomeric peptides consisting of two lysine and two glutamic acid units each. Cryo-TEM image shows nanocoils formed by peptide $K_sEEK_s$. **C)** Schematic representation showing formation of multi-component hydrogel from partially oxidized alginate, which is functionalized with TA and APTC and subsequently crosslinked with gelatin to form a hydrogel. The $H_2S$ release profile from the final hydrogel shows gradual release extending over hours. **D)** Structure of thiobenzamide precursor and PEGMA polymer functionalized with thiobenzamide. A hydrogel was obtained by crosslinking PEGMA polymer with EDGMA. Graph of $H_2S$ release from hydrogel G1 and polymer solution P1, showing similar release profiles. SATO, *S*-aroylthiooxime; TEM, transmission electron microscopy; APTC, 2-aminopyridine-5-thiocarboxamide; TA, tetraaniline; PEGMA, poly(ethylene glycol) methyl ether methacrylate; EDGMA, ethylene glycol dimethacrylate.

In 2015, our group reported a supramolecular, peptide-based $H_2S$-releasing hydrogel system containing a covalently bound SATO donor.[87] The 6-mer peptide sequence included a β-sheet-rich region (where peptide chains are arranged parallel/anti-parallel to each other and are stabilized by a network of intermolecular H-bonds), a hydrophilic region containing three glutamic acid residues, and the N-terminus functionalized with a SATO group. Driven by hydrophobic interactions and stabilized by hydrogen-bonding in the β-sheet rich region, the SATO-functionalized peptides self-assembled into nanofibers in aqueous solutions. At concentrations as low as 1 wt%, a robust hydrogel formed upon charge screening through the addition of $CaCl_2$. Due to shielding of the SATO groups in the nanofiber core, extended release was observed, with measurable $H_2S$ levels beyond 15 h. More recently we conducted deeper investigations into these peptide-based materials by varying substituents on and around the SATO group (Fig. 1.4A).[88, 89] Specifically, we found that R group substitution on the aroyl ring of the SATO unit affected the internal structure of the self-assembled nanofibers, which in turn regulated gel stiffness. $H_2S$ release rates from the hydrogels depended on a complex balance between substituent electronic effects and internal nanofiber morphology, but extended release profiles were observed for all hydrogels. These $H_2S$-releasing, peptide-based hydrogels may be ideal for localized $H_2S$ delivery because the peptide components of the gels can be degraded into benign metabolites.

Recently we reported a self-assembled $H_2S$-releasing system based on constitutionally isomeric peptides.[90] A series of three tetrapeptides were designed with two lysine (K) and two glutamic (E) acid units varying in their placement along the peptide backbone (Fig. 1.4B). The lysine

residues were modified with SATO groups, yielding three peptides, $K_sEEK_s$, $K_sEK_sE$, and $K_sK_sEE$ ($K_s$ = SATO-modified lysine). Peptide $K_sEEK_s$ self-assembled into an unusual nanocoil morphology, whereas the other two peptides formed conventional twisted nanoribbons. Interestingly, $H_2S$ release from the nanocoils was slower than release from the nanoribbons, which we attributed to slower diffusion of cysteine into nanocoils relative to nanoribbons. Furthermore, nanocoils were more effective compared to small molecule $H_2S$ donors (GYY4137 and $Na_2S$) as well as nanoribbons in rescuing H9C2 cardiomyocytes from doxorubicin toxicity. This work demonstrated that slowly releasing $H_2S$ donors (release over several hours) are more effective than burst release donors such as $Na_2S$ or even moderately faster donors. Comparisons in biological studies between comparable $H_2S$ donors with different release rates will be vital for determining the optimal rate in various settings. Tuning nanostructures through supramolecular approaches may offer a method to modify release rate without changing $H_2S$ donor chemistry or released byproducts, allowing for clear comparisons between $H_2S$ donors with variable release half-lives.

Recently, Liang and co-researchers reported a smart, $H_2S$-releasing hydrogel for potential treatment of myocardial infarction.[91] The researchers synthesized a macromolecular $H_2S$ donor by grafting 2-aminopyridine-5-thiocarboxamide (APTC), a thiol triggered $H_2S$ donor, onto partially oxidized alginate (Alg-CHO). The macromolecular donor was further functionalized by tetraaniline (TA) to impart conductivity to the final Alg-APTC-TA construct, which was crosslinked with gelatin to form an $H_2S$-releasing conductive hydrogel (Fig. 1.4C). The hydrogel showed strong adhesion to tissue due to presence of aldehyde groups on the hydrogel surface, which can react with nucleophilic amines in tissue proteins. The authors observed a significant

increase in $H_2S$ release half-life of small molecule APTC from 3 to 270 min by encapsulating it within the hydrogel, and the hydrogel showed extended $H_2S$ release exceeding 24 h. The hydrogel was evaluated in mice hearts, exhibiting positive effects on function and remodeling of the left ventricle by significantly reducing cardiac fibrosis and ventricle wall thickening. This multifunctional hydrogel system underscores the importance of localized $H_2S$ delivery for conditions like myocardial infarction and further demonstrates the potential for self-assembled systems to achieve these advanced drug delivery goals.

A light-responsive hydrogel was reported by Connal and co-workers in 2017.[92] They synthesized light sensitive thiobenzaldehyde precursors that released thioaldehydes upon irradiation. The released thioaldehydes further reacted with amines to form imines, releasing $H_2S$ as a byproduct. The small molecule thiobenzaldehyde precursors released a small amount of $H_2S$ upon irradiation followed by enhancement in $H_2S$ release rate upon addition of amines. The authors then synthesized a vinyl monomer incorporating the thiobenzaldeyhyde precursor group, which was copolymerized with polyethylene glycol methacrylate (PEGMA) to form water soluble, light-sensitive, $H_2S$-releasing polymers, and further crosslinked with ethylene glycol dimethacrylate (EGDMA) to provide light-sensitive $H_2S$ releasing hydrogels (Fig. 1.4D). Slow $H_2S$ release rates were observed from the hydrogels and linear polymers relative to the small molecule donor. To that end, the hydrogel was tested as a surface for cell-culture to study $H_2S$ delivery *in vitro* and showed successful growth of cells on the gel surface and subsequent $H_2S$ delivery.

*De-polymerizable $H_2S$-donating systems*

An area of macromolecular drug delivery strategies that holds great potential but is in its infancy is depolymerizable systems. In such systems, therapeutic agents are covalently attached to or physically entrapped in polymers which can systematically depolymerize (also called self-immolation) upon application of a specific stimulus.[93, 94] These strategies are appealing because they enable methods for triggered release of payloads and avoid the potentially long biological clearance times of polymer byproducts associated with conventional macromolecular drug delivery systems.

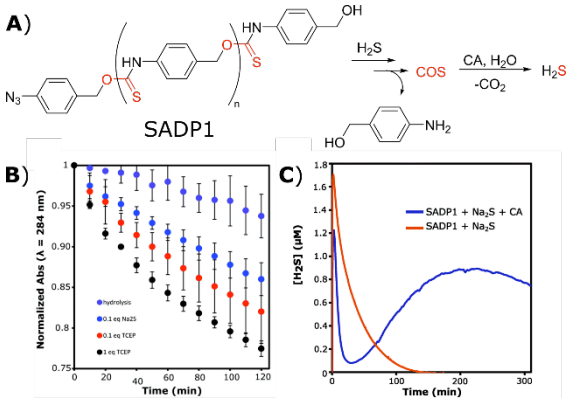


**Fig. 1.5. Depolymerizable $H_2S$-releasing polymers A)** Schematic illustration of $H_2S$-triggered depolymerization of SADP1 polymer. Reduction of the azide end group initiates de-polymerization of SADP1 polymer, generating COS, which is rapidly converted into $H_2S$ by the enzyme CA. **B)** Graph of depolymerization kinetics measured via UV-Vis spectroscopy comparing various triggers. **C)** Graph of $H_2S$ release curves from SADP1 polymer with $Na_2S$ as trigger. No $H_2S$ release from the polymer was observed in the absence of enzyme CA. SADP1, self-amplified depolymerizable polymer; COS, carbonyl sulfide; CA, carbonic anhydrase.

In 2019, we developed a depolymerizable COS/$H_2S$ donor based on oligo(thiourethanes).[95] A class of benzyl thiocarbamates developed by Pluth are COS/$H_2S$ donors that can be triggered by

a variety of stimuli.[96, 97] Operating through a 1,6-elimination mechanism, cleavage of a protecting group initiates the reaction, generating the COS product that can be converted into $H_2S$ by carbonic anhydrase. Inspired by this work, our group synthesized an aryl isothiocyanate monomer for use in a polyaddition reaction to form an oligothiourethane. This monomer was polymerized and end-capped with 4-azidobenzylalcohol to achieve an aryl azide end-capped oligothiourethane termed self-amplified depolymerizable polymer 1 (SADP1, Fig. 1.5A). The molecular weight was limited to 1,600 g/mol due to the low thermodynamic driving force for the polymerization, but depolymerization triggered by reducing agents revealed a decrease in polymer peaks and the appearance of peaks representative of 4-aminobenzylalcohol by UV-Vis spectroscopy (Fig. 1.5B). The $H_2S$ release profile of the oligothiourethane was observed by an $H_2S$-selective electrochemical probe (Fig. 1.5C). In the absence of carbonic anhydrase, addition of $Na_2S$ to a SADP1 solution showed only a spike in $H_2S$ concentration from the initial $Na_2S$ addition. However, the experiment performed in the presence of carbonic anhydrase produced a sudden spike followed by a gradual increase in $H_2S$ concentration over several hours. The gradual increase after the initial spike was a result of slow generation of COS through the depolymerization mechanism, which was then converted into $H_2S$ by carbonic anhydrase. In this way, the system self-amplified $H_2S$ production, where one equivalent of $H_2S$ reduced the azide end-group to trigger the depolymerization, generating several more equivalents of $H_2S$, which then went on to trigger more depolymerization, producing more $H_2S$. This work hints at the possibilities of depolymerizable polymers as carriers for delivery of "caged" small molecules such as $H_2S$, with potential to tune the triggering stimulus, the rate of $H_2S$ production, and the released byproducts.

### 1.4 Macromolecular systems with physically entrapped $H_2S$ donors

Physical entrapment of APIs within macromolecular or supramolecular materials is experimentally simpler than covalent binding of APIs to the scaffold. Consisting at a minimum of only a polymer and the drug to be delivered, no linker chemistry needs to be developed, so chemical designs are less elaborate. Additionally, a wide range of APIs can be sequestered in the same polymer matrix, and multiple APIs can be entrapped if desired. On the macroscale, physical entrapment tends to affect the physical properties of the polymer matrix less than covalent attachment, so physical, morphological, and biological properties of the matrix can be determined and optimized independent of the API. A number of delivery systems have been developed based on physically entrapping $H_2S$ donors.

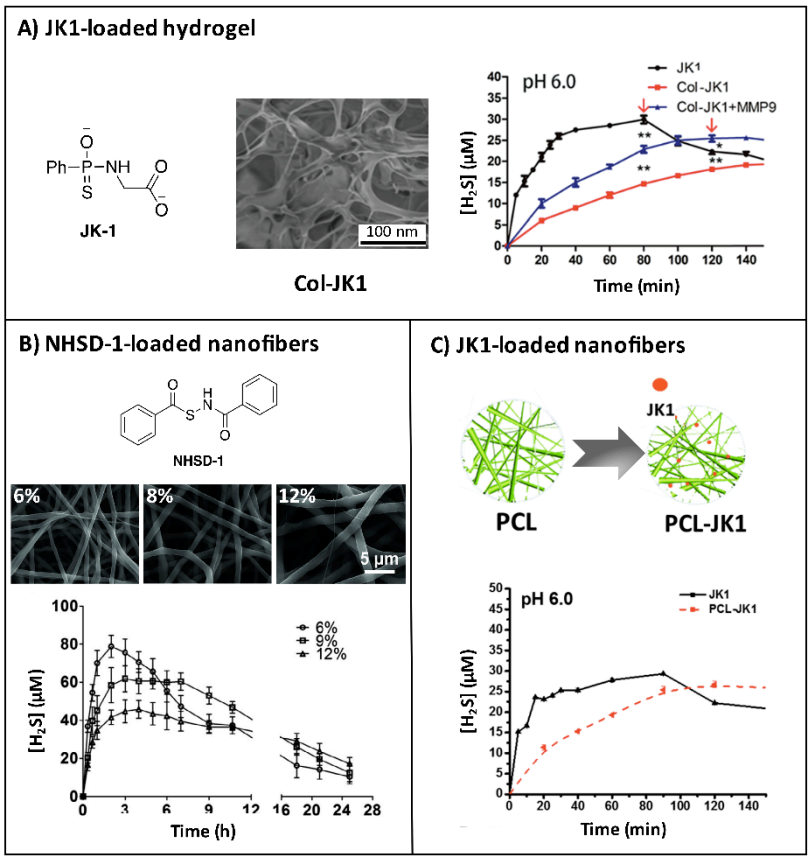


**Fig. 1.6. Hydrogels and nanofibers with physically entrapped $H_2S$ donors. A)** Chemical structure of pH sensitive JK1 donor and SEM images of Col-JK1 hydrogel. Graph of $H_2S$ release comparing hydrogels and small molecule JK1 donor. **B)** Chemical structure of NHSD-1 donor and SEM images of fibers with varying PCL concentrations. Graph of $H_2S$ release profile from fibers. **C)** Illustration showing JK1 donor embedded within PCL fibers and concentration vs. time graph showing $H_2S$ release profile. SEM, scanning electron microscopy; Col-JK1, collagen JK1; PCL, poly(caprolactone); NSHD-1, N-mercapto-based $H_2S$ donor.

*Hydrogels*

In 2019, Xiao et al. reported a dual pH- and enzyme-responsive $H_2S$-releasing hydrogel based on collagen for the potential treatment of indivertible disc degeneration (IDD).[98] A pH-sensitive small molecule $H_2S$ donor, JK1, was encapsulated within the porous network of the collagen hydrogel to generate Col-JK1 gel (Fig. 1.6A). Col-JK1 could be slowly degraded by MMP9, an

enzyme that is overexpressed under IDD conditions. Degradation of the collagen gel led to release of JK1 into the low pH environment of the inflamed tissue, where it underwent intramolecular cyclization to release $H_2S$. $H_2S$ release from Col-JK1 was slower compared to the small molecule donor alone and was accelerated in the presence of MMP9. Furthermore, Col-JK1 successfully inhibited apoptosis in nucleus pulposus cells and prevented degradation of extracellular matrix (ECM), indicating its potential for IDD treatment. Encapsulating the donor within the collagen hydrogel not only increased its retention time in the IDD lesion and prolonged the $H_2S$ release time, but it also created an enzyme-responsive, on-demand release system. However, $H_2S$ release from Col-JK1 gel in the absence of MMP9 was still substantial, highlighting the need for continued development of enzyme-responsive systems that release $H_2S$ only in the presence of the desired enzyme.

*Electrospun fibers*

A simple method to prepare drug-releasing polymers with control over release rates, mechanical properties, and matrix degradability is electrospinning. Electrospinning is a process of generating nano/microfibers by spraying a continuous stream of polymer solution and stretching it under high voltage. Electrospun fibers, like polymeric and self-assembled hydrogels, resemble the ECM in morphology and mechanical properties and therefore find use as materials for tissue engineering and regenerative medicine. Electrospun fibers, however, are much larger in diameter than peptide-based nanofibers or polymer chains (in the range of ~1 μm versus 1–10 nm). The large diameter allows the fibrous network to physically entrap and stabilize drugs and other bioactive molecules with high drug loading capacity. Chemical structure and morphology affect polymer degradation kinetics, as does fiber diameter, giving researchers several methods to alter

drug release profiles. With its tunability and versatility, the inexpensive technique of electrospinning is a natural fit for $H_2S$ releasing materials, where control of release rate is vital. Wang and co-workers reported the first electrospun $H_2S$-releasing microfibers in 2015 based on a biodegradable polycaprolactone (PCL) polymer matrix.[99] A solution of PCL at different concentrations (6%, 8%, and 12%) and a thiol activated $H_2S$-donor (NSHD1) were subjected to electrospinning to yield microfibers with diameters ranging from 0.5 to 1.5 μm (Fig. 1.6B). An increase in microfiber diameter was observed with increasing PCL concentration. SEM revealed smooth microfiber surfaces indicative of uniform distribution of NSHD-1 within the fibers, and FTIR spectroscopy confirmed NSHD-1 encapsulation. $H_2S$ release half-lives for the microfibers were longer than NSHD-1 alone, with measurable $H_2S$ levels extending past 24 h. Release rate depended on fiber thickness, with thicker fibers releasing more slowly than thinner ones. Additionally, these electrospun, $H_2S$-releasing microfibers protected H9C2 cardiomyocytes subjected to oxidative stress by addition of $H_2O_2$. They also enhanced proliferation of 3T3 fibroblasts, which is potentially useful for wound healing.

A few years later, the same group applied $H_2S$-releasing PCL nanofibers, with diameters near 300 nm, in the development of a nanofibrous coating for wound healing.[100] The fabrication and characterization of the nanofibers was similar to PCL-NSHD-1 nanofibers, but the pH-responsive $H_2S$ donor JK1 was included instead. $H_2S$ release from PCL-JK1 fibers was higher at pH 6 relative to physiological pH, and was significantly slower than small molecule JK1 donor alone, with measurable $H_2S$ levels past 2 h (Fig. 1.6C). One-time application of PCL-JK1 nanofibrous scaffolds to full-thickness cutaneous wound models in mice showed successful wound regeneration over 20 d with healing rates significantly higher than PCL fibers alone. It is

not clear how the release profile changed *in vivo* compared with the release over a few hours *in vitro*, but it likely released $H_2S$ for a much longer period based on the results from the *in vivo* studies.

In 2018 Melino and co-workers reported electrospun microfibrous polylactic acid (PLA) membranes containing garlic-derived organosulfur compounds (OSCs) fabricated using two different approaches.[101] In the first approach, garlic oil-soluble extract (GaOS) was directly coated onto the electrospun microfibers (~700 nm in diameter) to yield GaOS-coated PLA fiber membranes (PFM+GaOS). In the second approach, GaOS or diallyl disulfide (DADS) was encapsulated within the PFMs during the electrospinning process to generate GaOSPFM or DADSPFM fibers, respectively. Both doped fibers released substantially less $H_2S$ than the coated fibers. $H_2S$ release experiments were conducted in pH 8 buffer at 37 °C, and although the authors did not conduct a typical release experiment to measure cumulative or real-time $H_2S$ concentrations over time, the electrospun mats clearly protected the extracts in the dry state for several days. Studies on cardiac mesenchymal stem cells showed that the fiber mats protected the cells from oxidative stress.

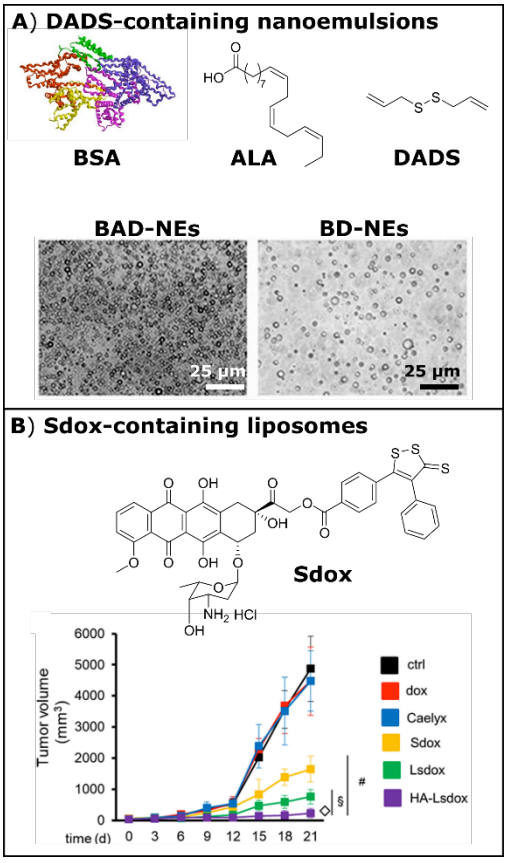


**Fig. 1.7**. **Nanoemulsions and liposomes with physically entrapped $H_2S$ donors. A)** Structures of BSA, ALA, and DADS. Optical micrographs depicting spherical particles for $H_2S$-releasing nanoemulsions with ALA (BAD-NEs) and without ALA (BD-NEs). **B)** Chemical structure of Dox modified with an $H_2S$ donor. BSA, bovine serum albumin; ALA, α-linoleic acid; DADS, diallyl disulfide; Dox, doxorubicin.

Nanoemulsions and liposomes physically loaded with $H_2S$ donors have similar therapeutic potential to polymer micelles described above. They can protect encapsulated APIs to improve stability, increase circulation times, and accumulate at sites of interest (e.g., tumors). These types of formulations are generally prepared through simple and scaleable processes such as

nanoprecipitation. Careful process control allows for tunable and uniform droplet sizes. The facile preparation and wide range of formulation possibilities are ideal for the development of various macromolecular $H_2S$ donor systems.

In 2016, Melino et al. reported on an $H_2S$-releasing protein nanoemulsion formulation utilizing DADS, α-linoleic acid (ALA), and bovine serum albumin (BSA) (Fig. 1.7A).[102] DADS is found in various natural extracts and releases small amounts of $H_2S$ upon reaction with a thiol.[103] Similarly, ALA promotes cardiovascular health, reduces the risk of cardiovascular attacks, and exhibits chemoprotective effects.[104, 105] The therapeutic applications of both DADS and ALA are limited by low aqueous solubility and stability. The authors suggested that a nanoemulsion formulation of both compounds may improve their bioavailability, thus increasing their therapeutic potential. Protein nanoemulsions of BSA-ALA-DADS (BAD-NEs) and BSA-DADS (BD-NEs) were prepared by sonication, with average diameters in the range of a few hundred nm. Interestingly, in thiol-containing buffer, BAD-NEs, which contained all three components, released more total $H_2S$ per unit of DADS relative to both BD-NEs, which lacked the ALA lipid component, and DADS alone. The authors attributed this result to both increased stability of DADS in the nanoemulsion and the antioxidant properties of ALA. Incubation of BAD-NE nanoemulsions with supercoiled plasmid DNA in an oxidative environment revealed superior antioxidant properties relative to ALA and DADS alone, as well as their binary mixture. Furthermore, BAD-NEs significantly decreased cell viability in MCF-7 mammary adenocarcinoma and HuT 78 T-cell lymphoma cells, suggesting their potential as an anti-cancer therapeutic.

In 2019, Arpicco, Riganti and coworkers reported on liposomal formulations of doxorubicin

(Dox) conjugated to an $H_2S$-donor (Sdox).[106] The Sdox compounds, reported by the authors in previous work,[107, 108, 109] showed reduced cardiotoxic effects compared with free Dox while retaining their efficacy against human bone osteosarcoma cells (characterized for their resistance to Dox). The authors suggested that encapsulation of Sdox in liposomes conjugated with hyaluronic acid (HA) might promote targeting to osteosarcoma cells due to their expression of the HA-receptor CD44. Liposomal Sdox (Lsdox) and hyaluronated liposomal Sdox (HA-Lsdox) were prepared through hydration of drug-lipid films, and successful insertion of Sdox into the liposomal membrane was confirmed by differential scanning calorimetry. HA-Lsdox showed a higher accumulation in CD44-expressing cells *in vitro* relative to Dox, Sdox, Lsdox, and Caelyx®, a commercial liposomal Dox formulation (Fig. 1.7B). Additionally, HA-Lsdox induced higher cell damage, apoptosis, and lower cell viability relative to the other formulations *in vitro*. *In vivo* studies revealed that HA-Lsdox greatly outperformed Sdox and the other liposomal Dox formulations with respect to inhibition of K7M2 tumor growth. This work highlights the potential for supramolecular donor systems in clinical applications of $H_2S$ therapy. Sdox is an advanced form of Dox that may reduce side effects of this common chemotherapy drug, but this work shows that drug delivery vehicles are still needed for Sdox to maximize its anti-cancer effects while limiting cardiotoxicity.

**1.5 Key Challenges and Future Perspectives**

In recent years it has become clear that $H_2S$, along with the other known gasotransmitters NO and CO, are molecules of supreme importance in mammalian physiology. Our understanding of the biological significance and therapeutic potential of $H_2S$ continues to expand, and there exists a need for a wide variety of strategies to deliver the gas at the desired location in the body, at the

intended time, for the appropriate duration, and with the chosen rate of release. Due to its reactivity and short half-life, controlled delivery becomes even more important for $H_2S$ than conventional small molecule drugs, which are typically selected from a variety of possible structures with considerations toward their pharmacokinetics and target specificity. Small molecule $H_2S$ donors remain vital in this endeavor, but $H_2S$-releasing macro- and supramolecular materials offer additional possibilities for regulating these key drug delivery parameters.

Polymers functionalized with $H_2S$ donors were the first macromolecular materials developed for $H_2S$ delivery, with initial reports in 2014. This strategy provides a straightforward method for extending the duration of $H_2S$ release and potentially altering its biodistribution and pharmacokinetics compared with small molecule donors. However, the polymer itself in this strategy typically brings limited if any additional control over release compared with small molecule analogs. Additionally, the fate of the polymeric byproduct(s) must be considered in these delivery systems. If the polymer is small enough, it may be renally excreted; otherwise it may accumulate if it is not biodegradable. Depolymerizable $H_2S$-releasing polymers, first reported in 2019, may hold advantages over functionalized non-degradable or slowly degradable polymers, including the potential for a specific trigger to initiate depolymerization.

Compared with soluble homopolymers and copolymers, $H_2S$-releasing block copolymers that form assemblies, such as micelles and liposomes, enhance release control. The hydrophilic block can protect $H_2S$ donors linked to or sequestered in the hydrophobic domain of a micelle or liposome, and micelle core mobility can regulate release rate. Beyond these advantages, micelles, liposomes, and other self-assembled structures have been studied extensively as drug delivery

vehicles, so $H_2S$-releasing components can be included in existing platforms. $H_2S$-releasing micelles with targeting groups on their peripheries hold potential for site-specific $H_2S$ delivery through systemic injection.

Localized $H_2S$ delivery may prove invaluable in studying the effects of $H_2S$ on specific organs because systemic drug delivery vehicles never have perfect targeting capacity. Hydrogels, either with covalently attached $H_2S$ donor motifs or sequestered donors, lead the way in localized $H_2S$ delivery. Hydrogels can be made from crosslinked water-soluble polymers (chemically crosslinked hydrogels) or from self-assembling small molecules such as peptides (physically crosslinked hydrogels). Both can be implanted (or injected from a needle in the case of shear-thinning hydrogels, which disassemble in response to shear stress during injection and reassemble in vivo after injection) at a site of interest to deliver $H_2S$ locally. Increased capacity to control the $H_2S$ release rate, hydrogel stiffness, and degradability of the hydrogel carrier material will further enhance the utility of $H_2S$-releasing hydrogels. The potential to functionalize hydrogels with additional bioactive units offers exciting possibilities in influencing cellular behavior and promoting healing. $H_2S$-releasing microspheres and electospun scaffolds, which may offer longer release periods than hydrogels, may also enable a number of biological studies and applications where long-term delivery (i.e., weeks to months) is desired. Both platforms, several types of which have thoroughly characterized degradation rates and mechanisms, are also well-suited to pairing $H_2S$ with other small molecule drugs where synergistic effects could be observed.

Many challenges remain in this field. While triggerable, small-molecule $H_2S$ donors have many

advantages over sulfide salts, they are inherently unstable compounds that must be handled with care to avoid triggering release prematurely. This need for careful handling and storage extends to $H_2S$-releasing materials, and it can limit storage times and shipment methods. The instability of $H_2S$ donors also limits delivery of $H_2S$ to active delivery, where exogenous $H_2S$ is administered *in response* to a specific condition. In contrast, proactive delivery strategies involve materials containing *latent* APIs that respond only to a biological trigger to release their payload. Development of proactive $H_2S$-releasing materials with precisely triggered release mechanisms are needed to continue moving the field forward.

Beyond stimuli-responsive delivery strategies, materials that release $H_2S$ over the course of weeks to months are needed. Most extended biological studies on the effects of $H_2S$ treatment in slow processes, for example chronic wound healing, are conducted using daily dosing of donor compounds. This dosing schedule results in fluctuations in $H_2S$ levels in circulation and/or at the treatment site. Delivery from materials, such as hydrogels, microparticles, electrospun scaffolds, or polymer films, has the potential to stabilize $H_2S$ levels through sustained release. Indeed, delivery from various materials is used widely to decrease dosing frequency in many common pharmaceuticals. Sustained delivery of $H_2S$ from materials has great therapeutic potential, but analytical challenges must be addressed in order to properly characterize $H_2S$ release profiles from these materials, both *in vitro* and *in vivo*. Methods for determining $H_2S$ release profiles, such as the methylene blue method, fluorescent sensing methods, and electrochemical probes, are well suited for measuring release times on the order of minutes to hours, but each has limitations beyond this time period. Reliable and sensitive methods for long-term measurement of $H_2S$ concentrations are needed.

Addressing these challenges in $H_2S$-releasing materials may provide insight into $H_2S$ biology and physiology and answer questions regarding potential $H_2S$ therapies. For example, will targeted and or localized delivery reduce the dose needed compared with systemic injection? Another question is how release rates affect therapeutic outcomes. Ongoing work in our lab and other labs is beginning to show that sustained $H_2S$ concentrations at low levels are more effective than instantaneous $H_2S$ donors or very long-acting donors. These results are consistent with a bell-shaped exposure-response curve, in which $H_2S$ exerts its maximum beneficial biological effect at intermediate concentrations. More efforts to compare similar donors with varying rates of $H_2S$ release are needed to verify these early results, and the outcomes of these experiments will inform clinical possibilities for $H_2S$ therapy. Compared with other drugs, the field of $H_2S$-releasing materials is in its infancy; drug delivery methods have been used clinically for decades and continue to be developed for other APIs. In the coming years, we expect to see materials capable of controlling many aspects of $H_2S$ delivery, revealing (patho)physiological insights and moving toward clinical applications.

## 1.6 References


(1) Bulbake, U.; Doppalapudi, S.; Kommineni, N.; Khan, W. Liposomal Formulations in Clinical Use: An Updated Review. *Pharmaceutics,* **2017**, 9, 1–33.

(2) Hu, Q. Q.; Li, H.; Wang, L. H.; Gu, H. Z.; Fan, C. H. DNA Nanotechnology-Enabled Drug Delivery Systems. *Chem. Rev.,* **2019**, 119, 6459–6506.

(3) Suk, J. S.; Xu, Q. G.; Kim, N.; Hanes, J.; Ensign, L. M. PEGylation as a strategy for improving nanoparticle-based drug and gene delivery. *Adv. Drug. Deliv. Rev.,* **2016**, 99, 28–51.

(4) Ekladious, I.; Colson, Y. L.; Grinstaff, M. W. Polymer-drug conjugate therapeutics: advances, insights and prospects. *Nat. Rev. Drug. Discov.,* **2019**, 18, 273–294.

(5) Barenholz, Y. Doxil® — The first FDA-approved nano-drug: Lessons learned. *J. Cont. Rel.* **2012** 160, 117–134.

(6) Dlugi, A. M.; Miller, J. D.; Knittle, J. Lupron depot (leuprolide acetate for depot suspension) in the treatment of endometriosis: a randomized, placebo-controlled, double-blind study. *Fertil. Steril.* **1990**, 54, 419–427.

(7) Ferrari, M. Cancer nanotechnology: opportunities and challenges. *Nat. Rev. Cancer* **2005**, 5, 161–171.

(8) Gordon, M. S.; Kinlock, T. W.; Vocci, F. J.; Fitzgerald, T. T. Memisoglu A and Silverman B. A Phase 4, Pilot, Open-Label Study of VIVITROL® (Extended-Release Naltrexone XR-NTX) for Prisoners. *J. Subst. Abus. Treat.* **2015**, 59, 52–58.

(9) Sanborn, G. E.; Anand, R.; Torti, R. E.; Nightingale, S. D.; Cal, S. X.; Yates, B.; Ashton, P.; Smith, T. Sustained-Release Ganciclovir Therapy for Treatment of Cytomegalovirus Retinitis: Use of an Intravitreal Device. *JAMA Ophthalmol.* **1992**, 110, 188–195.

(10) Allen, T. M.; Cullis, P. R. Liposomal drug delivery systems: From concept to clinical applications. *Adv. Drug. Deliv. Rev.* **201**3, 65, 36–48.

(11) Cho, K.; Wang, X.; Nie, S.; Chen, Z.; Shin, D. M. Therapeutic Nanoparticles for Drug Delivery in Cancer. *Clin. Cancer Res.* **2008**, 14, 1310–1316.

(12) Kataoka, K.; Harada, A.; Nagasaki, Y. Block copolymer micelles for drug delivery: design, characterization and biological significance. *Adv. Drug Deliv. Rev* **2001**, 47, 113–131.

(13) Mura, S.; Nicolas, J.; Couvreur, P. Stimuli-responsive nanocarriers for drug delivery. *Nat. Mater.* **2013**, 12, 991–1003.

(14) Petros, R. A.; DeSimone, J. M. Strategies in the design of nanoparticles for therapeutic applications. *Nat. Rev. Drug Discov.* **2010**, 9, 615–627.

(15) Uhrich, K. E.; Cannizzaro, S. M.; Langer, R. S.; Shakesheff, K. M. Polymeric Systems for Controlled Drug Release. *Chem. Rev.* **1999**, 99, 3181–3198.

(16) Mustafa, A. K.; Gadalla, M. M.; Snyder, S. H. Signaling by Gasotransmitters. *Sci Signal.* **2009**, 2, 1-8,.

(17) Wang, R. Two's company, three's a crowd: can $H_2S$ be the third endogenous gaseous transmitter? *FASEB J.* **2002**, 16, 1792–1798.

(18) Wang, R. Gasotransmitters: growing pains and joys. *Trends. Biochem. Sci.* **2014**, 39, 227–232.

(19) Carpenter, A. W.; Schoenfisch, M. H. Nitric oxide release: Part II. Therapeutic applications. *Chem. Soc. Rev.* **2012**, 41, 3742–3752.

(20) Ji, X.; Damera, K.; Zheng, Y.; Yu, B.; Otterbein, L. E.; Wang, B. Toward Carbon Monoxide–Based Therapeutics: Critical Drug Delivery and Developability Issues. *J. Pharm. Sci.* **2016**, 105, 406–416.

(21) Wallace, J. L.; Vaughan, D.; Dicay, M.; MacNaughton, W. K.; de Nucci, G. Hydrogen Sulfide-Releasing Therapeutics: Translation to the Clinic. *Antioxid. Redox. Signal.* **2017**, 28, 1533–1540.

(22) Wang, R. Shared signaling pathways among gasotransmitters. *Proc. Natl. Acad. Sci.* **2012**, 109, 8801–8802.

(23) Abe, K.; Kimura, H. The possible role of hydrogen sulfide as an endogenous neuromodulator. *J. Neurosci.* **1996**, 16, 1066–1071.

(24) Gadalla, M. M.; Snyder, S. H. Hydrogen sulfide as a gasotransmitter. *J Neurochem.* **2010**, 113, 14–26.

(25) Wang, R. Physiological Implications of Hydrogen Sulfide: A Whiff Exploration That Blossomed. *Physiol. Rev.* **2012**, 92, 791–896.

(26) Barr, L. A.; Calvert, J. W. Discoveries of Hydrogen Sulfide as a Novel Cardiovascular Therapeutic. *Circulation* **2014**, 78, 2111–2118.

(27) Calvert, J. W.; Jha, S.; Gundewar, S.; Elrod, J. W.; Ramachandran, A. Pattillo C. B.; Kevil, C. G.; Lefer, D. J. Hydrogen Sulfide Mediates Cardioprotection Through Nrf2 Signaling. *Circ. Res.* **2009**, 105, 365–374.

(28) Rajpal, S.; Katikaneni, P.; Deshotels, M.; Pardue, S.; Glawe, J.; Shen, X.; Akkus, N.; Modi, K.; Bhandari, R.; Dominic, P.; Reddy, P.; Kolluru, G. K.; Kevil, C. G. Total sulfane sulfur bioavailability reflects ethnic and gender disparities in cardiovascular disease. *Redox. Biol.* **2018**, 15, 480–489.

(29) Mustafa, A. K.; Sikka, G.; Gazi, S. K.; Steppan, J.; Jung S. M.; Bhunia A. K.; Barodka V. M.; Gazi, F. K.; Barrow, R. K.; Wang, R.; Amzel, L. M.; Berkowitz, D. E.; Snyder, S. H. Hydrogen Sulfide as Endothelium-Derived Hyperpolarizing Factor Sulfhydrates Potassium Channels. *Circ. Res.* **2011**, 109, 1259–1268.

(30) Tang, G.; Wu, L.; Liang, W.; Wang, R. Direct Stimulation of $K_{ATP}$ Channels by Exogenous and Endogenous Hydrogen Sulfide in Vascular Smooth Muscle Cells. *Mol. Pharmacol.* **2005**, 68, 1757–1764.

(31) Zhao, W.; Zhang, J.; Lu, Y.; Wang, R. The vasorelaxant effect of $H_2S$ as a novel endogenous gaseous $K_{ATP}$ channel opener. *EMBO J.* **2001**, 20, 6008–6016.

(32) Szabo, C. Hydrogen sulfide, an enhancer of vascular nitric oxide signaling: mechanisms and implications. *Am. J. Physiol. Cell Physiol.* **2016**, 312, C3–C15.

(33) Szabó, C.; Papapetropoulos, A. Hydrogen sulphide and angiogenesis: mechanisms and applications. *Br. J. Pharmacol.* **2011**, 164, 853–865.

(34) Wang, M. J.; Cai, W. J.; Zhu, Y. C. Mechanisms of angiogenesis: Role of hydrogen sulphide. *Clin. Exp. Pharmacol. Physiol.* **2010**, 37, 764–771.

(35) Whiteman, M.; Li, L.; Rose, P.; Tan, C-H.; Parkinson, D. B.; Moore, P. K. The Effect of Hydrogen Sulfide Donors on Lipopolysaccharide-Induced Formation of Inflammatory Mediators in Macrophages. *Antioxid. Redox. Signal.* **2009**, 12, 1147–1154.

(36) Zhang, H.; Zhi, L.; Moochhala, S.; Moore, P. K.; Bhatia, M. Hydrogen sulfide acts as an inflammatory mediator in cecal ligation and puncture-induced sepsis in mice by upregulating the production of cytokines and chemokines via NF-κB. *Am. J. Physiol. Lung Cell Mol. Physiol.* **2007**, 292, L960–L971.

(37) Kimura, Y.; Dargusch, R.; Schubert, D.; Kimura, H. Hydrogen Sulfide Protects HT22 Neuronal Cells from Oxidative Stress. *Antioxid. Redox. Signal.* **2006**, 8, 661–670.

(38) Kimura, Y.; Kimura, H. Hydrogen sulfide protects neurons from oxidative stress. *FASEB J.* **2004**, 18, 1165–1167.

(39) Whiteman, M.; Armstrong, J. S.; Chu, S. H.; Jia-Ling, S.; Wong, B-S.; Cheung, N. S.; Halliwell, B.; Moore, P. K. The novel neuromodulator hydrogen sulfide: an endogenous peroxynitrite 'scavenger'? *J. Neurochem.* **2004**, 90, 765–768.

(40) Olson, K. R. The therapeutic potential of hydrogen sulfide: separating hype from hope. *Am. J. Physiol. Regul. Integr. Comp. Physiol.* **2011**, 301, R297–R312.

(41) Szabó, C. Hydrogen sulphide and its therapeutic potential. *Nat. Rev. Drug Discov.* **2007**, 6, 917–935.

(42) Wallace, J. L.; Wang, R. Hydrogen sulfide-based therapeutics: exploiting a unique but ubiquitous gasotransmitter. *Nat. Rev. Drug Discov.* **2015**, 14, 329–345.

(43) Cirino, G.; Vellecco, V.; Bucci, M. Nitric oxide and hydrogen sulfide: the gasotransmitter paradigm of the vascular system. *Br. J. Pharmacol.* **2017**, 174, 4021–4031.

(44) Li, Z.; Polhemus, D. J.; Lefer, D. J. Evolution of Hydrogen Sulfide Therapeutics to Treat Cardiovascular Disease. *Circ. Res.* **2018**, 123, 590–600.

(45) Nagpure, B. V.; Bian, J-S. Brain, Learning, and Memory: Role of $H_2S$ in Neurodegenerative Diseases. In: *Chemistry, Biochemistry and Pharmacology of Hydrogen Sulfide*. edited by Moore PK, Whiteman M. Cham: Springer International Publishing; **2015**, 193–215.

(46) Wallace, J.; Buret, A.; Nagy, P.; Muscara, M.; Nucci, G. D. THU0464 phase 2 clinical trial of the GI safety of a hydrogen sulfide-releasing anti-inflammatory drug (ATB-346). *Ann. Rheum. Dis.* **2019**, 78, 522.

(47) Qian, Y.; Matson, J. B. Gasotransmitter delivery via self-assembling peptides: Treating diseases with natural signaling gases. *Adv. Drug Deliv. Rev.* **2017**, 110–111, 137–156.

(48) Blackstone, E.; Morrison, M.; Roth, M. B. $H_2S$ Induces a Suspended Animation-Like State in Mice. *Science* **2005**, 308, 518.

(49) Lau, N.; Pluth, M. D. Reactive sulfur species (RSS): persulfides, polysulfides, potential, and problems. *Curr. Opin. Chem. Biol.* **2019**, 49, 1–8.

(50) Powell, C. R.; Dillon, K. M.; Matson, J. B. A review of hydrogen sulfide ($H_2S$) donors: Chemistry and potential therapeutic applications. *Biochemical Pharmacology* **2018**, 149, 110–123.

(51) Xu, S.; Hamsath, A.; Neill, D. L.; Wang, Y.; Yang, C-T.; Xian, M. Strategies for the Design of Donors and Precursors of Reactive Sulfur Species. *Chem. Eur. J.* **2019**, 25, 4005–4016.

(52) Zheng, Y.; Ji, X.; Ji, K.; Wang, B. Hydrogen sulfide prodrugs—a review. *Acta. Pharm. Sin. B* **2015**, 5, 367–377.

(53) Connal, L. A. The benefits of macromolecular hydrogen sulfide prodrugs. *J. Mater. Chem. B* **2018**, 6, 7122–7128.

(54) Urquhart, M. C.; Ercole, F.; Whittaker, M. R.; Boyd, B. J.; Davis, T. P.; Quinn J. F., Recent advances in the delivery of hydrogen sulfide via a macromolecular approach. *Polym. Chem.* **2018**, 9, 4431–4439.

(55) Wang, H., Zhao. Y.; Wu, Y.; Hu, Y. L.; Nan, K. H.; Nie, G. J.; Chen, H. Enhanced anti-tumor efficacy by co-delivery of doxorubicin and paclitaxel with amphiphilic methoxy PEG-PLGA copolymer nanoparticles. *Biomaterials* **2011**, 32, 8281–8290.

(56) Wischke, C.; Schwendeman, S. P. Principles of encapsulating hydrophobic drugs in PLA/PLGA microparticles. *Int. J. Mol. Sci.* **2008**, 364, 298–327.

(57) Jeong, B.; Bae, Y. H.; Lee, D. S.; Kim, S. W. Biodegradable block copolymers as injectable drug-delivery systems. *Nature* 1997, 388, 860–862.

(58) Mura, S.; Nicolas, J.; Couvreur, P. Stimuli-responsive nanocarriers for drug delivery. *Nat. Mater.* **2013**, 12, 991–1003.

(59) Gabizon, A.; Shmeeda, H.; Barenholz, Y. Pharmacokinetics of pegylated liposomal doxorubicin - Review of animal and human studies. *Clin. Pharmacokinet.* **2003**, 42, 419–436.

(60) Liu, J.; Bu, W.; Pan, L; Shi, J. NIR-Triggered Anticancer Drug Delivery by Upconverting Nanoparticles with Integrated Azobenzene-Modified Mesoporous Silica. *Angew. Chem. Int. Ed*. **2013**, 52, 4375–4379.

(61) Yoo, H. S.; Park, T. G. Folate receptor targeted biodegradable polymeric doxorubicin micelles. *J. Cont. Rel.* **2004**, 96, 273–283.

(62) Govender, T.; Stolnik, S.; Garnett, M. C.; Illum, L.; Davis, S. S.; PLGA nanoparticles prepared by nanoprecipitation: drug loading and release studies of a water soluble drug. *J. Cont. Rel.* **1999**, 57, 171–185.

(63) Kalaria, D. R.; Sharma, G.; Beniwal, V.; Kumar, M. Design of Biodegradable Nanoparticles for Oral Delivery of Doxorubicin: *in vivo* Pharmacokinetics and Toxicity Studies in Rats. *Pharm. Res.* **2009**, 26, 492–501.

(64) Sahana, D. K.; Mittal, G.; Bhardwaj, V., Kumar, M. PLGA nanoparticles for oral delivery of hydrophobic drugs: Influence of organic solvent on nanoparticle formation and release Behavior in vitro and in vivo using estradiol as a model drug. *J. Pharm. Sci.* **2008**, 97, 1530–1542.

(65) Song, Z. M.; Feng, R. L.; Sun, M.; Guo, C. Y.; Gao, Y.; Li, L. B.; Zhai, G. X. Curcumin-loaded PLGA-PEG-PLGA triblock copolymeric micelles: Preparation, pharmacokinetics and distribution *in vivo*. *J. Colloid. Interface Sci.* **2011**, 354, 116–123.

(66) Hamada, T.; Nakane, T.; Kimura, T.; Arisawa, K.; Yoneda, K.; Yamamoto, T.; Osaki, T.; Treatment of Xerostomia with the Bile Secretion-Stimulating Drug Anethole Trithione: A Clinical Trial. *Am. J. Med. Sci.* **1999**, 318, 146–151.

(67) Hasegawa, U. van der Vlies, A. J. Design and Synthesis of Polymeric Hydrogen Sulfide Donors. *Bioconjugate Chem.,* **2014**, 25, 1290–1300.

(68) Foster J. C.; Matson, J. B. Functionalization of Methacrylate Polymers with Thiooximes: A Robust Postpolymerization Modification Reaction and a Method for the Preparation of $H_2S$-Releasing Polymers. *Macromolecules,* **2014**, 47, 5089–5095.

(69) Foster, J. C.; Powell, C. R.; Radzinski, S. C.; Matson, J. B. *S*-aroylthiooximes: a facile route to hydrogen sulfide releasing compounds with structure-dependent release kinetics. *Org. Lett.,* **2014***,* 16, 1558–1561.

(70) Powell, C. R.; Foster, J. C.; Okyere, B.; Theus, M. H.; Matson, J. B. Therapeutic Delivery of $H_2S$ via COS: Small Molecule and Polymeric Donors with Benign Byproducts. *J. Am. Chem. Soc.,* **2016**, 138, 13477–13480.

(71) Steiger, A. K.; Zhao, Y.; Pluth, M. D. Emerging Roles of Carbonyl Sulfide in Chemical Biology: Sulfide Transporter or Gasotransmitter? *Antioxid. Redox Signal.* **2017**, 28, 1516–1532.

(72) Li, Z.; Li, D.; Wang, L.; Lu, C.; Shan, P.; Zou, X.; Li, Z. Photocontrollable water-soluble polymeric hydrogen sulfide ($H_2S$) donor. *Polymer,* **2019**, 168, 16–20.

(73) Soo, C. H.; Liu, W.; Misra. P.; Tanaka, E.; Zimmer, J. P.; Itty, I. B. Bawendi MG and Frangioni JV. Renal clearance of quantum dots. *Nat. Biotechnol.,* **2007**, 25, 1165–1170.

(74) Kataoka, K.; Harada, A.; Nagasaki, Y. Block copolymer micelles for drug delivery: Design, characterization and biological significance. *Adv. Drug Deliv. Rev.,* **2012**, 64, 37–48.

(75) Maeda, H.; Wu, J.; Sawa, T.; Matsumura, Y.; Hori, K. Tumor vascular permeability and the EPR effect in macromolecular therapeutics: a review. *J. Control. Rel.,* **2000**, 65, 271–284.

(76) Hasegawa, U.; van der Vlies, A. J. Polymeric micelles for hydrogen sulfide delivery. *MedChemComm,* **2015**, 6, 273–276.

(77) Foster, J. C.; Radzinski, S. C.; Zou, X.; Finkielstein, C. V.; Matson, J. B. $H_2S$-Releasing Polymer Micelles for Studying Selective Cell Toxicity. *Mol. Pharm.,* **2017**, 14, 1300–1306.

(78) Foster, J. C.; Carrazzone, R. J.; Spear, N. J.; Radzinski, S. C.; Arrington, K. J.; Matson, J. B. Tuning $H_2S$ Release by Controlling Mobility in a Micelle Core. *Macromolecules,* **2019**, 52, 1104–1111.

(79) Ercole, F.; Mansfeld, F. M.; Kavallaris, M.; Whittaker, M. R.; Quinn, J. F.; Halls, M. L.; Davis, T. P. Macromolecular Hydrogen Sulfide Donors Trigger Spatiotemporally Confined Changes in Cell Signaling. *Biomacromolecules,* **2016**, 17, 371–383.

(80) Yu, S. H.; Ercole, F.; Veldhuis, N. A.; Whittaker, M. R.; Davis, T. P.; Quinn, J. F. Polymers with acyl-protected perthiol chain termini as convenient building blocks for doubly responsive $H_2S$-donating nanoparticles. *Polym. Chem.,* **2017**, 8, 6362–6367.

(81) Ercole, F.; Whittaker, M. R.; Halls, M. L.; Boyd, B. J.; Davis, T. P.; Quinn, J. F. Garlic-inspired trisulfide linkers for thiol-stimulated $H_2S$ release. *Chem. Commun.,* **2017**, 53, 8030–8033.

(82) Arbach, M.; Santana, T. M.; Moxham, H.; Tinson, R.; Anwar, A.; Groom, M.; Hamilton, C. J. Antimicrobial garlic-derived diallyl polysulfanes: Interactions with biological thiols in Bacillus subtilis. *Biochim. Biophys. Acta-Gen Subj.,* **2019**, 1863, 1050–1058.

(83) Benavides, G. A.; Squadrito, G. L.; Mills, R. W.; Patel, H. D.; Isbell, T. S.; Patel, R. P.; Darley-Usmar, V. M.; Doeller, J. E.; Kraus, D. W. Hydrogen sulfide mediates the vasoactivity of garlic. *Proc. Natl. Acad. Sci. U. S. A.,* **2007**, 104, 17977–17982.

(84) Vo, C. D.; Kilcher, G. Tirelli, N. Polymers and Sulfur: what are Organic Polysulfides Good For? Preparative Strategies and Biological Applications. *Macromol. Rapid Commun.,* **2009**, 30, 299–315.

(85) Long, T. R.; Wongrakpanich, A.; Do, A.-V., Salem, A. K.; Bowden, N. B. Long-term release of a thiobenzamide from a backbone functionalized poly(lactic acid). *Polym. Chem.,* **2015**, 6, 7188–7195.

(86) Lin, L.; Qin, H.; Huang, J.; Liang, H.; Quan, D.; Lu, J. Design and synthesis of an AIE-active polymeric $H_2S$-donor with capacity for self-tracking. *Polym. Chem.,* **2018**, 9: 2942–2950.

(87) Carter, J. M.; Qian, Y.; Foster, J. C.; Matson, J. B. Peptide-based hydrogen sulphide-releasing gels. *Chem. Commun.,* **2015**, 51, 13131–13134.

(88) Kaur, K.; Qian, Y.; Gandour, R. D.; Matson, J. B. Hydrolytic Decomposition of S-Aroylthiooximes: Effect of pH and *N*-Arylidene Substitution on Reaction Rate. *J. Org. Chem.,* **2018**, 83, 13363–13369.

(89) Qian, Y.; Kaur, K.; Foster, J. C.; Matson, J. B. Supramolecular Tuning of $H_2S$ Release from Aromatic Peptide Amphiphile Gels: Effect of Core Unit Substituents. *Biomacromolecules,* **2019**, 20, 1077–1086.

(90) Wang, Y.; Kaur, K.; Scannelli, S. J.; Bitton, R.; Matson, J. B. Self-Assembled Nanostructures Regulate $H_2S$ Release from Constitutionally Isomeric Peptides. *J. Am. Chem. Soc.,* **2018**, 140, 14945–14951.

(91) Liang, W.; Chen, J.; Li, L.; Li, M.; Wei, X.; Tan, B.; Shang, Y.; Fan, G.; Wang, W.; Liu, W. Conductive Hydrogen Sulfide-Releasing Hydrogel Encapsulating ADSCs for Myocardial Infarction Treatment. *ACS Appl. Mater. Interfaces.,* **2019**, 11: 14619–14629.

(92) Xiao, Z.; Bonnard, T.; Shakouri-Motlagh, A.; Wylie, R. A. L.; Collins, J.; White, J.; Heath, D. E.; Hagemeyer, C. E.; Connal, L. A. Triggered and Tunable Hydrogen Sulfide Release from Photogenerated Thiobenzaldehydes. *Chem. Eur. J.,* **2017**, 23, 11294–11300.

(93) Peterson, G. I.; Larsen, M. B.; Boydston, A. J. Controlled Depolymerization: Stimuli-Responsive Self-Immolative Polymers. *Macromolecules,* **2012**, 45, 7317–7328.

(94) Shabat, D. Self-immolative dendrimers as novel drug delivery platforms. *J. Polym. Sci. A,* **2006**, 44, 1569–1578.

(95) Powell, C. R.; Foster, J. C.; Swilley, S. N.; Kaur, K.; Scannelli, S. J.; Troya, D.; Matson, J. B. Self-amplified depolymerization of oligo(thiourethanes) for the release of COS/$H_2S$. *Polym. Chem.,* **2019**, 10, 2991–2995.

(96) Levinn, C. M.; Steiger, A. K.; Pluth, M. D. Esterase-Triggered Self-Immolative Thiocarbamates Provide Insights into COS Cytotoxicity. *ACS Chem. Biol.,* **2019**, 14, 170–175.

(97) Steiger, A. K.; Pardue, S.; Kevil, C. G. Pluth, M. D. Self-Immolative Thiocarbamates Provide Access to Triggered $H_2S$ Donors and Analyte Replacement Fluorescent Probes. *J. Am. Chem. Soc.,* **2016**, 138, 7256–7259.

(98) Zheng, Z.; Chen, A.; He, H.; Chen, Y.; Chen, J.; Albashari, A. A.; Li, J.; Yin, J.; He, Z.; Wang, Q.; Wu, J.; Wang, Q.; Kang, J.; Xian, M.; Wang, X.; Xiao, J. pH and enzyme dual-responsive release of hydrogen sulfide for disc degeneration therapy. *J. Mater. Chem. B,* **2019**, 7, 611–618.

(99) Feng, S.; Zhao, Y.; Xian, M.; Wang, Q. Biological thiols-triggered hydrogen sulfide releasing microfibers for tissue engineering applications. *Acta. Biomater.,* **2015**, 27, 205–213.

(100) Wu, J.; Li, Y.; He, C.; Kang, J.; Ye, J.; Xiao, Z.; Zhu, J.; Chen, A.; Feng, S.; Li, X.; Xiao, J.; Xian, M.; Wang, Q. Novel $H_2S$ Releasing Nanofibrous Coating for *in Vivo* Dermal Wound Regeneration. *ACS Appl. Mater. Interfaces,* **2016**, 8, 27474–27481.

(101) Cacciotti, I.; Ciocci, M.; Di Giovanni, E.; Nanni, F.; Melino, S. Hydrogen Sulfide-Releasing Fibrous Membranes: Potential Patches for Stimulating Human Stem Cells Proliferation and Viability under Oxidative Stress. *Int. J. Mol. Sci.,* **2018,** 1–19.

(102) Matteo Ciocci, E. I.; Felicia, C.; Haneen, A.; Khashoggi, F. N.; Sonia, M. $H_2S$-releasing nanoemulsions: a new formulation to inhibit tumor cells proliferation and improve tissue repair. *Oncotarget*, **2016**, 84338–84358.

(103) Cai, Y-R.; Hu, C-H. Computational Study of $H_2S$ Release in Reactions of Diallyl Polysulfides with Thiols. *J. Phys. Chem. B,* **2017**, 121, 6359–6366.

(104) Bhattacharya, A.; Banu, J.; Rahman, M.; Causey, J.; Fernandes, G. Biological effects of conjugated linoleic acids in health and disease. *J. Nutr. Biochem.,* **2006**, 17, 789–810.

(105) Zhao, G. X.; Etherton, T. D.; Martin, K. R.; West, S. G.; Gillies, P. J.; Kris-Etherton, P. M. Dietary alpha-linolenic acid reduces inflammatory and lipid cardiovascular risk factors in hypercholesterolemic men and women. *J. Nutr.,* **2004**, 134, 2991–2997.

(106) Gazzano, E.; Buondonno, I.; Marengo, A.; Rolando, B.; Chegaev, K.; Kopecka, J.; Saponara, S.; Sorge, M.; Hattinger, C. M.; Gasco, A.; Fruttero, R.; Brancaccio, M.; Serra, M.; Stella, B.; Fattal, E.; Arpicco, S.; Riganti, C. Hyaluronated liposomes containing $H_2S$-releasing doxorubicin are effective against P-glycoprotein-positive/doxorubicin-resistant osteosarcoma cells and xenografts. *Cancer Lett.,* **2019**, 456, 29–39.

(107) Bigagli, E.; Luceri, C.; De Angioletti, M.; Chegaev, K.; D'Ambrosio, M.; Riganti, C.; Gazzano, E.; Saponara, S.; Longini, M.; Luceri, F.; Cinci, L. New NO- and $H_2S$-releasing doxorubicins as targeted therapy against chemoresistance in castration-resistant prostate cancer: in vitro and in vivo evaluations. *Invest. New Drug,* **2018**, 36, 985–998.

(108) Buondonno, I.; Gazzano, E.; Tavanti, E.; Chegaev, K.; Kopecka, J.; Fanelli, M.; Rolando, B.; Fruttero, R.; Gasco, A.; Hattinger, C.; Serra, M.; Riganti, C. Endoplasmic reticulum-targeting doxorubicin: a new tool effective against doxorubicin-resistant osteosarcoma. *Cell. Mol. Life Sci.,* **2019**, 76, 609–625,.

(109) Chegaev, K.; Rolando, B.; Cortese, D.; Gazzano, E.; Buondonno, I.; Lazzarato, L.; Fanelli, M.; Hattinger, C. M.; Serra, M.; Riganti, C.; Fruttero, R.; Ghigo, D.; Gasco, A. $H_2S$-Donating Doxorubicins May Overcome Cardiotoxicity and Multidrug Resistance. *J. Med. Chem.,* **2016**, 59, 4881–4889.

## Chapter 2: Hydrolytic decomposition of *S*-aroylthiooximes: Effect of pH and *N*-arylidene substitution on reaction rate

Reprinted with permissions from *Hydrolytic decomposition of* S-*aroylthiooximes: Effect of pH and* N-*arylidene substitution on reaction rate*, Journal of Organic Chemistry, **2018**, 83, 21, 13363–13369. Copyright: 2018, American Chemical Society. The final publication is available online at: https://pubs.acs.org/doi/abs/10.1021/acs.joc.8b02151

### 2.1 Authors

Kuljeet Kaur, Yun Qian, Richard D. Gandour, and John B. Matson

Department of Chemistry, Virginia Tech, Virginia Tech Center for Drug Discovery, Macromolecules Innovation Institute, Virginia Tech, Blacksburg, VA, 24061

### 2.2 Abstract

The hydrolytic decomposition of four peptides containing *S*-aroylthiooximes (SATOs) with variable *N*-arylidene substituents was investigated in 10 aqueous buffer solutions at pH values ranging from 6.0 to 10.9. UV-Vis spectroscopy was employed to study the reaction kinetics, which revealed V-shaped pH-rate profiles for all peptides with a minimum near pH 8, suggesting a change from an acid-catalyzed to a base-activated reaction. Hammett plots showed positive ρ values above pH 8 and negative ρ values below pH 8, providing further evidence for a mechanism change. Based on these data, along with mass spectrometry evidence, we propose a specific acid catalysis under mildly acidic and neutral conditions and multiple base-promoted decomposition reactions under mildly basic conditions.

## 2.3 Introduction

Functional groups containing carbon–nitrogen double bonds, (e.g., imines, hydrazones, and oximes) are easy to prepare and are relatively stable in aqueous media near neutral pH.[1] Under acidic conditions, however, these functional groups hydrolyze rapidly.[2] As a result of this pH-dependent stability, functional groups containing C=N bonds find use in several applications, including drug delivery,[3] and tissue engineering.[4] For example, hydrazones are linkers in cancer therapeutics, where active drugs can be released in the acidic tumor microenvironment,[5-7] and oximes are used widely in bio-conjugation and in constructing hydrogels as matrices for cell encapsulation.[8-10]

Despite extensive knowledge of the pH-dependent hydrolyses of functional groups with structures $R^1R^2C{=}N{-}X$ where X = $R^3$, $NHR^3$, or $OR^3$ (imines, hydrazones, and oximes, respectively), little is known about the sulfur-containing analogues (X = $SR^3$) of oximes.[11] Our recent investigations of *S*-aroylthiooximes (SATOs), which are sulfur analogues of oximes, have the general structure $R^1R^2C{=}NSC(O)Ar$.[12] SATOs decompose upon reaction with a thiol to release hydrogen sulfide ($H_2S$), a biological signaling gas with many physiological roles and extensive therapeutic potential.[13-16] Since our initial report on SATOs in 2014, others have studied synthetic routes to compounds with C=N–S linkages,[17,18] and we have employed SATOs as $H_2S$ donors in polymers,[19] polymer micelles,[20] and peptide-based gels.[21]

SATOs are prepared through a condensation reaction between an *S*-aroylthiohydroxylamine and an aldehyde or ketone. In our original report on SATOs, we noted that in addition to thiol-triggered decomposition to produce $H_2S$, SATOs can also undergo hydrolysis in a reaction that is the reverse of the condensation reaction through which they form. They are fairly stable near

physiological pH, with hydrolysis half-lives ranging from days to weeks for most compounds. Despite the stability of SATOs at near-neutral pH, significant hydrolysis of SATO-containing peptides occurs when purified under basic conditions. In an effort to increase the stability of these $H_2S$-releasing peptides, we quantify the kinetics and probe the mechanism(s) of hydrolytic decomposition at pH 6–10.9 of four water-soluble, SATO-containing peptides.

## 2.4 Results

### Design and synthesis of SATO-peptides

To probe how pH affects SATO decomposition, we designed four SATO-peptides for this study. We attached a short peptide chain with the sequence IAVEEE, as we have used previously,[21] to promote water solubility. Each SATO-peptide consists of a central aromatic linker, an arylidene, that is attached on one side to IAVEEE and on the other side to SATO (Fig. 2.1A). Only the linker varies among the four compounds; we selected linkers to include both electron-donating (–$OCH_2C(O)$–), and electron-withdrawing groups (–C(O)–, –$SO_2$–), plus a group with extended conjugation (–CH=CHC(O)–) (Fig. 2.1B).

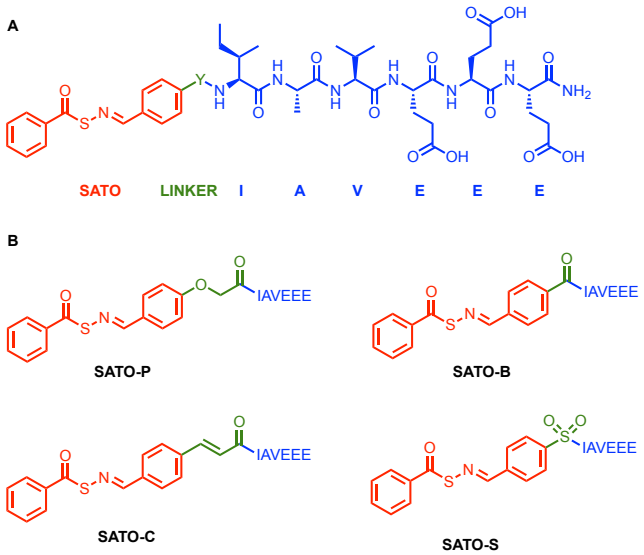

**Fig. 2.1. (A)** Complete general structure of SATO-peptides with the SATO group in red, the linker (Y) in green, and the peptide chain (IAVEEE) in blue **(B)** Structures of SATO-containing peptides with the various linkers, Y, shown in green.

Peptides were constructed by using Fmoc-based solid phase peptide synthesis, installing the linker in the final coupling step. After cleavage from the resin and isolation of each functionalized peptide, *S*-benzoylthiohydroxylamine was added to each peptide aldehyde in a condensation reaction before purification by preparative HPLC. Peptides are named with a two-unit code, where the first unit indicates the thiooxime part of the peptide (SATO in all cases) and the second unit consists of a letter that indicates the type of the linker (P, C, B, or S, as indicated in Fig. 2.1). For example, peptide SATO-C refers to a thiooxime containing peptide with a cinnamoyl linker.

## Kinetic hydrolytic decomposition of SATO-containing peptides

Hydrolytic decomposition rate measurements of SATO-peptide solutions were carried out at rt in buffered water at 10 different pH values ranging from 6.0–10.9 (Scheme 2.1). Reactions were followed via UV–Vis absorption spectroscopy by monitoring the decrease in the absorption maximum near 330 nm. Figure 2.2 includes representative time-dependent spectra for peptide SATO-C at pH 7.7; data for the other peptides can be found in Appendices (Figure 1S3-1S12). We observed an isosbestic point near 300 nm for each hydrolysis at each pH value (Fig. 2.2A).

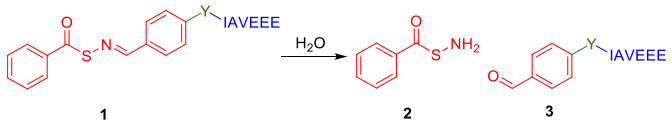


**Scheme 2.1**. General scheme representing hydrolysis of SATO-peptides **(1)** to *S*-benzoylthiohydroylamine **(2)** and the corresponding peptide aldehyde unit **(3)**.

First-order kinetics plots based on these spectral data revealed straight lines, and the pseudo-first-order rate constants were calculated from the slope of these lines (Fig. 2.2 B). Using this method for each peptide at each pH, we obtained 40 pseudo-first-order rate constants (Table 2.1).

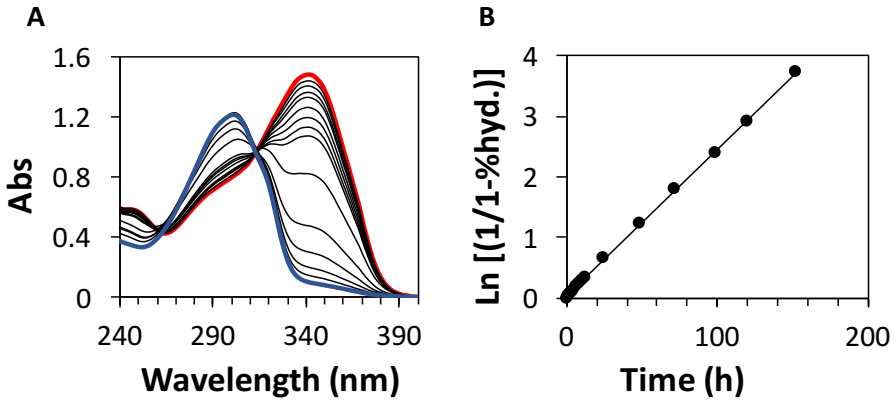


**Fig. 2.2.** (A) Example UV–Vis absorbance curves for peptide SATO-C at 50 μM in aqueous phosphate buffer solution (10 mM) at pH 7.7. The red and blue traces correspond to the first and final timepoints, respectively, with intermediate timepoints in black. (B) First-order kinetics plot of peptide C3 exhibiting a straight-line fit corresponding to pseudo-first-order kinetics.

| | $k_{obs}*10^3$ ($min^{-1}$) | | | | ρ |
|---|---|---|---|---|---|
| **pH** | **SATO-P** | **SATO-C** | **SATO-B** | **SATO-S** | **value** |
| **6.0** | 27 ± 2 | 18 ± 1 | 17 ± 1 | 13 ± 1 | –0.3 |
| **6.7** | 6.4 ± 0.1 | 4.4 ± 0.1 | 4.3 ± 0.3 | 3.2 ± 0.3 | –0.4 |
| **7.0** | 3.4 ± 0.3 | 2.1 ± 0.1 | 1.8 ± 0.1 | 1.4 ± 0.1 | –0.5 |
| **7.4** | 1.3 ± 0.1 | 0.87 ± 0.04 | 0.87 ± 0.02 | 0.69 ± 0.02 | –0.3 |
| **7.7** | 0.67 ± 0.03 | 0.52 ± 0.02 | 0.46 ± 0.03 | 0.39 ± 0.03 | –0.3 |
| **8.0** | 0.50 ± 0.04 | 0.33 ± 0.03 | 0.33 ± 0.02 | 0.28 ± 0.01 | –0.3 |
| **8.5** | 0.35 ± 0.02 | 0.53 ± 0.08 | 0.63 ± 0.05 | 0.62 ± 0.05 | 0.3 |
| **9.3** | 0.57 ± 0.04 | 0.81 ± 0.04 | 1.1 ± 0.1 | 2.1 ± 0.1 | 0.8 |
| **10.2** | 3.1 ± 0.2 | 6.9 ± 0.8 | 10 ± 1 | 8.9 ± 0.2 | 0.6 |
| **10.9** | 13 ± 0.6 | 34 ± 3 | 49 ± 1 | 37 ± 3 | 0.5 |

[a]Rate constants and standard deviations of measurement were calculated from the average of three replicates. Buffers (all 10 mM) were as follows: pH 6.0–8.0: phosphate buffer; pH 8.5: Bicine buffer; pH 9.3-10.9: carbonate buffer.

**Table 2.1.** Hydrolytic decomposition rate constants of SATO-peptides

Four pH–rate profiles (Fig. 2.3) were constructed to identify the hydrolytic decomposition mechanisms of the SATO-peptides. For each SATO-peptide, a pH–rate profile was generated by graphing Log pseudo-first-order rate constants vs. pH, yielding V-shaped profiles for each peptide with minima in the region of pH 8.0–8.5 (Fig. 2.3). Comparing the nearly identical pH–rate profiles among the 4 SATO-peptides revealed only one notable difference. The minimum Log $k_{obs}$ was at pH 8.5 for SATO-P but was at pH 8.0 for SATO-B, SATO-C, and SATO-S. For all peptides, linear regression of Log $k_{obs}$ in the range of pH 6.0–8.0 gave a slope of approximately –0.9, indicating a linear dependence of rate on $[H_3O^+]$, which is consistent with an acid-catalyzed reaction. A similar analysis in the range of pH 8.5–10.9 gave a slope in all plots of approximately 0.8, indicative of a linear dependence of the rate on $[^-OH]$, which is consistent with a base-activated reaction.

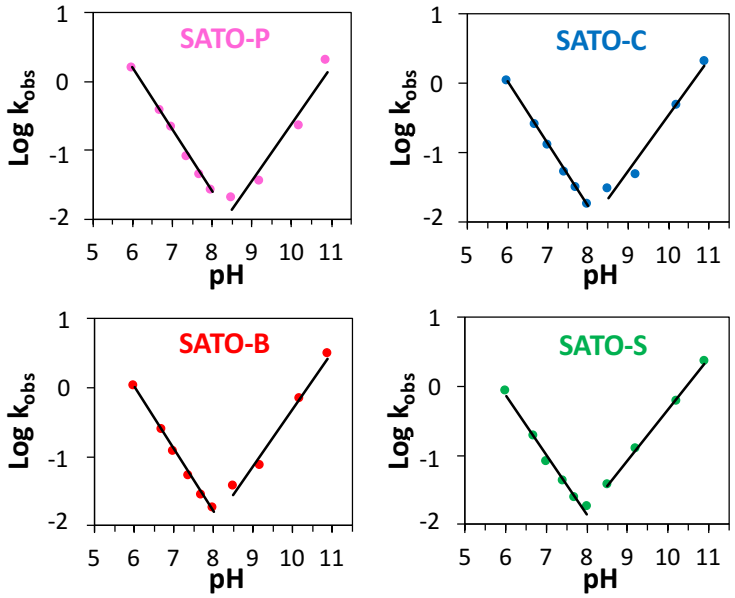


**Fig. 2.3.** Plots showing pH-rate profiles for all four SATO-containing peptides. Lines are linear regressions of Log $k_{obs}$ at pH 6.0-8.0 and 8.5-10.9 in each profile.

## Hammett plots at different pH values

To evaluate how different substituents affect rates of hydrolytic decomposition of SATO-containing peptides, we plotted Log $k_{obs}$ versus Hammett sigma (σ) of the linker at given pH values (Fig. 2.4). We estimated Hammett σ values for the linkers by first plotting predicted p$K_a$ values[22] for eight *para*-substituted benzoic acid derivatives against their known Hammett σ values.[22,23] The plot revealed a strong linear correlation for these eight known compounds (Fig. 1S14). We then estimated Hammett σ values for the linkers by applying predicted p$K_a$ values for para HOOC-$C_6H_4$-Y-NHMe to the fitted line for p$K_a$'s of eight known acids versus their Hammett σ values (see appendices).

At pH 6.0–8.0, good correlations were observed in the Hammett plots, with ρ values around –0.3 (Table 2.1). At pH 8.5, Hammett ρ was 0.3; for pH 9.3, 10.0, and 10.9 Hammett ρ was 0.8, 0.6, and 0.5, respectively. This change in the sign of ρ observed for crossover from acidic to basic conditions supported the proposed change in mechanism. Electron-withdrawing and electron-donating substituents affected the acidic and basic reactions in opposite ways.

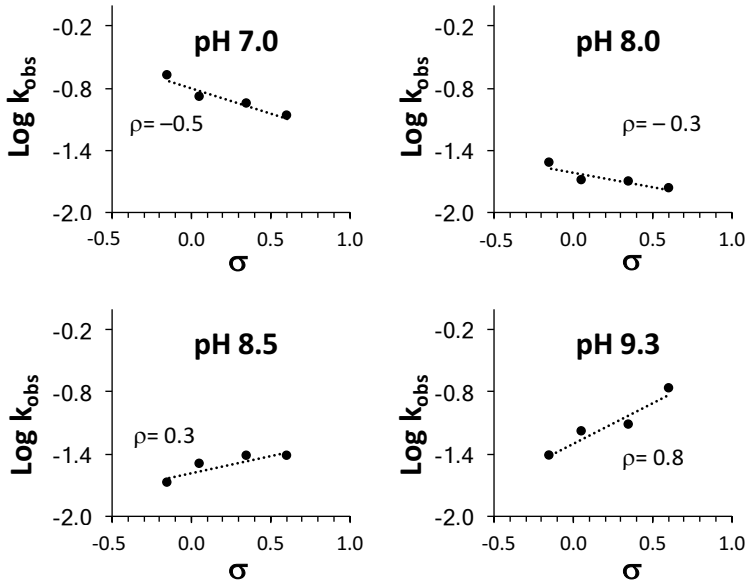

**Fig. 2.4.** Hammett plots at pH 7.0, 8.0, 8.5, and 9.3, illustrating the change in sign of values of ρ as the pH moves from acidic to basic.

### Identification of products at different pH values

Mass spectrometric analysis of the SATO-peptide fragments formed at various pH values after 5 min provided information on the products of hydrolytic decomposition (see Discussion). A mass spectrum for SATO-B at pH 6.0 (Fig. 2.5A) showed evidence for the formation of peptide aldehyde at m/z = 819.4 (the product of C=N bond hydrolysis) and peptide nitrile at m/z = 816.4 (a decomposition product). At pH 10.9, the same products were observed, along with peptide imine thiol (the product of thioester hydrolysis) at m/z = 850.7 (Fig. 2.5B).

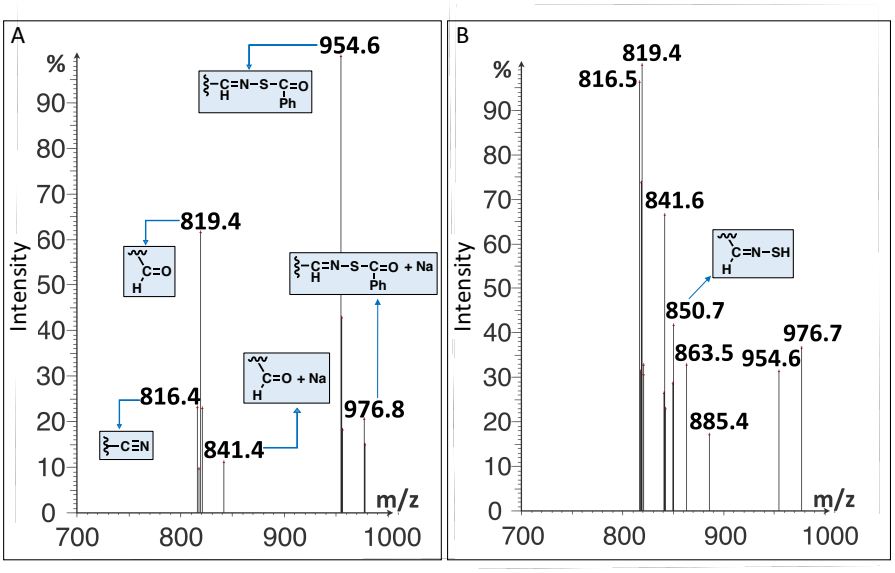


**Fig. 2.5.** Mass spectra for peptide SATO-B after 5 min depicting reaction progress and products at pH a) 6.0 and B) 10.9

## 2.5 Discussion

### Possible mechanisms as a function of pH

A V-shape in pH–rate profiles indicates a change in mechanism when transitioning from acidic to basic conditions. The minima in the pH–rate profiles indicate either a minimum in the sum of

the rates for the acid-catalyzed and base-activated reactions, or an uncatalyzed reaction, as has been observed for some imines.[2,24-26]

In general, three mechanisms are possible for the hydrolysis reactions involving C=N bonds (Scheme 2.2)[24,25] These include (**I**) equilibrium protonation of –C=N– followed by the addition of water to –C=$NH^+$– to form a protonated carbinolamine adduct (specific acid-catalyzed); (**II**) addition of water to neutral –C=N– (with concomitant proton transfer from water and proton transfer to the imine N atom) or addition of $^-$OH to cationic –C=$NH^+$– to form a neutral carbinolamine; and (**III**) addition of $^-$OH to neutral –C=N– to form an anionic carbinolamine adduct (base-activated), which likely picks up a proton immediately to form neutral carbinolamine (vertical arrow) or forms the neutral carbinolamine in a mechanism of synchronous $^-$OH addition and proton transfer (diagonal arrow). All forms of carbinolamine adducts decompose in subsequent steps to give the hydrolyzed products, an aldehyde and *S*-benzoylthiohydroxylamine in this case. The formation or decomposition of the carbinolamine adduct can both act as rate-determining steps depending on the reaction conditions and substrate structure.[27] The shape of the pH-rate profiles suggests a crossover from acid-catalyzed to base-mediated hydrolytic decomposition.

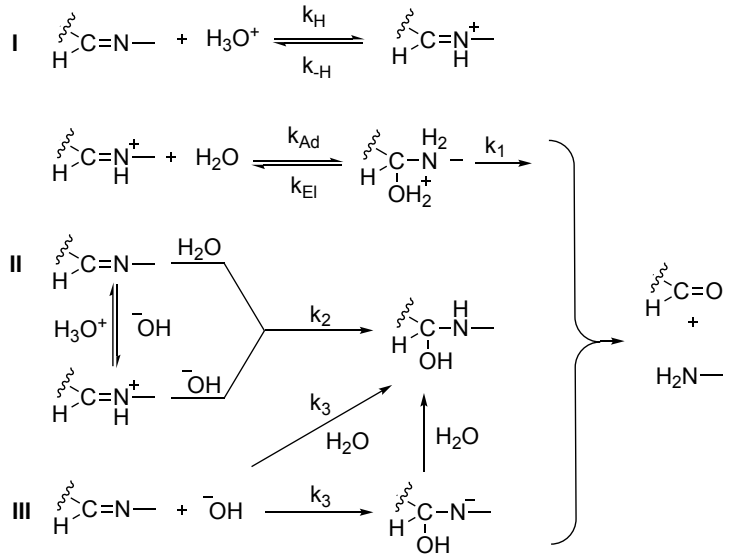

**Scheme 2.2.** General representation of rate-determining steps possible during the hydrolysis of C=N. The constants $k_1$–$k_3$ represent the respective rate constants of the reactions.

Based on the reactions of *O*-acylaldoximes,[28] three additional decomposition mechanisms might operate in *S*-acylaldoximes. These include (**IV**) water addition to the carbonyl of the thioester (with concomitant proton transfer from water and proton transfer to the carbonyl O atom) followed by elimination of thiohydroxylamine (R-C=N-SH); (**V**) addition of $^{-}$OH to C=O to form an anionic tetrahedral adduct (base-activated) followed by elimination of thiooximate (R–C=N–S$^{-}$); and (**VI**) proton transfer from C—H with synchronous elimination of thiocarboxylate to form a nitrile. For *O*-acylaldoximes, mechanism **IV** predominates at pH < 7; mechanisms **V** and **VI** operate at a ratio of 3:1 at pH >7.

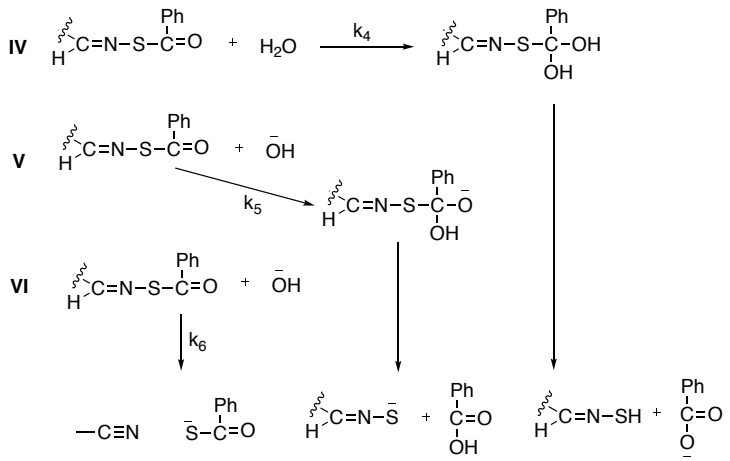

**Scheme 2.3.** General representation of rate-determining steps possible during the reactions not involving hydrolysis of C=N. The constants $k_4$–$k_6$ represent the respective rate constants of the reactions.

## Hydrolysis in mildly acidic to neutral media (pH 6.0–7.7)

The rate of hydrolysis in this region increases linearly with increasing solution acidity, as evidenced by the slope near –1 in the pH–rate profiles (Fig. 2.3). Under mildly acidic to neutral conditions, the reaction likely proceeds via a fast equilibrium protonation of the –C=N– group followed by addition of water to –C=$NH^+$– to give a protonated carbinolamine adduct, which then decomposes to give the final products (Scheme 1.2, Mechanism **I**). Breakdown of the carbinolamine intermediate is likely rate-determining.[27,29] The proposed rate law is therefore given by the following equation:

$$\boxed{Rate = k_{obs}[-C=N-][H_3O^+] \quad where\ k_{obs} = k_1\left(\frac{k_H}{k_{-H}}\right)\left(\frac{k_{Ad}}{k_{El}}\right)}$$

Further verification of this mechanism comes from the negative values of ρ obtained from the Hammett plots in this pH range. Negative values of ρ indicate that the transition state is electron deficient compared to the reactant; therefore, addition of water or breakdown of the tetrahedral intermediate must be rate-determining. Electron-withdrawing groups therefore increase the electrophilicity of the carbon atom in –C=N–, decreasing the stability of the cationic intermediate

and decelerating the reaction. A more negative value of ρ (closer to –1) would be expected if protonation of the imine were rate determining. This mechanism is consistent with results obtained on the hydrolyses of oximes and hydrazones, where Kalia and Raines concluded that protonated carbinolamine adduct formation is rate-determining under mildly acid and neutral conditions. The appearance of nitrile in the mass spectrum (Fig. 2.5A) suggests an elimination mechanism may be operating as well (Scheme 2.3, Mechanism **VI**). The mechanistic details of such an elimination reaction at this pH remain to be explored.

**Reactions in basic media (pH 9.3–10.9)**

In the range of pH 9.3–10.9, hydrolytic decomposition rates increase with increasing basicity with a slope near 1, which corresponds to the increase in concentration of $^{-}$OH. Therefore, three mechanisms are possible. (Scheme 2.2, Mechanism **III** and Scheme 2.3, Mechanisms **V** and **VI**). The corresponding rate law is 1$^{st}$ order in both $^{-}$OH and C=N (2$^{nd}$ order overall), as indicated by the rate equation below:

$$\boxed{Rate = k_{obs}[C=N][\ ^{-}OH\ ] \quad where\ k_{obs} = k_3 + k_5 + k_6}$$

Values of ρ in this pH region are positive, which is opposite in sign to those in the acidic pH region, indicating build-up of negative charge in the transition state. These data are consistent with addition of $^{-}$OH to the neutral C=N (Mechanism **III**), addition of $^{-}$OH to the neutral thioester (Mechanism **V**), or proton abstraction from the imine carbon by $^{-}$OH (Mechanism **VI**) as the rate determining step. The expected values of ρ would likely be similar for each mechanism.

The pH–rate profiles for the hydrolyses of oximes,[30] hydrazones,[30] and *O*-acylaldoximes[28] provide precedence for predicting mechanisms. For oximes and hydrazones, pH–rate profiles

have negative slopes at pH 5–9. This observation likely rules out Mechanism **III**, where a positive pH-rate profile under basic conditions would be observed. For *O*-acylaldoximes, pH–rate profiles have a zero slope at pH 4.8–6.6 and positive slopes starting at pH 7.2–9.5. These measurements support Mechanisms **V** and **VI**. Further evidence for Mechanisms **V** and **VI** comes from mass spectral product analysis (Figure 2.5B). The data reveal the formation of three major species: 1) A peptide nitrile (m/z = 816.5), which supports mechanism **VI**; 2) A peptide thiooxime (m/z = 850.7), which supports mechanism **V**; and 3) A peptide aldehyde (m/z = 819.4, along with additional Na-adduct peaks at m/z = 841.6, 863.5 and 885.4), which may come from hydrolysis of the thiooximate product in Mechanism **V**, as we and others have previously suggested.[12,31]

**Reactions in mildly basic media (pH 8.0–8.5)**

At pH 8 and 8.5, the reaction proceeds slowly and the rate constants for all four peptides are close. The lack of a plateau region in any of the four pH–rate profiles suggests that this changeover region reflects a sum of rates for acid-catalyzed (**I**) and base activated (**V** and **VI**) mechanisms. Thus, $k_{obs}$ would comprise $k_1(k_H/k_{-H})[H_3O^+] + (k_5 + k_6)[^-OH]$. However, we cannot exclude mechanisms **II** and **IV**. These two mechanisms both generate neutral intermediates, presumably with small values of ρ. The values of ρ flip from negative to positive in this pH range (–0.3 for pH 8.0; 0.3 for pH 8.5). Unfortunately, one cannot distinguish among the mechanisms as an observed ρ is a weighted average of all contributing mechanisms. Because multiple processes likely occur in this pH range, the rate law cannot be explicitly determined.

**Hammett ρ values**

At pH 6.0–8.0, values of ρ hover near –0.3; at pH >8.5, they increase to approximately 0.6. The crossover point from negative to positive ρ values occurs between pH 8.0 and pH 8.5 (Table 2.1). The change in sign of ρ agrees with the change from the proposed acid-catalyzed to base-activated mechanisms.

At pH 6.0–8.0, equilibrium protonation of –C=N– precedes rate-determining addition of water to the cationic intermediate. The equilibrium protonation of –C=N– is favored by electron-donating substituents, whereas the attack of water is favored by the electron-withdrawing substituents. As a result of these competing forces, the positive charge build-up in the transition state is small, leading to a small negative value of ρ. The appearance of the nitrile in the mass spectrum at pH 6 (Fig. 2.5A) suggests a contribution from a mechanism that may have a small positive or near zero value of ρ. This contribution means that the observed value would be less negative than if acid-catalyzed hydrolysis of C=N were the only mechanism.

Interestingly, the absolute values of ρ at higher pH are larger than those at lower pH. Above pH 8.5, values of ρ increase in magnitude. Presuming mechanisms **V** and **VI** operate at high pH, one would expect the value of ρ would be higher for mechanism **VI**. Precedence for a large positive value of ρ derives from formation of nitriles in *O*-pivaloyloximes in acetonitrile.[32] Our previous study[12] on hydrolysis of arylidenethiooximes at pH 7.4 in water/acetonitrile suggests a very small positive value of ρ for mechanism **V**. The values in Table 2.1 and the mass spectrum at pH 10.9 (Fig. 2.5B) suggest that both mechanisms operate.

## 2.6 Conclusion

In summary, we have studied in detail the hydrolytic decomposition kinetics of a series of SATO-peptides in aqueous buffer to increase our knowledge of the sulfur-containing analogues

of imines and oximes. Based on pH-rate profile data, Hammett plots at different pH values, and mass spectral data, we conclude that several mechanisms for hydrolytic decomposition of SATO-peptides operate under acidic and basic conditions. Consistent with C=N functional groups, SATOs undergo acid-catalyzed hydrolysis under mildly acidic to neutral conditions (pH 6.0–7.4), and base-activated decomposition reactions under basic conditions (pH 9.3–10.9). Rates are slowest under mildly basic conditions (pH 7.7–8.5), where crossover occurs. This study provides further insight into the chemistry of sulfur-containing analogues of imines and oximes at physiologically relevant pH. Such insight may be useful in designing new $H_2S$ donors and exploiting the reactivity of these compounds for therapeutic purposes.

## 2.7 Experimental

*Materials*

Fmoc-protected amino acids and Rink amide MBHA resin were purchased from P3biosystems and used as received. Other reagents for peptide synthesis were purchased from commercial vendors and used as received unless otherwise noted. All the solvents employed for peptide synthesis were reagent grade.

*Methods*

Synthesis of the SATO-peptides was accomplished in two steps: 1) The peptides were made by using solid-phase peptide synthesis (SPPS), with installation of the linker on resin; 2) After cleavage of the peptide from the resin and purification by preparative HPLC, *S*-benzoylthiohydroxylamine was added to form the SATO group in a condensation reaction. Final SATO peptides were then purified again by preparative HPLC. Detailed synthetic conditions are provided below.

For all four SATO-peptides, IAVEEE was synthesized either manually or by using a Liberty1 microwave-assisted peptide synthesizer (CEM) following standard procedures[21] for Fmoc-based SPPS. For peptides SATO-P, SATO-C and SATO-B, the linkers (2-(4-formylphenoxy)acetic acid, 4-formyl cinnamic acid, and 4-formylbenzoic acid, respectively) were coupled respectively to the peptide N-terminus on-resin under identical coupling conditions as those for the amino acids. Peptide SATO-S was synthesized by following a different procedure. First, 4-formylsulfonylchloride was coupled to L-isoleucine in water under microwave heating by using a modified literature procedure (further details and characterization appear in the Supporting Information).[33] This unit was added under standard SPPS conditions to the AVEEE peptide on-resin. After cleavage and isolation, peptides were dissolved in water containing 0.1% $NH_4OH$ and filtered through a 0.45 μm PTFE filter before purifying. Purification by preparative-scale reverse phase-high performance liquid chromatography (RP-HPLC) was carried out on an Agilent Technologies 1260 Infinity HPLC system, eluting with a gradient of 2% ACN to 90% ACN in milliQ $H_2O$ over 33 min on an Agilent PLRP-S column (100-Å particle size, 25 x 150 mm) and monitoring at 220 nm. To both mobile phases, 0.1% $NH_4OH$ was added to aid in solubility. Fractions were analyzed by mass spectrometry (Advion ExpressIon Compact Mass Spectrometer (CMS)), and product-containing fractions were combined, rotovapped to remove ACN, and lyophilized (LabConco).

The lyophilized linker-containing peptides were dissolved in dry DMSO; *S*-benzoylthiohydroxylamine along with catalytic TFA were added to afford the final SATO-peptides—SATO-P, SATO-C, SATO-B, and SATO-S (Figure 1B). Peptides were dissolved in 10 mM phosphate buffer at pH 7.4 and filtered through a 0.45 μm PTFE filter before injecting onto the HPLC. Purification was carried out by RP-HPLC, eluting with a gradient of 2% ACN to

90% ACN in milliQ $H_2O$ without any additives. The protocol for analyzing and recovering the peptides was the same as described above. The final SATO-peptides were dissolved in milliQ water and distributed into aliquots (100 mg each). Aliquots were frozen, lyophilized, and stored at –20 $^oC$.

*pH measurements*

Buffer solutions (10 mM) were freshly prepared in milliQ $H_2O$ from their respective salts in calibrated volumetric glassware. Phosphate, carbonate, and bicine buffers were used to achieve the required pH range of 6.0–8.0, 9.3–10.9, and 8.5, respectively. The pH of the buffer solutions was checked with a calibrated digital pH-meter equipped with an external glass electrode (Accument Basic [AB15 Plus], Fisher Scientific). Required adjustments were made by adding $H_3PO_4$ and NaOH for phosphate buffers or only NaOH for bicine buffer. The pH for the carbonate buffers was not adjusted.

*Spectral measurements*

Peptides (100 μg lyophilized aliquots) were dissolved in buffer (2 mL) to achieve a final concentration of about 50 μM. Once homogeneous, solutions were transferred into a 10-mm quartz cuvette (Starna Cells) for analysis. UV–Vis absorption spectra were recorded at pre-determined timepoints from 400 to 200 nm on a Varian Cary 100 UV–Vis spectrophotometer with a scanning speed of 600 nm $\cdot$ $min^{-1}$ with light source changeover set to 400 nm. Spectral data were analyzed and plotted as described in the Supporting Information.

*Mass spectrometry*

For mass spectrometry analysis, peptides were dissolved at 200 μM in the indicated buffer (10 mM) and vortexed. After 5 min, an aliquot was removed and directly injected into the mass

spectrometer (Advion CMS with a resolution of 0.5–0.7 m/z units) in negative electrospray ionization mode.

## 2.8 References


(1) Jencks, W. P. Mechanism and Catalysis of Simple Carbonyl Group Reaction. *Prog. Phys. Org. Chem.,* **1964**, 2, 63–128.

(2) Cordes, E. H.; Jencks, W. P. On the Mechanism of Schiff Base Formation and Hydrolysis. *J. Am. Chem. Soc.,* **1961**, 84, 832–837.

(3) Matson, J. B.; Stupp, S. I. Drug Release from Hydrazone-Containing Peptide Amphiphiles. *Chem. Commun.,* **2011**, 47, 7962–7964.

(4) Grover, G. N.; Lam, J.; Nguyen, T. H.; Segura, T.; Maynard, H. D. Biocompatible Hydrogels by Oxime Click Chemistry. *Biomacromolecules,* **2012**, 13, 3013–3017.

(5) Baul, T. S.; Basu, S.; de Vos, D.; Linden, A. Amino Acetate Functionalized Schiff Base Organotin(IV) Complexes as Anticancer Drugs: Synthesis, Structural Characterization, and *in vitro* Cytotoxicity Studies. *Invest. New Drugs,* **2009**, 27, 419–431.

(6) da Silva, C. M.; Silva, M. M.; Reis, F. S.; Ruiz, A.; de Carvalho, J. E.; Santos, J. C. C.; Figueiredo, I. M.; Alves, R. B.; Modolo, L. V.; de Fatima, A. Studies on Free Radical Scavenging, Cancer Cell Antiproliferation, and Calf Thymus DNA Interaction of Schiff Bases. *J. Photochem. Photobiol. B,* **2017**, 172, 129–138.

(7) Feng, X.; Li, D.; Han, J.; Zhuang, X.; Ding, J. Schiff Base Bond-Linked Polysaccharide-Doxorubicin Conjugate for Upregulated Cancer Therapy. *Mater. Sci. Eng. C Mater. Biol. Appl.,* **2017**, 76, 1121–1128.

(8) Rashidian, M.; Mahmoodi, M. M.; Shah, R.; Dozier, J. K.; Wagner, C. R.; Distefano, M. D. A Highly Efficient Catalyst for Oxime Ligation and Hydrazone-Oxime Exchange Suitable for Bioconjugation. *Bioconjug. Chem.,* **2013**, 24, 333–342.

(9) Lin, F.; Yu, J.; Tang, W.; Zheng, J.; Defante, A.; Guo, K.; Wesdemiotis, C.; Becker, M. L. Peptide-Functionalized Oxime Hydrogels with Tunable Mechanical Properties and Gelation Behavior. *Biomacromolecules,* **2013**, 14, 3749–3758.

(10) Mukherjee, S.; Hill, M. R.; Sumerlin, B. S. Self-healing Hydrogels Containing Reversible Oxime Crosslinks. *Soft Matter,* **2015**, 11, 6152–6161.

(11) Barton, D. H. R.; Magnus, P. D.; Pennanen, S. I. Evidence for the Existence of a Thio-oxime. *J.C.S. Chem. Commun.,* **1974**, 1007.

(12) Foster, J. C.; Powell, C. R.; Radzinski, S. C.; Matson, J. B. S-aroylthiooximes: A Facile Route to Hydrogen Sulfide Releasing Compounds with Structure-Dependent Release Kinetics. *Org. Lett.,* **2014**, 16, 1558–1561.

(13) Olson, K. R. The Therapeutic Potential of Hydrogen Sulfide: Separating Hype from Hope. *Am. J. Physiol. Regul. Integr. Comp. Physiol.,* **2011**, 301, R297–312.

(14) Szabo, C. Hydrogen Sulphide and its Therapeutic Potential. *Nat. Rev. Drug Discov.,* **2007**, 6, 917–935.

(15) Wallace, J. L.; Wang, R. Hydrogen Sulfide-Based Therapeutics: Exploiting a Unique but Ubiquitous Gasotransmitter. *Nat. Rev. Drug Discov.,* **2015**, 14, 329–345.

(16) Wang, R. Physiological Implications of Hydrogen Sulfide: A Whiff Exploration that Blossomed. *Physiol. Rev.,* **2012**, 92, 791–896.

(17) Lee, C.; Wang, X.; Jang, H. Y. Copper-Catalyzed Oxidative N-S Bond Formation for the Synthesis of N-sulfenylimines. *Org. Lett.,* **2015**, 17, 1130–1133.

(18) Long, W.; Qiu, W.; Li, C.; Song, L.; Bai, G.; Zhang, G.; He, H. Direct Synthesis of N-sulfenylimines through Oxidative Coupling of Amines with Disulfides/Thiols Over Copper Based Metal–Organic Frameworks. *RSC Adv.,* **2016**, 6, 40945–40952.

(19) Foster, J. C.; Matson, J. B. Functionalization of Methacrylate Polymers with Thiooximes: A Robust Postpolymerization Modification Reaction and a Method for the Preparation of H2S-Releasing Polymers. *Macromolecules,* **2014**, 47, 5089–5095.

(20) Foster, J. C.; Radzinski, S. C.; Zou, X.; Finkielstein, C. V.; Matson, J. B. $H_2S$-Releasing Polymer Micelles for Studying Selective Cell Toxicity. *Mol. Pharm.,* **2017**, 14, 1300–1306.

(21) Carter, J. M.; Qian, Y.; Foster, J. C.; Matson, J. B. Peptide-Based Hydrogen Sulphide-Releasing Gels. *Chem. Commun.,* **2015**, 51, 13131–13134.

(22) Scifinder Scholar, Chemical Abstracts Service: Columbus, OH (accessed April, 2018); pka values calculated using Advanced Chemistry Development (ACD/Labs) software, version V11.02; (ACD/Labs 1994–2006)

(23) Hansch, C.; Leo, A.; Taft, R. W. A Survey of Hammett Substituent Constants and Resonance and Field. *Chem. Rev.,* **1991**, 91, 165–195.

(24) Dash, A. C.; Dash, B.; Praharaj, S. Hydrolysis of Imines: Kinetics and Mechanism of Spontaneous Acid-, Base-, and Metal Ion-Induced Hydrolysis of *N*-salicylidene-2-aminothiazole. *Dalton Trans.,* **1961**, 2063–2069.

(25) Dash, A. C.; Dash, B.; Mahapatra, P. K. Hydrolysis of Imines. Part 2. Kinetics and Mechanism of Hydrolysis of N-Salicylidene-2-aminopyridine in the Presence and Absence of the Copper (I) Ion. A Study of the Catalytic Effects of some Mixed-Ligand Complexes of Copper. *Dalton Trans.,* **1983**, 1503–1509.

(26) Reeves, R. L. Schiff Bases. Kinetics of Hydrolysis of p-Trimethylammoniumbenzylidene-p'-hydroxyaniline chloride in Aqueous Solution from pH 1 to 11.5. *J. Am. Chem. Soc.,* **1961**, 84, 3332–3337.

(27) Rosenberg, S.; Silver, S. M.; Sayer, J. M.; Jencks, W. P. Evidence for Two Concurrent Mechanisms and a Kinetically Significant Proton Transfer Process in Acid-Catalyzed O-Methyloxime Formation. *J. Am. Chem. Soc.,* **1974**, 96, 7986–7998.

(28) Blanch, J. H.; Onsager, O. T. Stability of N-Heterocyclic Oxime Derivatives. Part I. Decomposition of *N*-Methylpyridinium 3- and 4-O- Acetylaldoxime Iodides in Aqueous Solution. *J. Chem. Soc.* **1965**, 0, 3729–3724.

(29) More O'Ferral, R. A.; O'Brien, D. M.; Murphy, D. G. Rate and Equilibrium Constants for Formation and Hydrolysis of 9-Formylfluorene xime: Diffusion- Controlled Trapping of a Protonated Aldehyde by Hydroxylamine. *Can. J. Chem.,* **2000**, 78, 1594–1612.

(30) Kalia, J.; Raines, R. T. Hydrolytic Stability of Hydrazones and Oximes. *Angew. Chem. Int. Ed. Engl.,* **2008**, 47, 7523–7526.

(31) Branchaud, B. P. Studies on the Preparation and Reactions of Tritylsulfenimines. *J. Org. Chem.,* **1983**, 48, 3531–3538.

(32) Cho, B. R.; Cho, N. S.; Lee, S. K. Elimination Reactions of (E)- and (Z)-Benzaldehyde O-Pivaloyloximes. Transition-State Differences for the Syn and Anti Eliminations Forming Nitriles. *J. Org. Chem.,* **1997**, 62, 2230–2233.

(33) Milne, H. B.; Peng, C. H. The use of Benzylsulfonyl Chloride in Peptide Synthesis. *J. Am. Chem. Soc.,* **1956**, 79, 639–644.

## Appendix A

### Synthesis of ((4-formylphenyl)sulfonyl)-L-isoleucine

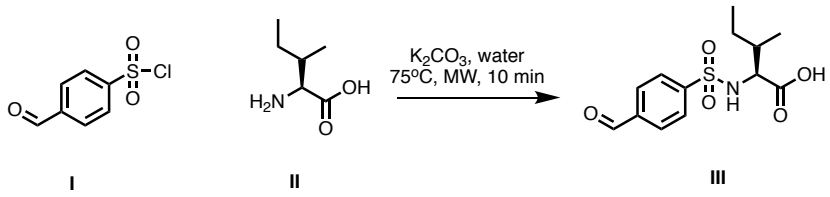


**Scheme 1.S1**: Synthesis of (4-formylphenyl)sulfonyl)-L-isoleucine

Modified amino acid ((4-formylphenyl)sulfonyl)-L-isoleucine was synthesized according to literature procedures.[1] Briefly, a microwave reaction tube was charged with 4-formylsulfonyl chloride (0.100 g, 0.5 mmol), L-isoleucine (0.064 g, 0.5 mmol), $K_2CO_3$ (0.146 g, 1.0 mmol), and water (2 mL) to give a suspension. The reaction mixture was sonicated for 30–45 min to afford a turbid solution. The reaction mixture was subjected to microwave heating, at 75 $^oC$ for 10 min to yield a clear, pale yellow solution. Reaction progress was monitored by TLC, eluting with 100 % EtOAc (UV visualization). Once the starting material had been completely consumed, the reaction mixture was acidified by addition of 1N HCl, and the mixture was extracted with EtOAc (2 × 10 mL) in a separatory funnel. The organic layers were then combined and washed with brine (1 × 10 mL). The clear solution was then dried over $Na_2SO_4$ and concentrated under vacuum to afford the product as a light orange solid (0.093 g, 63 % yield). The final product was used directly in the next step without further purification. $^1$H NMR (DMSO-$d_6$): δ 0.78 (m, 6H), 1.13 (m, 1H) δ 1.38 (m, 1H), 1.68 (m, 1H) δ 3.63 (t, 1H), 7.96 (d, 2H) δ 8.06 (d, 2H), 8.34 (d, 1H) δ 10.10 (s, 1H), 12.62 (bs, 1H). $^{13}$C NMR (DMSO-$d_6$): δ 11.3, δ 15.8, δ 24.7, δ 37.2, δ 60.7, δ 127.7, δ 130.4, δ 138.7, δ 146.4, δ 172.4, δ 193.1.

## NMR spectra

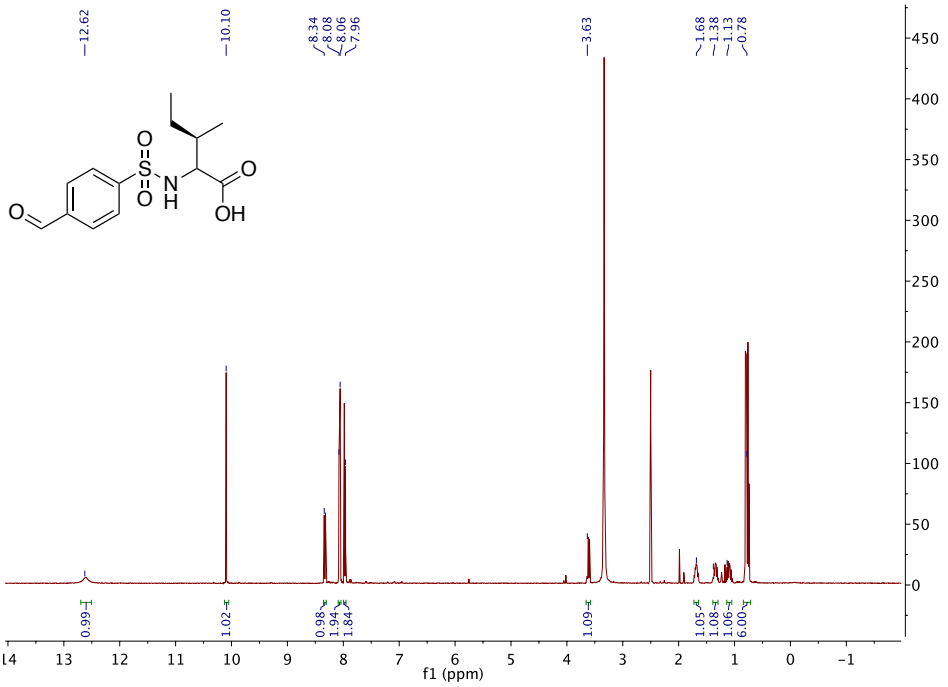


**Fig 1.S1**: $^{1}$H-NMR of ((4-formylphenyl)sulfonyl)-L-isoleucine **(III)**

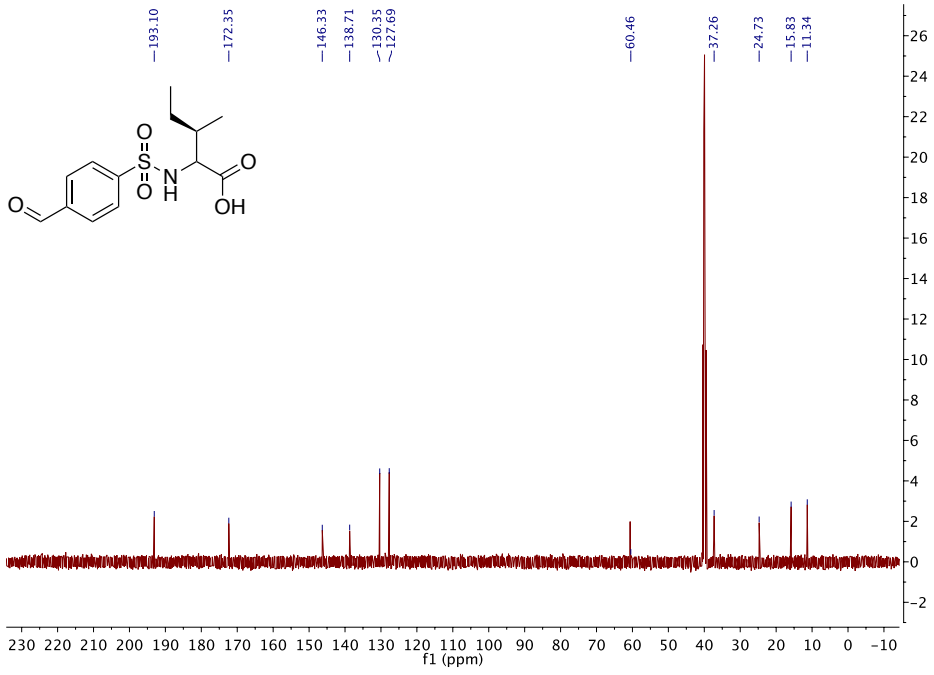


**Fig 1.S2**: $^{13}$C-NMR of ((4-formylphenyl)sulfonyl)-L-isoleucine **(III)**

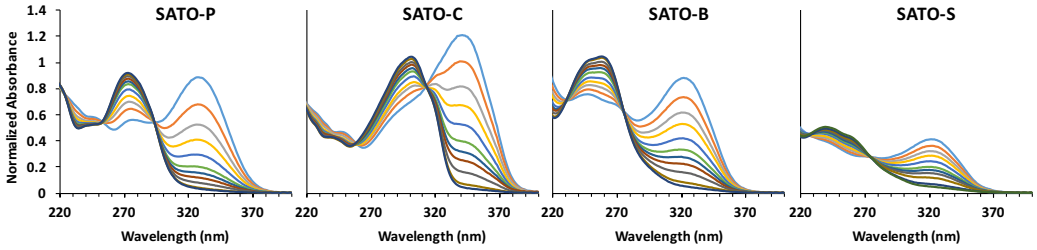


**Fig 1.S3:** UV–Vis absorption spectra of SATO-P, SATO-C, SATO-B, and SATO-S at pH 6.0

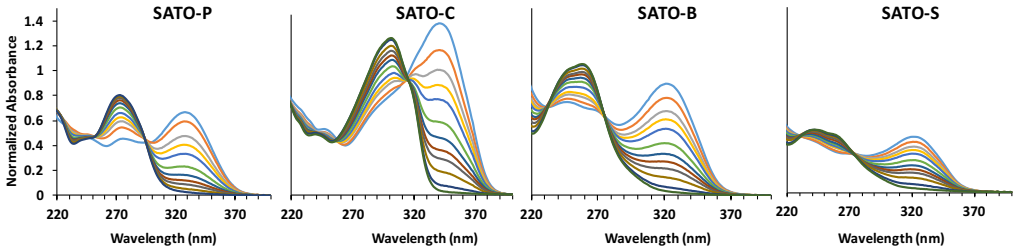


**Fig 1.S4:** UV–Vis absorption spectra of SATO-P, SATO-C, SATO-B, and SATO-S at pH 6.7

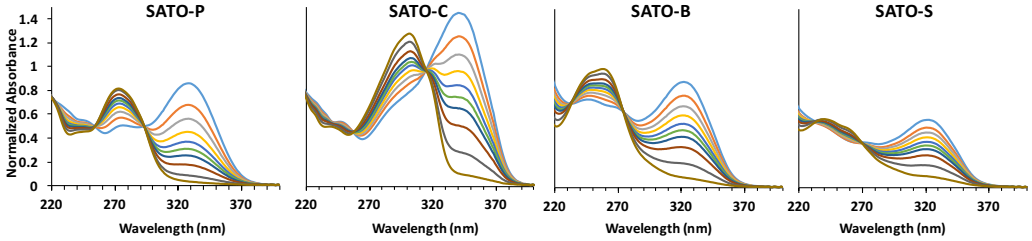


**Fig 1.S5:** UV–Vis absorption spectra of SATO-P, SATO-C, SATO-B, and SATO-S at pH 7.0

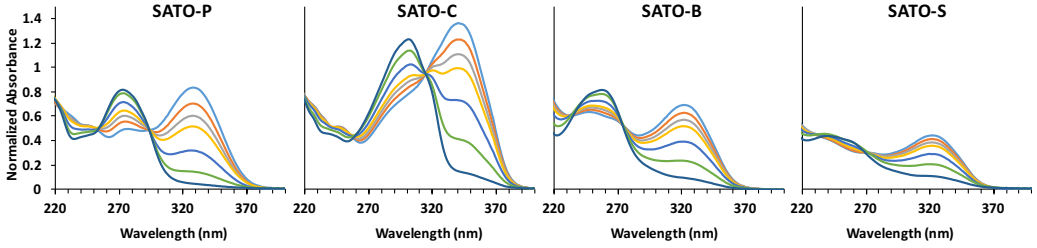


**Fig 1.S6:** UV–Vis absorption spectra of SATO-P, SATO-C, SATO-B, and SATO-S at pH 7.4

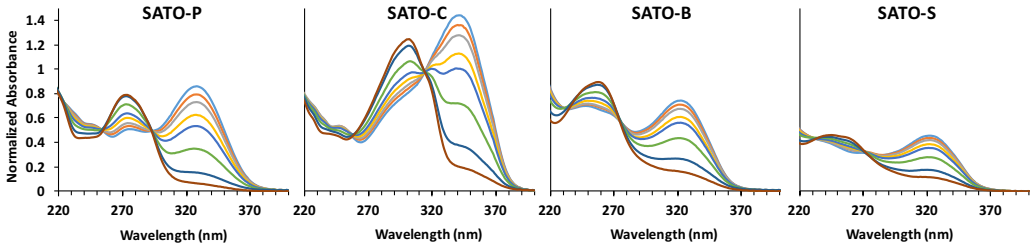


**Fig 1.S7:** UV–Vis absorption spectra of SATO-P, SATO-C, SATO-B, and SATO-S at pH 7.7

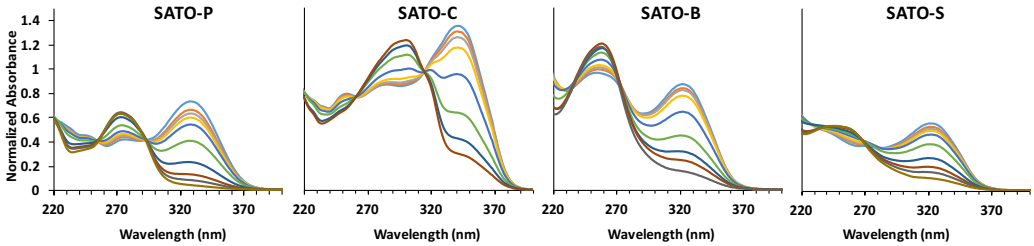


**Fig 1.S8:** UV–Vis absorption spectra of SATO-P, SATO-C, SATO-B, and SATO-S at pH 8.0

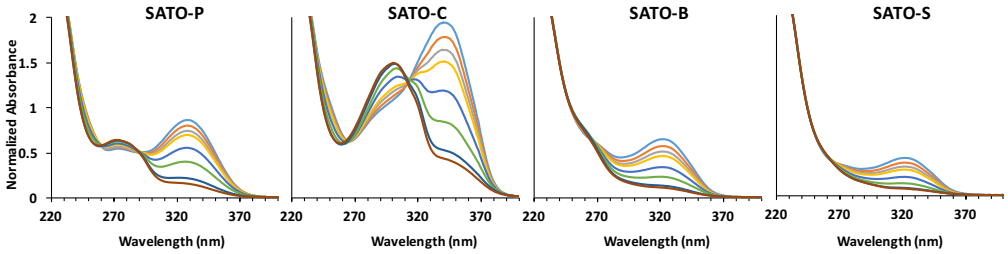


**Fig 1.S9:** UV–Vis absorption spectra of SATO-P, SATO-C, SATO-B, and SATO-S at pH 8.5

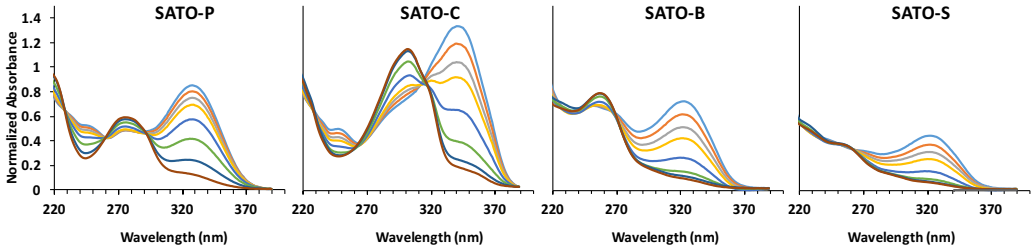


**Fig 1.S10:** UV–Vis absorption spectra of SATO-P, SATO-C, SATO-B, and SATO-S at pH 9.3

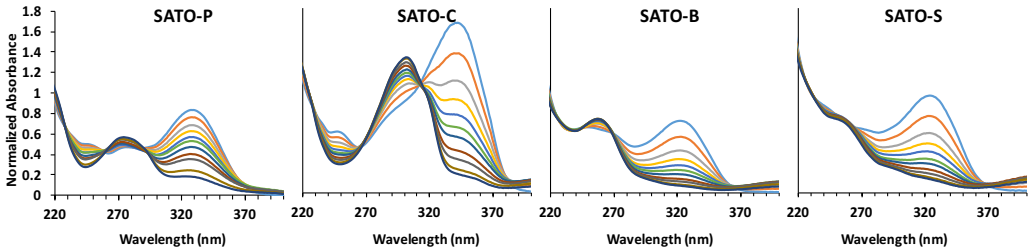


**Fig 1.S11:** UV–Vis absorption spectra of SATO-P, SATO-C, SATO-B, and SATO-S at pH 10.2

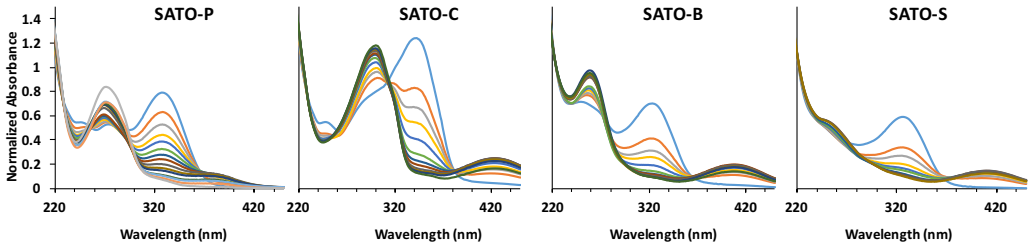


**Fig 1.S12:** UV–Vis absorption spectra of SATO-P, SATO-C, SATO-B, and SATO-S at pH 10.9

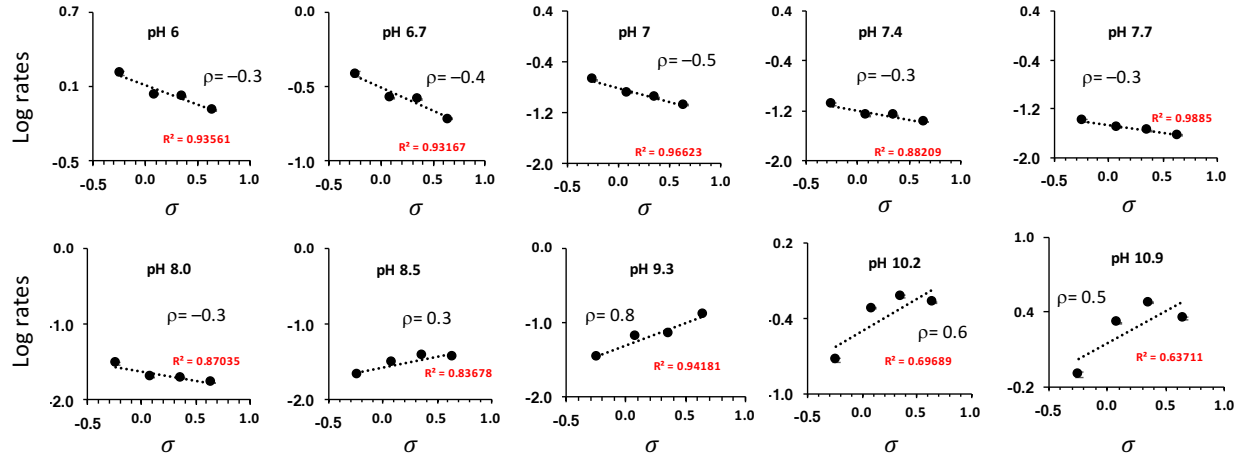


**Fig 1.S13:** Hammett plots for pH range 6.0–10.9.

## Calculations

The SATO absorbance peak was compared to the isosbestic point for each hydrolysis experiment. The % hydrolysis was calculated using the following equation.[2]

$$\%\text{hydrolysis} = \frac{[\text{I}]}{[\text{I}] + [\text{III}]} = \left(\frac{A_{\text{peak I}}}{A_{\text{iso}}} - \frac{\varepsilon_{\text{peak I}}}{\varepsilon_{\text{iso}}}\right)\left(\frac{\varepsilon_{\text{iso}}}{\varepsilon_{\text{peak I}} - \varepsilon_{\text{peak III}}}\right)$$

Where:

$A_{peakI}$ = absorbance of at $\lambda_{max}$ for SATO-peptide at given time point.

$A_{iso}$ = absorbance at the isosbestic point at given time point.

$\varepsilon_{peak\ I}$ = Extinction coefficient of SATO-peptide at $\lambda_{max}$.

$\varepsilon_{iso}$ = Extinction coefficient at isosbestic point.

$\varepsilon_{peak\ III}$ = Extinction coefficient of linker-peptide aldehyde (without SATO unit) at $\lambda_{max}$ for the corresponding to SATO-peptide.

The equation for %hydrolysis was programmed into Excel with all the known components except for the extinction coefficient ( $\varepsilon_{peak\ I}$). The solver function was used to estimate $\varepsilon_{peak\ I}$ for the linker-peptide unit at 100% hydrolysis by maximizing the $R^2$ value. The estimated extinction coefficient was then applied to the equation for %hydrolysis to calculate the % hydrolysis at various time points. Pseudo-first-order kinetic plots were obtained by plotting time vs ln(1/(1 – %hydrolysis)), and half-lives were obtained using $t_{1/2}$=ln(2)/slope.

**Estimates of sigma values for linkers**

Using the estimates of p$K_a$ with the ACD software in SciFinder®, we approximated values of sigma for the linkers by replacing the Y-NH-IAVEEE by Y-NH-Me. First, we plotted known values of sigma versus predicted p$K_a$ for common para substituents over a large range of values from strong electron-donating groups to strong electron-withdrawing groups. We included some

common groups that are models for the linkers. We plotted the data (Figure S14) for these compounds and performed linear regression in Excel.

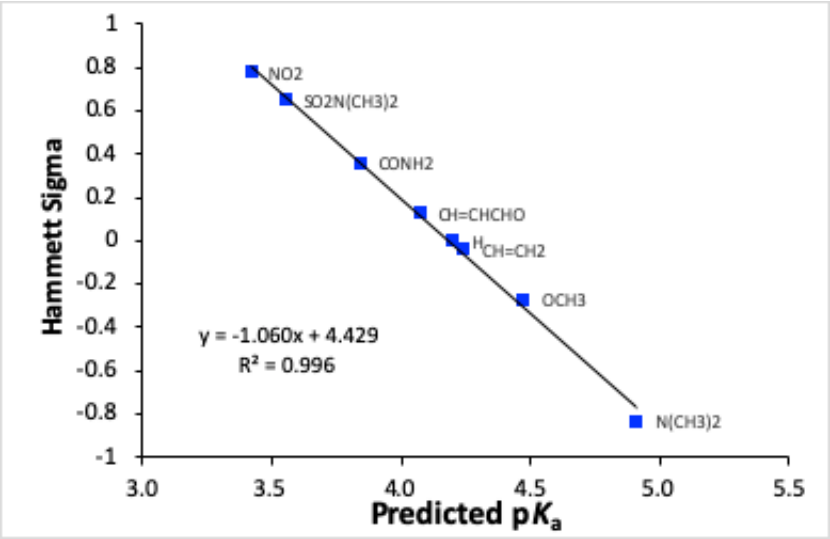


**Fig 1.S14:** Plot of predicted values of p$K_a$ versus sigma. Linear regression analysis displayed.

Using the equation generated by linear regression, we calculated the sigma values for models for linkers Y in para-HOOC-$C_6H_4$-Y from the estimated p$K_a$s (see Table S1).

| Y | Predicted p$K_a$ | Known σ | Calc'd σ | Difference in σ |
|---|---|---|---|---|
| $NO_2$ | 3.42 | 0.78 | **0.80** | –0.02 |
| $SO_2N(CH_3)_2$ | 3.55 | 0.65 | **0.67** | –0.02 |
| $CONH_2$ | 3.84 | 0.36 | **0.36** | 0.00 |
| CH=CHCHO | 4.07 | 0.13 | **0.12** | 0.01 |
| H | 4.20 | 0 | **–0.02** | 0.02 |
| $CH=CH_2$ | 4.24 | –0.04 | **–0.06** | 0.02 |
| $OCH_3$ | 4.47 | –0.27 | **–0.31** | 0.04 |
| $N(CH_3)_2$ | 4.91 | –0.83 | **–0.77** | –0.06 |
| **Models for linkers** | | | | |
| $CH=CHCONHCH_3$ | 4.12 | | **0.06** | |
| $OCH_2CONHCH_3$ | 4.31 | | **–0.14** | |

| | | | | |
|---|---|---|---|---|
| $SO_2NHCH_3$ | 3.60 | | **0.61** | |
| $CONHCH_3$ | 3.84 | | **0.36** | |

**Table 1.S1**. Data used to estimate Hammett sigma for group Y in para-HOOC-$C_6H_4$-Y

## References


(1) Milne, H. B.; Peng, C. H. The use of Benzylsulfonyl Chloride in Peptide Synthesis *J. Am. Chem. Soc.,* **1956**, 79, 639–644.

(2) Foster, J. C.; Powell, C. R.; Radzinski, S. C.; Matson, J. B. S-aroylthiooximes: A Facile Route to Hydrogen Sulfide Releasing Compounds with Structure-Dependent Release Kinetics *Org. Lett.,* **2014**, 16, 1558–1561.

## Chapter 3: Hydrogen Sulfide-releasing peptide hydrogel limits the development of intimal hyperplasia in human vein segments

Reprinted with permissions from *Hydrogen sulfide-releasing peptide hydrogel limits the development of intimal hyperplasia in human vein segments*, Acta Biomaterialia, **2019**, 97, 374–384.  The final publication is available online at: https://www.sciencedirect.com/science/article/pii/S1742706119305318

### 3.1 Authors

Alban Longchamp[a], Kuljeet Kaur[b], Diane Macabrey[a], Celine Dubuis[a], Jean-Marc Corpataux[a], Sébastien Déglise[a], John B. Matson[b] and Florent Allagnat[a]

[a]Department of Vascular Surgery, Centre Hospitalier Universitaire Vaudois (CHUV), Lausanne, Switzerland

[b]Virginia Tech Department of Chemistry, Macromolecules Innovation Institute, and Virginia Tech Center for Drug Discovery, Blacksburg, VA, USA

### 3.2 Abstract

Currently available interventions for vascular occlusive diseases suffer from high failure rates due to re-occlusive vascular wall adaptations, a process called intimal hyperplasia (IH). Naturally occurring hydrogen sulfide ($H_2S$) works as a vasculoprotective gasotransmitter *in vivo*. However, given its reactive and hazardous nature, $H_2S$ is difficult to administer systemically. Here, we developed a hydrogel capable of localized slow release of precise amounts of $H_2S$ and tested its benefits on IH. The $H_2S$-releasing hydrogel was prepared from a short peptide attached to an *S*-aroylthiooxime $H_2S$ donor. Upon dissolution in aqueous buffer, the peptide self-assembled into

nanofibers, which formed a gel in presence of calcium. This new hydrogel delivered $H_2S$ over the course of several hours, in contrast with fast-releasing NaHS. The $H_2S$-releasing peptide/gel inhibited proliferation and migration of primary human vascular smooth muscle cells (VSMCs), while promoting proliferation and migration of human umbilical endothelial cells (ECs). Both NaHS and the $H_2S$-releasing gel limited IH in human great saphenous vein segments obtained from vascular patients undergoing bypass surgery, with the $H_2S$-releasing gel showing efficacy at a 5x lower dose than NaHS. These results suggest local perivascular $H_2S$ release as a new strategy to limit VSMC proliferation and IH while promoting EC proliferation, hence re-endothelialization.

### 3.3 Introduction

Despite remarkable technological advances, the rate of restenosis due to intimal hyperplasia (IH) one year following endovascular reconstruction or bypass surgery reaches 30%.[1] IH is driven by the dysfunction of endothelial cells (EC) lining the inner part of the vessels, which results in a reprogramming of the vascular smooth muscle cells (VSMCs) from a differentiated to a proliferating and migrating phenotype and the formation of an occlusive neo-intima layer at the site of injury.[2] The available systemic drug therapies used to prevent restenosis are generally poorly tolerated and show narrow therapeutic ranges.[3, 4] Localized treatments include drug-eluting angioplasty balloons and stents, which limit VSMC proliferation and reduce IH, but they also delay re-endothelization, limiting their efficacy and prolonging the need for anti-thrombotic medication.[5]

Hydrogen sulfide ($H_2S$) is an endogenous gasotransmitter with important cytoprotective and anti-inflammatory properties, which may protect against atherosclerosis, chronic heart failure and vascular restenosis.[6, 7] In humans, plasma $H_2S$ concentration declines with age,[8] and the circulating levels of $H_2S$ are reduced in patients suffering from cardiovascular diseases.[9, 10]

Administration of exogenous $H_2S$ may reduce the symptoms of cardiovascular diseases, but its gaseous nature and rapid *in vivo* half-life nature create a delivery challenge.

To tap the therapeutic potential of this gasotransmitter, numerous sulfur-containing small molecules called $H_2S$ donors have been developed that release $H_2S$ either by hydrolysis or in response to a specific trigger.[11] However, $H_2S$ delivery via small molecule donors is often limited by short release periods, low water solubility, lack of target specificity, and toxicity in some cases.[11, 12] To limit toxicity and extend the $H_2S$ release period, $H_2S$ donors have been incorporated into water-soluble polymers, micelles, hydrogels, nanofibers, and films.[13-17] However, there is still a growing need for $H_2S$-releasing materials capable of delivering $H_2S$ directly at a site of interest for an extended period of time.[18, 19] Peptide-based hydrogels have been widely used for tissue engineering and regenerative medicine,[20] but only a handful of reports detail their use in delivering gasotransmitters.[21-23]

Here, we developed and tested the safety and therapeutic potential of a self-assembling aromatic peptide amphiphile, employing an $H_2S$-releasing *S*-aroylthiooxime (SATO) group as the aromatic component. We found that our $H_2S$-releasing hydrogel, which is capable of localized $H_2S$ delivery, promotes EC function while inhibiting VSMC expansion and IH formation in human veins at a significantly lower dose than NaHS.

### 3.4 Results

#### Design and synthesis of an $H_2S$-releasing peptide and a control peptide

Self-assembling aromatic peptide amphiphiles rely on a combination of aromatic stacking of N-terminal aromatic groups and hydrogen bonding in a short peptide chain consisting of 2-6 amino acids to drive self-assembly in aqueous solution.[29-32] We based the peptide design for this study on our recent report on the first $H_2S$-releasing aromatic peptide amphiphile.[22] Using an N-

terminal SATO group as the aromatic component and a pentapeptide sequence modified from our original design, the sequence used for the $H_2S$-releasing peptide (termed Pep-$H_2S$) was SATO–FBA–IAVEE, where SATO represents the aromatic $H_2S$ donor, FBA represents 4-formylbenzoic acid, and IAVEE represents the peptide sequence using 1-letter codes. We chose the IAVEE sequence compared with previously published IAVEEE sequence because we envisioned that removing one Glu residue would increase gel stiffness. We also prepared a control peptide (termed Pep-Ctrl) incapable of releasing $H_2S$ with the sequence OBHA–FBA-IAVEEEE, where OBHA represents *O*-benzyl hydroxylamine. Pep-Ctrl contains an oxime linkage in place of the acylthiooxime linkage in Pep-$H_2S$, but the peptides are otherwise identical. In initial rheological studies, we found that two additional C-terminal Glu residues were needed in Pep-Ctrl compared with Pep-$H_2S$ to afford hydrogels with similar storage moduli. We speculate that stronger aromatic stacking and/or hydrogen bonding in the OBHA component vs. the SATO component leads to this requirement for a longer hydrophilic sequence, which tends to decrease storage modulus, in Pep-Ctrl.

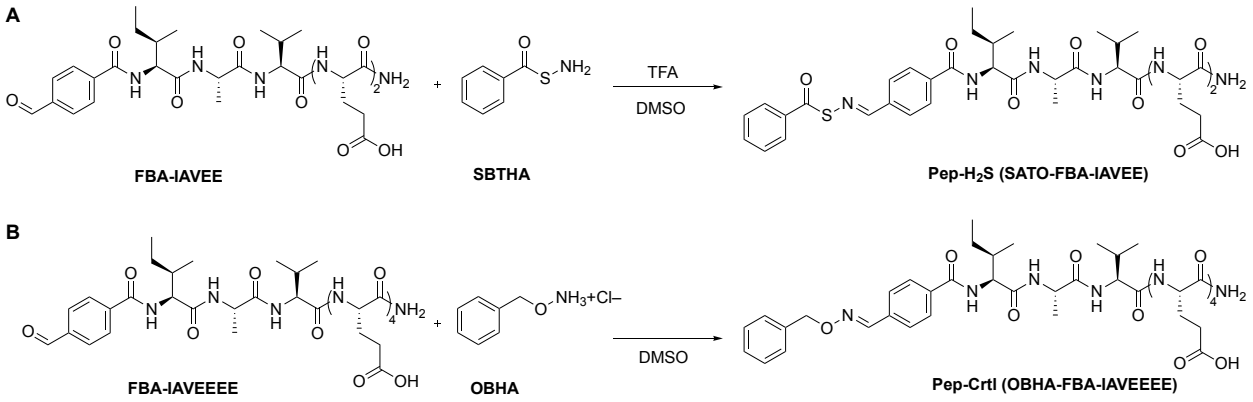


**Fig. 3.1: A)** Synthesis of Pep-$H_2S$ (sequence SATO-FBA-IAVEE). **B)** Synthesis of Pep-Ctrl (sequence OBHA-FBA-IAVEEEE).

Peptides FBA-IAVEE and FBA-IAVEEEE were synthesized using Fmoc-based solid-phase peptide synthesis. The FBA units were coupled to the peptides on-resin before cleavage and purification. The two peptide aldehydes were then further derivatized to form the final aromatic peptide amphiphile products (Fig 3.1). Pep-$H_2S$ was prepared by condensing the N-terminal aldehyde in FBA-IAVEE with *S*-benzoylthiohydroxylamine to form the final molecule. Pep-Ctrl was synthesized similarly, condensing FBA-IAVEEEE with hydroxylamine OBHA. Both peptides were purified by preparative HPLC after the condensation step, lyophilized, and aliquoted for further analysis.

**Peptides self-assemble into nanoribbons**

Self-assembly is typically observed in amphiphilic molecules, where the hydrophobic component drives assembly as it excludes water. In dilute solution, amphiphiles are molecularly dissolved, but self-assembly occurs above a given concentration, termed the critical aggregation concentration (CAC). Here we used the Nile red assay to determine the CAC for both Pep-$H_2S$ and Pep-Ctrl. The hydrophobic Nile red dye, which is non-fluorescent in a hydrophilic environment incorporates within the hydrophobic core of the self-assembled nanostructures, resulting in a fluorescence enhancement proportional to the peptide concentration. The CAC is then defined as the point of abrupt change in the fluorescence intensity and refers to a minimum concentration above which the molecule exists primarily in a self-assembled state. In our experiments on Pep-$H_2S$, we measured a CAC of 0.9 mM (near 1 mg/mL) for both peptides.

With CAC values in hand, we next explored the molecular packing of the self-assembled aromatic peptide amphiphiles Pep-$H_2S$ and Pep-Ctrl. Circular dichroism (CD) spectra were measured for both Pep-$H_2S$ and Pep-Ctrl at 10 mM in 1X PBS buffer to evaluate secondary structure formation. Prominent minima at 217 nm and 220 nm for Pep-$H_2S$ and Pep-Ctrl,

respectively, indicated the presence of β-sheets (Fig. 3.2). Typically, β-sheet signals in the CD spectra of short, self-assembling peptides indicates the formation of extended, 1-dimensional nanostructures, which are necessary for gelation.[33]

To explore further the self-assembled structures, we used conventional TEM with negative staining to image the nanostructures formed by Pep-$H_2S$ and Pep-Ctrl (Fig. 3.2B, C). Aromatic peptide amphiphiles can take on many types of morphologies, including spheres, cylinders, flat or twisted ribbons, sheets, and others.[30, 34] When long, one-dimensional objects are observed, they may entangle under certain conditions to form gels. In both cases, we observed flat nanoribbons many several microns in length, with widths around 6–7 nm, which was consistent with the CD spectra depicting β-sheets. The nanoribbons were uniform in width, likely due to the fact that both peptide nanostructures are assembled from pure, single molecules with no molecular weight dispersity.

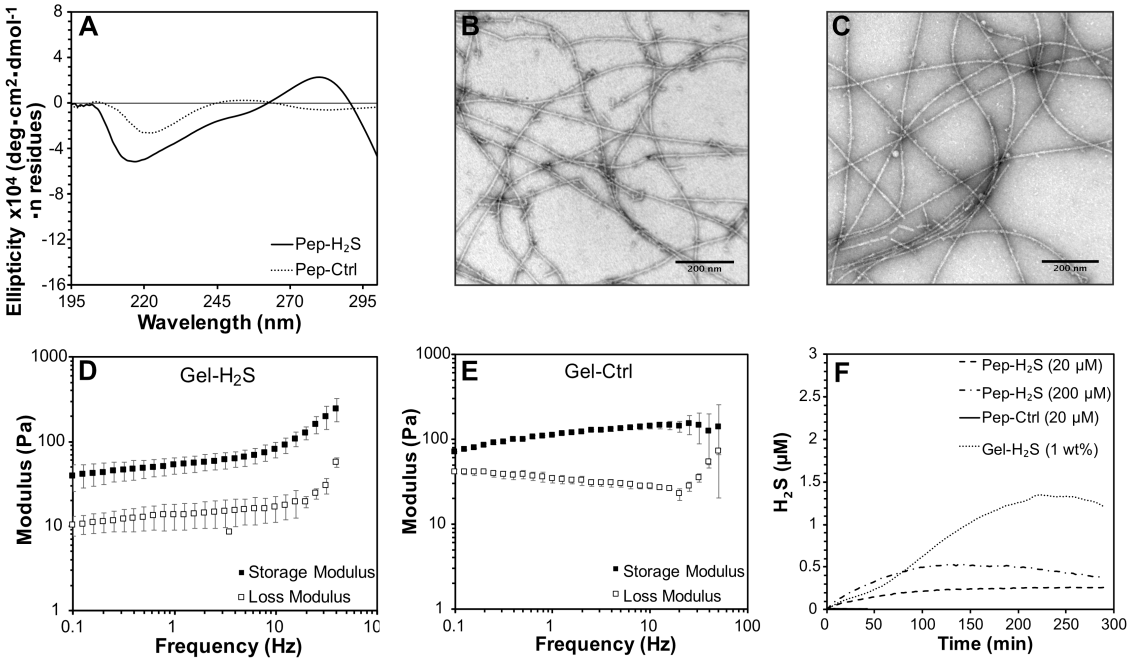


**Fig. 3.2: A**) CD spectra for 10 mM Pep-$H_2S$ and Pep-Ctrl solution in 1X PBS buffer. **B** and **C**) Conventional TEM images for Pep-$H_2S$ and Pep-Ctrl, respectively. Peptides were dissolved at 10 mM in 50 mM phosphate buffer at pH 7.4. Samples were diluted to 500 μM immediately before casting and stained with 2% uranyl acetate solution. **D** and **E**) Frequency sweep oscillatory rheology for hydrogels Gel-$H_2S$ and Gel-Ctrl, respectively, prepared at 1 wt% in 1 X PBS at pH 7.4 and gelled with $CaCl_2$. **F**) $H_2S$ release curves measured on an $H_2S$-selective electrochemical probe comparing Gel-$H_2S$, Pep-$H_2S$ (200 μM and 20 μM), and Pep-Ctrl.

## Calcium salts trigger peptide gelation to form soft hydrogels

As noted above, aromatic peptide amphiphiles that form long, one-dimensional aggregates may gel under conditions that promote entanglement of the nanostructures. We found that addition of $CaCl_2$ promoted the rapid gelation of both Pep-$H_2S$ and Pep-Ctrl. This is likely due to two factors: 1) charge screening of the negatively charged Glu residues, which reside on the nanofiber surface and cause the fibers to repel each other under low salt conditions; and 2) formation of salt bridges between the nanofibers due to the divalent nature of the calcium ion.

The gelation and viscoelastic properties of the hydrogels, termed Gel-$H_2S$ and Gel-Ctrl when in the gel state, were evaluated by rheological measurements. Peptide solutions were first prepared

at 1 wt. % (~10 mM) in 1X PBS, and solutions were added directly to the rheometer. Next, a solution of $CaCl_2$ in water was added to the peptide solutions to afford a final $CaCl_2$ concentration of 8 mM. After a brief waiting period to allow for gelation throughout the sample, each hydrogel was measured. Frequency sweeps of both Gel-$H_2S$ and Gel-Ctrl revealed that the storage modulus (G') was higher than the loss modulus (G") throughout the range tested, indicating that both peptides formed robust, soft hydrogels (Fig. 3.2D, E). Gel-$H_2S$ showed a storage modulus of 50 Pa at intermediate frequencies, while Gel-Ctrl showed a storage modulus of 100 Pa. Both hydrogels were soft and easily manipulated by a spatula or syringe. At frequencies above 10 Hz, both hydrogels showed increases in both G' and G". This behavior is characteristic of materials with non-covalent cross-linking such as peptide-based hydrogels.[35]

**Peptide gel exhibit slow and sustained $H_2S$ release**

SATOs are thiol-triggered $H_2S$ donors[24] so we aimed to evaluate $H_2S$ release from the peptides in solution and gel form in the presence of thiols. To obtain $H_2S$ release curves using real-time monitoring, we used an $H_2S$-selective microelectrode probe (Fig. 3.2F). A solution of Pep-$H_2S$ at 20 μM, triggered with a 10-fold excess of L-Cys, showed a steady rise in $H_2S$ concentration up to 0.2 μM over 120 min, after which it remained steady. Because $H_2S$ is constantly oxidizing and volatilizing, we typically observe peaking concentrations at values much lower than the starting concentration of the $H_2S$ donor. We also measured release at a 10-fold higher concentration to evaluate how this increase would affect the release rate. Similar to the 20 μM case, the $H_2S$ release profile for Pep-$H_2S$ at 200 μM showed a gradual release with a peaking time at 130 min at a concentration of 0.5 μM. As expected, Pep-Ctrl did not show any $H_2S$ release. We also tested release from Gel-$H_2S$, prepared by addition of $CaCl_2$ to $H_2S$-Pep, into a large volume of PBS. Release was slow and steady and continued rising slowly over 220 min up to a peak

concentration of 1.3 μM before tapering off. As measuring $H_2S$ release from Pep-$H_2S$ and Gel-$H_2S$ required different conditions, the peaking times and concentrations cannot be directly compared; however, the peak shapes for the peptide under both solution and gel conditions show slow and steady release, which we expect may be ideal for localized delivery of $H_2S$.

**$SF_7$-AM signal in VSMC and HUVEC upon addition of Pep-Ctrl and Pep-$H_2S$.**

Live VSMCs or HUVECs were incubated with the fluorescent $H_2S$ probe $SF_7$-AM, and fluorescence was measured continuously before and after addition of 200 μM Pep-Ctrl, Pep-$H_2S$, or 100 μM NaHS. Experiments were performed in VSMC or HUVEC culture media containing 200 μM L-Cys. No additional thiol was added to trigger $H_2S$ release. Time-lapse imaging of $SF_7$-AM in the presence of VSMCs demonstrated that VSMCs produced little endogenous $H_2S$, as evidenced by the slow and low buildup of the $SF_7$-AM signal (Ctrl and Pep-Ctrl conditions, Fig. 3.3A). The rate of endogenous $H_2S$ production was two-fold higher in HUVECs as compared to VSMCs (Fig. 3.3B, C). As expected, addition of NaHS rapidly raised the $SF_7$-AM signal to similar levels in both cell types, while Pep-$H_2S$ induced a 4-fold slower release in both cell types (Fig. 3.3C). Of note, 200 μM Pep-$H_2S$ was not sufficient to surpass significant endogenous $SF_7$-AM signal in HUVECs, but it significantly raised the signal in VSMCs above controls (Fig. 3.3C). Lower Pep-$H_2S$ concentration (20 μM) was not sufficient to generate detectable amounts of $H_2S$ in either cell type (data not shown).

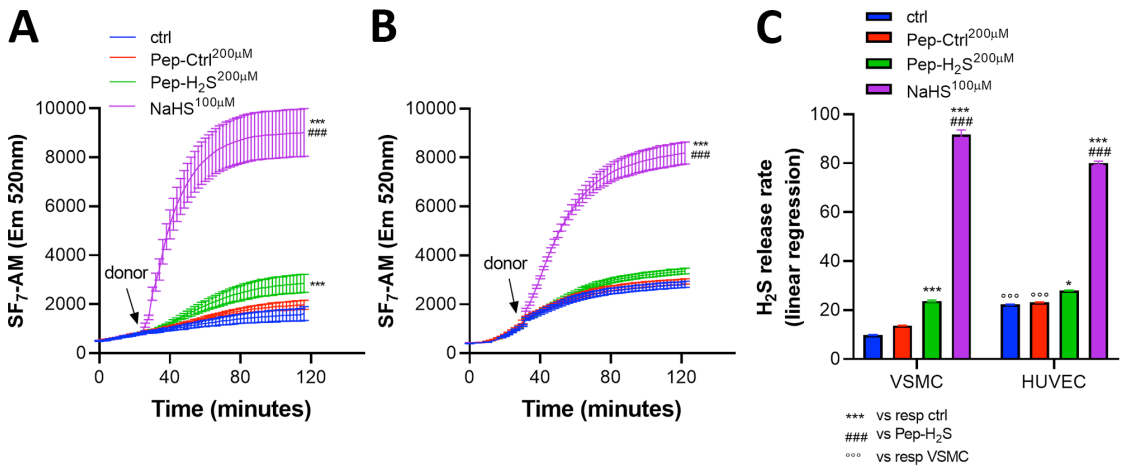


**Fig. 3.3: A)** $SF_7$-AM fluorescent signal in live primary VSMCs exposed or not (Ctrl) to 100 µM NaHS, 200 µM Pep-Ctrl or 200 µM Pep-$H_2S$ for the indicated time. **B**) $SF_7$-AM fluorescent signal in HUVECs exposed or not (Ctrl) to 100 µM NaHS, 200 µM Pep-Ctrl or 200 µM Pep-$H_2S$ for the indicated time. **C**) Linear regression of $SF_7$-AM fluorescence curves to estimate $H_2S$-releasing rates. Data are mean ± SEM of 4 independent experiments. *P<0.05, ***P<0.001 vs. respective ctrl; $^{###}$P<0.001 vs. Pep-$H_2S$; °°°p<0.001 vs. respective condition in VSMCs, as determined by two-way ANOVA with post-hoc t-test with Tukey's correction for multiple comparisons.

## Ex vivo treatment with the $H_2S$-releasing gel prevent development of IH in human saphenous vein segments

To explore the application of Gel-$H_2S$ in vascular diseases, we obtained human vein segments, which were placed in culture for 7 d with or without Gel-$H_2S$ or Gel-Ctrl (10-20 µL gel/mL media, equivalent to ~100 or ~200 µM sulfide, respectively). The RPMI culture medium contained 200 µM L-Cys, and no additional thiol was added to trigger $H_2S$ release. NaHS (100 µM) was used as a positive control of exogenous $H_2S$ supply.

Histomorphometric analysis of intima and media thickness after 7 d in culture revealed that treatment of human vein segments with Gel-$H_2S$ or NaHS fully blocked the increase in intima thickness or intima over media thickness (I/M) over 7 d in culture. (Fig. 3.4A). Importantly, treatment with Gel-$H_2S$, Gel-Ctrl, or NaHS did not affect the media thickness, suggesting no cytotoxic effect of exogenous $H_2S$ treatment. Next, we analyzed cell proliferation in the vein

segments using PCNA immunostaining. We observed a two-fold increase in cell proliferation in the control conditions (D7 and Gel-Ctrl) compared to the baseline (D0), while the Gel-$H_2S$ treatment lowered the proliferation to D0 levels (Fig. 4B).

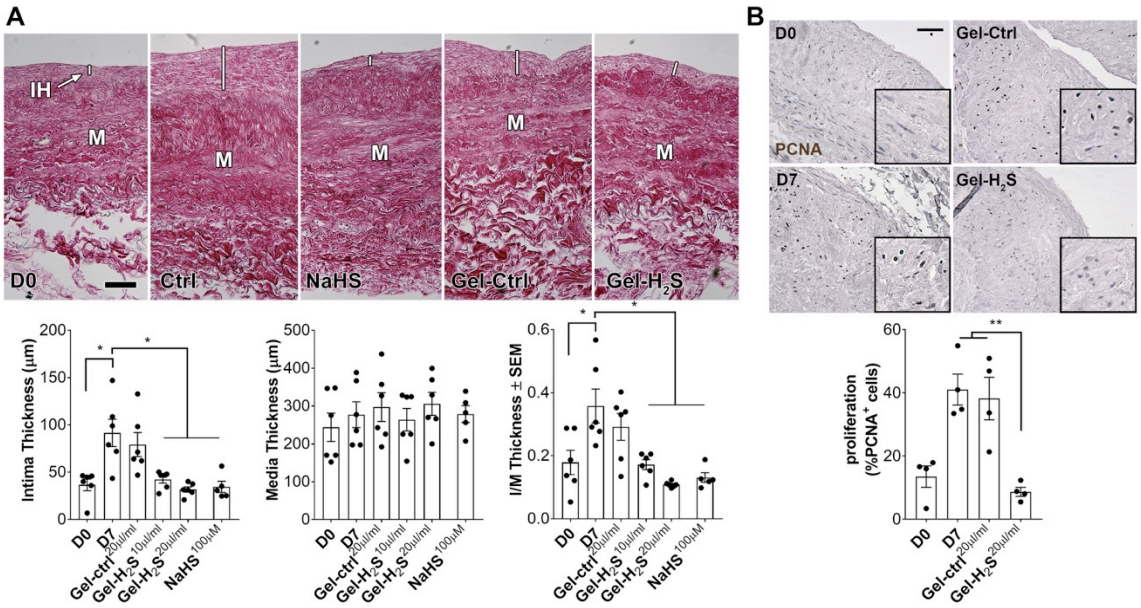


**Fig. 3.4:** Human great saphenous vein segments were put or not (D0) in static culture for 7 days in presence or not (D7) of NaHS (100 µM), Gel-Ctrl (20 µL/mL) or Gel-$H_2S$ (10 or 20 µL/mL). **A**) Representative VGEL staining (scale bar represents 200 µm) and scatter plots with mean±SEM of media, intima thicknesses, and intima/media ratio (I/M) in 5 vein segments. **B**) Representative PCNA immunostaining (black nuclei) counterstained with hematoxylin (blue nuclei) and scatter plots with mean±SEM of PCNA immunostaining. Insets are 3x magnification of main image. Scale bar represents 150 µm. *P<0.05; **P<0.01 vs D7 as determined by one-way ANOVA with post-hoc t-test with Dunnet's correction for multiple comparisons.

## The $H_2S$-releasing peptide/gel decreased VSMC proliferation and transmigration

To understand further the cell-based effects of Pep-$H_2S$ and Gel-$H_2S$, we examined human EC and VSMC proliferation and migration *in vitro*. In line with our *ex-vivo* data on human vein segments, *in vitro* studies of VSMCs derived from human vein segments revealed that Pep-$H_2S$ inhibited cell proliferation in a dose-dependent manner, while Pep-Ctrl had no effect (Fig. 3.5A). Importantly, 10 µM Pep-$H_2S$ had a similar effect to 100 µM NaHS. Media thickness data in

human veins (Fig 3.4) suggested that the donors had no cytotoxic effect on VSMCs. To further test this observation, *in vitro* assessment of cell apoptosis using Hoechst-propidium iodide staining was conducted. The results confirmed that Pep-$H_2S$, Pep-Ctrl, and NaHS had no toxic effect on VSMCs after 48 h exposure (Fig. 3.5B). Thapsigargin (TG) was used as a positive control to induce apoptosis (Fig 3.5B). Finally, using a transmigration assay in Boyden chambers, we observed that, as compared to the pre-conditioned EC culture medium alone (control$^+$), the addition of NaHS or Gel-$H_2S$ (10 μL/mL), but not Gel-Ctrl, inhibited VSMC transmigration. Interestingly, Gel-$H_2S$ was significantly more potent than NaHS, fully blocking VSMC transmigration (Fig. 3.5C).

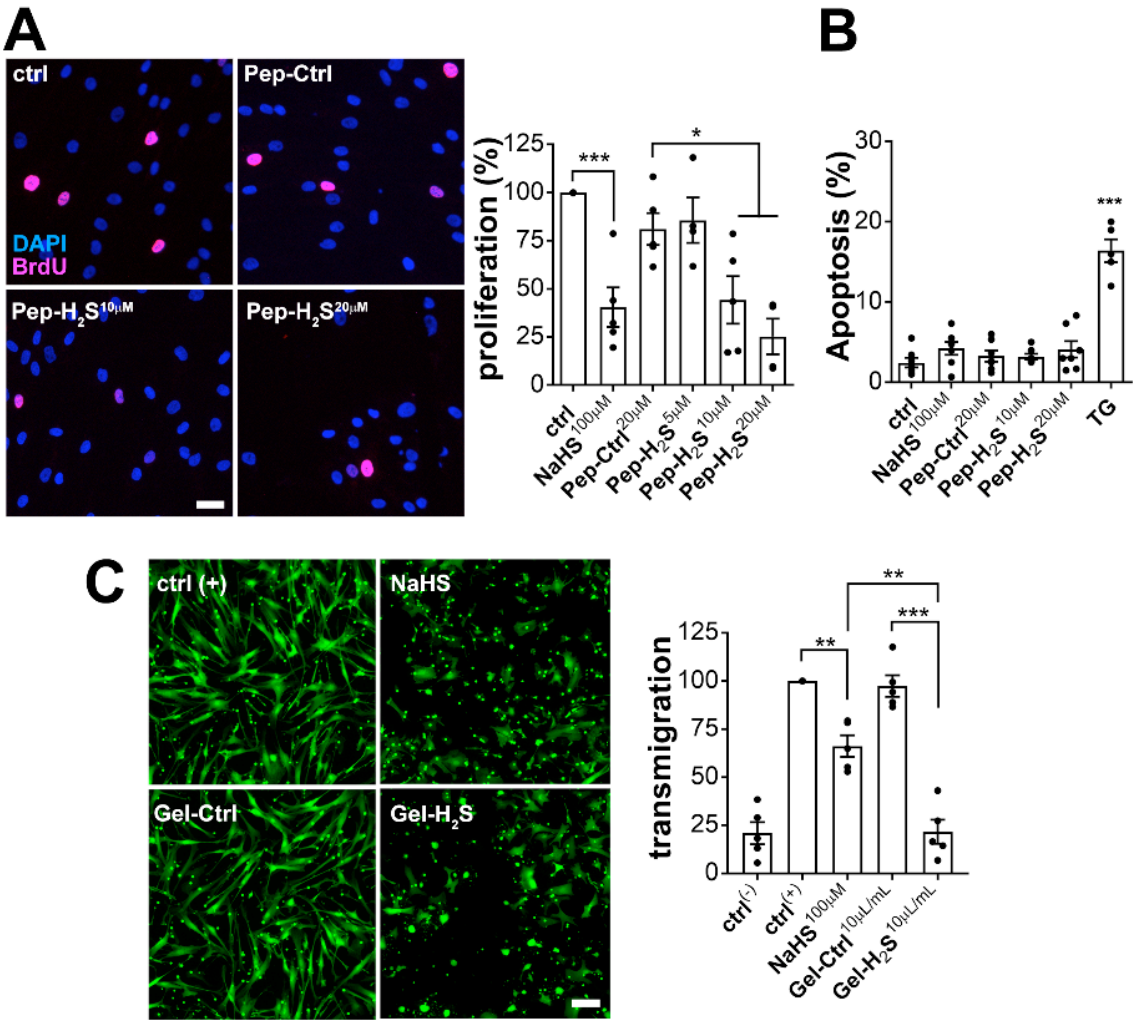


**Fig. 3.5: A)** VSMCs were exposed or not (Ctrl) to 100 µM NaHS, Pep-Ctrl, or Pep-$H_2S$ for 24 h in presence of BrdU. Scale bar represents 20 µm. Proliferation was calculated as the ratio of BrdU-positive nuclei over total DAPI-stained nuclei and expressed as % of proliferation in control condition**. B**) VSMC apoptosis levels after 48 h exposure to 100 µM NaHS, Pep-Ctrl, Pep-$H_2S$, or a 24 h exposure to 100 nM thapsigargin as a positive control. **C)** VSMC transmigration through an artificial membrane toward pre-conditioned medium of HUVECs (EGM-2 medium) supplemented or not ($ctrl^{(+)}$) with 100 µM NaHS, 10 µL/mL of Gel-Ctrl or Gel-$H_2S$ for 16 h. Scale bar represents 50 µm. All data are scatter plots with mean ± SEM. *P<0.05, **P<0.01, ***P<0.001 vs $ctrl^{(+)}$ as determined by one-way ANOVA with post-hoc t-test with Tukey's correction for multiple comparisons.

Further Western blot analyses of VSMC phenotype using two VSMC-specific proteins, calponin and SM22α, did not reveal major changes, although calponin levels tended to decrease in VSMCs exposed to the highest dose of Pep-$H_2S$ (20 µM) (Fig. 3.6A, B). Further immunocytochemistry analysis revealed that NaHS and Pep-$H_2S$ (20 µM) disrupted the typical

cytoskeleton staining for calponin and SM22α (Fig. 3.6C), which may account for the reduced proliferation and mobility of VSMCs exposed to $H_2S$.

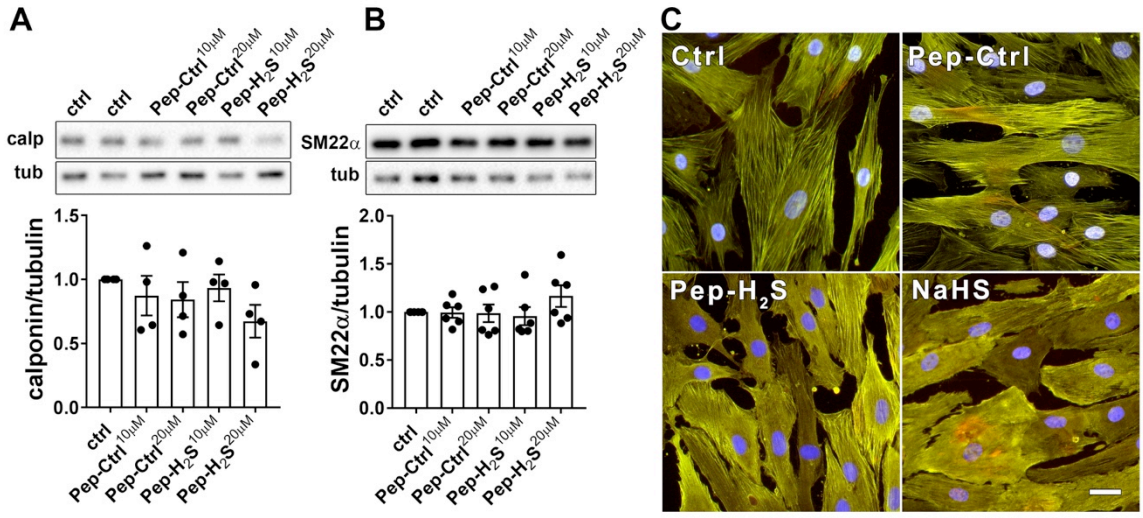


**Fig. 3.6:** VSMCs were exposed or not (ctrl) to NaHS (100 μM), Pep-Ctrl (10 or 20 μM), or Pep-$H_2S$ (10 or 20 μM) for 24 h. **A, B**) Western blot analysis of calponin (**A**) and SM22α (**B**), over tubulin levels. **C**) VSMC immunofluorescent staining for calponin (red), SM22α (green), and nuclei (DAPI staining in blue). Images are overlays of the 3 channels, representative of 5 independent experiments. Scale bar represents 20 μm.

### The $H_2S$-releasing peptide/gel increased EC proliferation and transmigration

We then performed similar experiments on HUVECs. $H_2S$ promotes EC proliferation, migration, and angiogenesis [36]. As expected, NaHS and Pep-$H_2S$ increased HUVEC proliferation, Pep-$H_2S$ being effective at a 10-fold lower dose than NaHS (Fig. 3.7A). We also tested HUVEC transmigration toward basic EC medium without growth factors (EBM™-2; control$^{(-)}$) or full HUVEC culture medium (EGM™-2 Bullet kit™; control$^{(+)}$). The EGM™-2 Bullet kit stimulated transmigration as expected. Consistently, and in contrast with VSMCs, NaHS and Gel-$H_2S$ (10 μL/mL) promoted HUVEC transmigration (Fig. 3.7B).

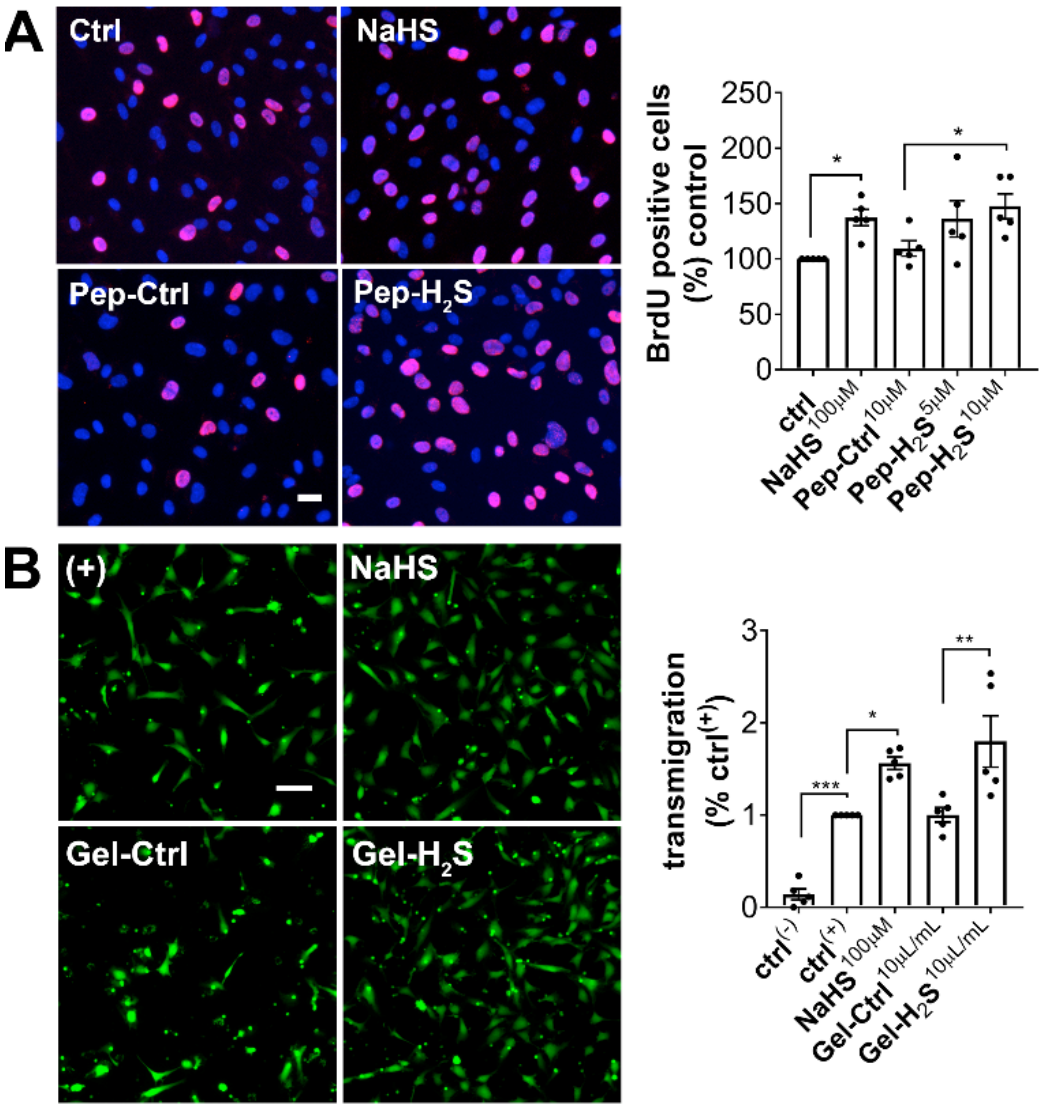


**Fig. 3.7: A)** HUVECs were exposed or not (ctrl) to 100 µM NaHS, Pep-Ctrl, Pep-$H_2S$ for 8h in the presence of BrdU. Proliferation was calculated as the ratio of BrdU-positive nuclei over total DAPI-stained nuclei and expressed as % of proliferation in the ctrl condition. Scale bar represents 20 µm. **B)** HUVEC transmigration through an artificial membrane toward EGM-2 medium supplemented or not (+) with 100 µM NaHS, 10 µL/mL Gel-Ctrl, or 10 µL/mL Gel-$H_2S$ for 6 h. Data are mean ± SEM of calcein-AM fluorescence signal measured on a fluorescence plate reader ($\lambda_{ex}$ = 495 nm; $\lambda_{em}$ = 517 nm). Scale bar represents 50 µm. All data are scatter plots with mean ± SEM. *P<0.05, **P<0.01, ***P<0.001 vs $ctrl^{(+)}$ as determined by one-way ANOVA with post-hoc t-test with Dunnet's correction for multiple comparisons.

### 3.5. Discussion

Previous studies in animal models have reported protection from IH with exogenous NaHS administration in rats,[37] rabbits,[38] and mice.[39, 40] However, human evidence of $H_2S$ donor efficacy against IH was lacking. Here we report, for the first time in human tissue, that a peptide hydrogel with sustained release of low levels of $H_2S$ inhibits VSMC proliferation and IH in an *ex-vivo* model of human vein culture.

Controlling the amount of $H_2S$ released is critical as relatively high doses of exogenous $H_2S$ (over 500–1000 ppm) lead to respiratory distress and death, hindering the use of $H_2S$ medications in humans. $H_2S$ donors release $H_2S$ by either hydrolysis or in response to a specific trigger such as a thiol or other nucleophiles.[11] We employed a thiol-triggered donor motif, which adds a level of control to the release and ensures more sustained release compared to passive hydrolysis. The peptide is highly soluble and self-assembles to form long nanoribbons stabilized by β-sheets, resulting in steady release in the range of hours, in stark contrast to the instantaneous release of $H_2S$ from NaHS. Importantly, Pep-$H_2S$ reduces IH at a 10-fold lower total sulfide dose than NaHS, which is likely due to the slower release kinetics, leading to better $H_2S$ bioavailability. In addition to reduced toxicity, a sustained release strategy is crucial for the prevention of IH in patients because the acute stage of IH development typically occurs during the first 30 days following the intervention.[41]

Local biodegradable sheaths, wraps, meshes, membranes, and cuffs have all been tested for perivascular applications. However, these solid solutions adapt poorly to the elasticity of vascular tissue. While solid forms are more stable over time, injectable semi-solid formulations, in particular hydrogels, present exciting alternatives as they are easily positioned and provide adequate coverage of the vessel.[42] Due to their ability to self-assemble into nanoribbons, both

Pep-$H_2S$ and Pep-Ctrl spontaneously form soft hydrogels at 1 wt. %, as measured by rheology, in aqueous solution in the presence of $CaCl_2$. Gel-$H_2S$ provides extended release compared to Pep-$H_2S$, with potentially increased efficacy in reducing IH *in-vivo.*[41] Most current hydrogel formulations involve the combination of a gel and a drug. The $H_2S$-releasing gel developed here has advantages over polymer-based gels because it is a fully biodegradable single small molecule with no polydispersity, and it requires no covalent crosslinking beyond addition of salt.

The protective effect of the $H_2S$-releasing peptide against IH is probably largely imparted by a direct inhibition of VSMC proliferation. Indeed, in line with previous reports,[39] we show that Pep-$H_2S$/Gel-$H_2S$ and NaHS inhibit human VSMC proliferation and transmigration, which are important features of pathogenic synthetic VSMCs involved in IH.[2] We further observed that the $H_2S$-releasing peptide and NaHS disrupt the normal cytoskeleton architecture of VSMCs, as evidenced by a modified pattern of calponin and SM22α immunostaining. Given the prominent role of cytoskeleton dynamics and remodeling during mitosis and cell migration, this disrupted pattern likely contributes to reduced VSMC proliferation and migration. Whether or not the protection imparted by the donors is directly mediated by $H_2S$ remains unknown. *S*-Aroylthiooxime compounds release $H_2S$ in the presence of thiols with intermediate formation of thiocysteine (cysteine persulfide).[23] Thus, the observed biological effects of Pep-$H_2S$/Gel-$H_2S$ may be attributable, at least in part, to cysteine persulfide or other related reactive sulfide species. Further studies will be conducted to identify the mechanism underlying the effects of $H_2S$/persulfide on the VSMC cytoskeleton.

In contrast to VSMCs, EC proliferation and transmigration is stimulated by Pep-$H_2S$/Gel-$H_2S$, consistent with previous reports showing that exogenous $H_2S$ stimulates HUVEC proliferation and migration *in vitro* [43,44] and has pro-angiogenic properties *in vivo*. [45, 46] This feature is of

particular interest in the context of IH. Indeed, EC dysfunction and death during vascular surgery plays a major role in the development of IH, and the pro-angiogenic effects of $H_2S$ might accelerate endothelium recovery following vascular trauma.[2]

Currently available local therapies, such as drug-eluting stents and balloons, are coated with non-specific cytotoxic (paclitaxel) and cytostatic (sirolimus) drugs. These devices may improve long-term vessel patency when compared with standard "bare" stents and balloons.[47, 48] However, their long-term effects on patient outcomes remain unclear, and recent evidence suggests a negative outcome for paclitaxel-coated devices and increased rate of complications.[5] Thus, local perivascular application of an $H_2S$-releasing gel might provide a unique therapeutic opportunity, with benefits on both VSMCs and ECs and without systemic toxicity.

### 3.6. Conclusion

To summarize, we developed and evaluated the therapeutic potential of an $H_2S$-releasing biodegradable hydrogel to limit the development of IH in human veins. The thiol-triggered, controlled $H_2S$ release from peptide hydrogels provides sustained $H_2S$ concentrations over a period of hours. Consequently, extended release of low levels of $H_2S$ from the peptide hydrogel inhibits VSMC proliferation and IH in human vein models more effectively than sulfide salts (NaHS). In contrast to its inhibitory effects on VSMCs, the $H_2S$-releasing peptide hydrogel facilitates *in vitro* HUVEC proliferation and transmigration, which may further assist in preventing IH and help the recovery after vascular intervention. In future efforts, we will evaluate the therapeutic potential of the perivascular application of $H_2S$-releasing gels at the site of vascular trauma following surgery in animal models of IH. Overall, we propose that application of such $H_2S$-releasing self-assembling peptide hydrogels may constitute a viable solution to limit IH in human vein grafts.

## 3.7. Experimental

*Chemicals*

Rink Amide MBHA resin and 9-fluorenylmethoxy carbonyl (Fmoc) protected L-amino acids were purchased from P3Biosystems and used as received. HBTU, *N*-methylpiperidine, DBU, and other reagents for peptide synthesis were purchased from commercial vendors and used as received unless otherwise noted. The solvents employed for peptide synthesis were reagent grade.

*Peptide synthesis and purification*

Peptides were synthesized either manually or using a Liberty1 microwave-assisted peptide synthesizer (CEM) using solid-phase peptide synthesis (SPPS) via standard Fmoc protocols as described previously.[23] 4-formylbenzoic acid was coupled to the N-terminus of the peptide on resin using HBTU and DIEA in DMF. After cleavage and isolation, peptides were dissolved in water containing 0.1% $NH_4OH$ and filtered through a 0.45 μm PTFE filter before purification. Purification by preparative-scale reverse phase high-performance liquid chromatography (RP-HPLC) was carried out on an Agilent Technologies 1260 Infinity HPLC system, eluting with a gradient of 2% ACN to 90% ACN in milliQ $H_2O$ over 33 min using an Agilent PLRP-S column (100 Å particle size, 25 x 150 mm) and monitoring at 220 nm. To both mobile phases was added 0.1% $NH_4OH$ to aid in solubility. Fractions were analyzed by mass spectrometry (Advion ExpressIon Compact Mass Spectrometer), and product-containing fractions were combined, rotovapped to remove ACN, and lyophilized (LabConco).

The lyophilized peptide FBA-IAVEE was dissolved in dry DMSO and reacted with *S*-benzoylthiohydroxylamine (SBTHA) in the presence of catalytic TFA to afford the final SATO-

FBA-IAVEE peptide. Peptide FBA-IAVEEEE was similarly reacted with *O*-benzyl hydroxylamine hydrochloride (OBHA·HCl) in dry DMSO, but without using TFA, to afford the non-$H_2S$-releasing control peptide OBHA-FBA-IAVEEEE. Peptides were dissolved in a mixture of phosphate buffer (100 mM at pH 7.4) and acetonitrile (5:2 v/v) and filtered through a 0.45 μm PTFE filter before purification. Purification was carried out using RP-HPLC, eluting with a gradient of 2% ACN to 90% ACN in milliQ $H_2O$ without any additives. The protocol for analysing and recovering the peptides was the same as described above. The final peptides were dissolved in milliQ water and distributed into aliquots (100 μg each). Aliquots were frozen, lyophilized, and stored at -20 $^oC$.

*Critical aggregation concentration (CAC) measurements*

Nile red stock solution in acetone (1 mg/mL) was diluted in milliQ water to a concentration of 0.01 mg/mL and was used to make all peptide solutions. A peptide stock solution was prepared at 4 mg/mL in the Nile red stock solution and was further diluted to the concentration of 3 mg/mL, 2 mg/mL, 1 mg/mL, 0.5 mg/mL, 0.25 mg/mL, 0.1 mg/mL, 0.01 mg/mL, 0.001 mg/mL, and 0.0001 mg/mL. All peptide dilutions were vortexed/sonicated for a few seconds, then 300 μL of each was transferred to a 96-well plate, and the plate was allowed to sit in dark for 15–20 min. Florescence spectra were recorded using a Varian Cary Eclipse fluorescence spectrophotometer (FL1105M003) with an excitation wavelength of 550 nm. Fluorescence intensity measured at 628 nm was plotted against log[concentration], and the final CAC values were estimated to be the point of intersection between the linear fits of high and low concentration regimes.

*Circular Dichroism (CD) Spectroscopy*

CD spectra were measured at room temperature using a Jasco J-815 CD spectrometer (Jasco Inc.) with a preset $N_2$ flow at 120 mL/min. The range of wavelengths employed was 250 to 190 nm (50 nm/min) with a response time of 8 s. Samples for both Pep-$H_2S$ and Pep-Ctrl were freshly prepared at 10 mM (20 μL) in 1X PBS (pH 7.4) and were analyzed using a dismountable quartz cuvette with path length of 0.2 mm with 3 iterations for each sample. Raw spectra were converted to mean residual ellipticity for comparison.

*Hydrogelation*

Both Pep-$H_2S$ and Pep-Ctrl formed hydrogels in PBS solutions (Gel-$H_2S$ and Gel-Ctrl) at physiological pH upon addition of 4 μL of $CaCl_2$ solution (200 mM in water) to 90 μL of peptide solution (10 mM in 1X PBS). The final concentration of $CaCl_2$ in the hydrogels was 8 mM.

*Rheology*

Rheological experiments were done on an AR-2000 (TA instruments) using a 25 mm parallel plate geometry. Buffered peptide solutions (240 μL, 1 wt.% peptide, ~10 mM) were prepared for each peptide in 1X PBS (pH 7.4) and quickly transferred to the rheometer's bottom geometry. Gelation was initiated upon addition of 10 μL $CaCl_2$ solution (200 mM in water), and the resulting solution was mixed thoroughly with a pipet tip to ensure homogeneity. After allowing the solution to gel for 10 min, the upper geometry was lowered to a pre-set gap of 500 μm, and a dynamic time sweep was performed at a frequency of 1 Hz and 0.5% strain to measure storage (G') and loss (G") moduli. Each time sweep was followed by a dynamic frequency sweep (0.010-100 Hz at 0.5% strain) and a strain sweep (1 Hz at 0.5-100% strain).

*Morphology analysis via TEM*

Peptide solutions (10 mM in 0.05 M phosphate buffer at pH 7.4) were prepared and allowed to age overnight, then diluted with water to 500 μM. Next, 10 μL of the peptide solution was deposited on a carbon-coated copper TEM grid (300 mesh, Electron Microscopy Sciences), allowed to sit for 5–6 min, and then gently blotted with filter paper. The grid was then washed by adding a drop of MilliQ water, allowing it to stand for 1 min, and then blotting with filter paper. Samples were stained with 10 μL of a 2% uranyl acetate aqueous solution for 5–6 min, blotted with filter paper, and allowed to dry in air before TEM observation. Images were taken on a Philips EM420 TEM with a slow scan CCD camera.

*$H_2S$ release measurements using an electrode probe*

$H_2S$ release from the peptides was measured amperometrically using an electrode probe (ISO-$H_2S$-100-CXX, World Precision Instruments). A solution of either Pep-$H_2S$ or Pep-Ctrl (20 μL of 0.1 mM solution in 1X PBS) was placed in an inner well inside a specially designed glass vial equipped with a stir bar. An additional 76 μL of 10 mM PBS buffer at pH 7.4 was then added to the well, followed by 4 μL L-Cys solution (5 mM in water). The final concentrations in the inner well were 20 μM in peptide and 0.2 mM (10 equiv) in L-Cys. The well was immediately covered with the gas-permeable membrane (Breathe easier, Diversified Bioteck), and PBS buffer at pH 7.4 (4.95 mL) mixed with 50 μL of diethylenetriaminepentaacetic acid (DTPA) solution (10 mM in water) was added into the vial, covering the inner well. The $H_2S$-selective microelectrode was then immersed in the PBS solution, and the output signal was recorded. Similarly, $H_2S$ release from Pep-$H_2S$ at 200 μM was measured by mixing 20 μL of peptide solution (1 mM) with 80 μL of PBS in the well followed by addition of 1 μL (10 equiv) L-Cys solution (200 mM in water).

$H_2S$ release from Gel-$H_2S$ was measured by placing 96 μL of the peptide solution (10 mM in 1X PBS) in the inner well followed by 4 μL of $CaCl_2$ to form a hydrogel. 10 μL L-Cys solution (200 mM in water) was added, the well was covered with the membrane, and output signal was measured as above. Calibration was carried out as previously reported.[24]

*Cell culture*

Human veins were obtained from donors who underwent lower limb bypass surgery.[25] For static vein cultures, 5 mm segments were kept for 7 days in RPMI-1640 Glutamax supplemented with 10 % FBS and 1% antibiotic solution (10,000 U/mL penicillin G, 10,000 U/mL streptomycin sulphate) at 37 °C, 5% $CO_2$ and 5% $O_2$. The cell culture medium was changed every 48 h. The hydrogels were prepared by dissolving the peptides at 10 mM in PBS, then adding 8 mM final concentration of $CaCl_2$ to achieve gelation. The hydrogels (10 or 20 μL/mL) were then added to the vein segments in the media. No remaining gel was found after 48 h of culture. Freshly prepared gel was added when changing the media every 48 h.

The segments of vein were then fixed in 4% formalin and paraffin-embedded for histological analysis. Five distinct vein segments coming from five different patients were used in this study.

Human smooth muscle cells were prepared from these human saphenous vein segments as previously described.[25] Briefly, 1–2 mm vein explants were plated on the dry surface of a 6-well culture plate coated with 1% Gelatin type B (Sigma-Aldrich) and maintained in RPMI, 10% FBS 1% antibiotic solution medium in a 37 °C, 5% $CO_2$, 5% $O_2$ environment. Because ECs could not be isolated from the vein segments, HUVECs purchased from Lonza were maintained in EGM™-2 (Endothelial Cell Growth Medium-2 BulletKit™) at 37 °C, 5% $CO_2$ and 5% $O_2$. Passages 1 to 8 were used for the experiments.

*Histomorphometry and Immunohistochemistry*

Segments of vein (5 mm) embedded in paraffin were cut into 5 µm sections. 2-mm out of 5-mm were cut in 4 series of 10 slides with 5 sections per slides with a 250 µm interval between the series. One slide per series was stained using Van Gieson-elastin (VGEL) staining. 3 images per section were taken at 100x magnification to cover the whole vein area. 8 measurements of the intima and media thicknesses were made from the images, evenly distributed along the length of the vein wall.[26] Thus, for each vein, the intima and media thicknesses values are a mean of 4 series x 3 images x 8 measures = 96 independent measures. Morphometric measurements were done by two independent researchers, one of them blind to the experimental groups, using the Leica Qwin® software (Leica, Switzerland).

PCNA (proliferating cell nuclear antigen) immunohistochemistry was performed on paraffin sections. After rehydration and antigen retrieval (TRIS-EDTA buffer, pH 9, 15 min in a microwave at 600 watts), human vein sections were incubated overnight with the proliferating cell nuclear antigen antibody (PCNA; M087901, Dako, Baar, Switzerland), washed and revealed using the EnVision +/HRP, DAB+ system according to manufacturer's instructions (Dako, Baar, Switzerland), and counterstained with hematoxylin.[27] One slide per series was assessed and 3 images per section were taken at 100x magnification. The PCNA and hemotoxlin positive nuclei were manually counted by two independent observers unaware of the conditions.

*Immunofluorescent staining*

Cell immunostaining was performed on cells grown on glass coverslips ($10^6$ cells per well in 24 well plates) and fixed for 5 min in methanol at −20 °C. Cells were then permeabilized in PBS supplemented with 2 wt. % BSA and 0.3 vol. % Triton X-100 for 30 min, blocked in PBS

supplemented with 2 wt. % BSA and 0.1 vol. % Tween 20 for another 30 min, and incubated overnight with the primary antibodies diluted in the same buffer. BrdU immunostaining was performed using mouse anti-BrdU (BD Bioscience 55627, 1:200) and fluorescent-labelled anti-mouse secondary antibodies (AlexaFluor 568; 1/500, Thermo Fisher Scientific). BrdU positive nuclei were automatically detected using the ImageJ software and normalized to the total number of DAPI-positive nuclei. Double calponin/SM22α immunofluorescent staining was performed using mouse anti human calponin (DAKO; M3556; 1/200) and rabbit anti-human SM22α, (Abcam; 4106; 1/400). Cells were then washed 3 times for 5 min in PBS supplemented with 0.1 vol. % Tween 20, and incubated for 1 h at room temperature with a mix of fluorescent-labelled secondary antibodies (anti-rabbit AlexaFluor 488 and anti-mouse AlexaFluor 568; 1/500).

*Live-cell hydrogen sulfide measurement*

Free sulfide was measured in cells using the $SF_7$-AM fluorescent probe[28] (Sigma-Aldrich cat: 748110). The probe was dissolved in anhydrous DMF at 5 mM. $10^5$ cells per well were plated in a 96 well plate. After 24 h, $SF_7$-AM (5 μM) was added to VSMCs or HUVECs, and fluorescence intensity ($\lambda_{ex}$ = 495 nm; $\lambda_{em}$ = 520 nm) was measured continuously in a Synergy Mx fluorescent plate reader at 37 °C before and after addition of various donors as indicated. Linear regressions of the $SF_7$-AM fluorescent signal were calculated during the linear part of the curves generated to measure the $H_2S$ release rate.

*Transmigration assays*

The chemotactic-induced cell transmigration across a matrix barrier was investigated using a Boyden chamber made of a polycarbonate membrane insert with 8 mm pores (Falcon; BD Biosciences) placed in 24-well culture plates. $10^5$ VSMCs resuspended in 300 μL of RPMI 1640 medium were plated onto the transwell. Transwells with VSMCs were placed in a 24-well plate

with 400 µL of EGM-2 culture medium after 48 h in contact with HUVECs. $10^5$ HUVECs resuspended in 300 µL of EBM™-2 (Endothelial Cell Growth Basal Medium-2, no supplements from Lonza) were plated in a transwell and placed in a 24-well plate with 400 µL of fresh complete EGM-2 BulletKit™ culture medium (with full supplements). In experiments with gels (Gel-$H_2S$ and Gel-Ctrl), 10 µL/mL of gel (1 wt. %) was placed in the 24-well plate. After 8 h, calcein-AM (5 µg/mL, Thermo) was added to the well to stain the cells on the outer surface of the membrane of the transwell. After 30 min and two washes with PBS, fluorescence was measured using a fluorescent plate reader ($\lambda_{ex}$ = 485 nm; $\lambda_{em}$ = 530 nm). Cells were also imaged using an inverted fluorescent microscope (Leica AG).

*Statistical analyses*

All experiments were quantitatively analyzed using GraphPad Prism® 6, and results are shown as mean ± SEM. One-way ANOVA tests were performed followed by multiple comparisons using *post-hoc* t-tests with the appropriate correction for multiple comparisons.

### 3.8. References


(1) Simpson, E. L.; Kearns, B.; Stevenson, M. D.; Cantrell, A. J.; Littlewood, C.; Michaels, J. A. Enhancements to angioplasty for peripheral arterial occlusive disease: systematic review, cost-effectiveness assessment and expected value of information analysis. *Health. Technol. Assess.* **2014**, 18, 1–252.

(2) Curcio, A.; Torella, D.; Indolfi, C. Mechanisms of smooth muscle cell proliferation and endothelial regeneration after vascular injury and stenting: approach to therapy. *Circul. J.* **2011**, 75, 1287–1296.

(3) Sharma, S.; Christopoulos, C.; Kukreja, N.; Gorog, D. A. Local drug delivery for percutaneous coronary intervention. *Pharmacol. Therapeut.* **2011**, 129, 260–266.

(4) Seedial, S. M.; Ghosh, S.; Saunders, R. S.; Suwanabol, P. A.; Shi, X.; Liu, B.; Kent, K.C. Local drug delivery to prevent restenosis. *J. Vasc. Surg.* **2013**, 57, 1403–1414.

(5) Katsanos, K.; Spiliopoulos, S.; Kitrou, P.; Krokidis, M.; Karnabatidis, D. Risk of Death Following Application of Paclitaxel-Coated Balloons and Stents in the Femoropopliteal Artery of the Leg: A Systematic Review and Meta-Analysis of Randomized Controlled Trials. *J. Am. Heart Assoc.* **2018**, 7, 011245.

(6) Szabo, C. A timeline of hydrogen sulfide (H2S) research: From environmental toxin to biological mediator. *Biochem. Pharmacol.,* **2018**, 149, 5-19.

(7) Wallace, J. L.; Wang, R. Hydrogen sulfide-based therapeutics: exploiting a unique but ubiquitous gasotransmitter. *Nat. Rev. Drug. Discov.* **2015**, 14, 329-345.

(8) Chen, Y. H.; Yao, W. Z.; Geng, B.; Ding, Y. L.; Lu, M.; Zhao, M. W.; Tang, C. S. Endogenous hydrogen sulfide in patients with COPD. *Chest* **2005**, 128, 3205-3211.

(9) Rajpal, S.; Katikaneni, P.; Deshotels, M.; Pardue, S.; Glawe, J.; Shen, X.; Akkus, N.; Modi, K.; Bhandari, R.; Dominic, P.; Reddy, P.; Kolluru, G. K.; Kevil, C. G. Total sulfane sulfur bioavailability reflects ethnic and gender disparities in cardiovascular disease. *Redox. Biol.* **2018**, 15, 480-489.

(10) Islam, K. N.; Polhemus, D. J.; Donnarumma, E.; Brewster, L. P.; Lefer, D. J. Hydrogen Sulfide Levels and Nuclear Factor-Erythroid 2-Related Factor 2 (NRF2) Activity Are Attenuated in the Setting of Critical Limb Ischemia (CLI). *J. Am. Heart Assoc.* **2015,** 4, 1-10.

(11) Powell, C. R.; Dillon, K. M.; Matson, J. B. A review of hydrogen sulfide (H2S) donors: Chemistry and potential therapeutic applications. *Biochem. Pharmacol.* **2018**, 149, 110-123.

(12) Hartle, M. D.; Pluth, M. D. A practical guide to working with H2S at the interface of chemistry and biology. *Chem. Soc. Rev*. **2016**, 45, 6108-6117.

(13) Xiao, Z.; Bonnard, T.; Shakouri-Motlagh, A.; A L Wylie, R.; Collins, J.; Heath, D.; Hagemeyer, C.; Connal, L. A. Triggered and Tunable Hydrogen Sulfide Release from Photo-Generated Thiobenzaldehydes. *Chem. Eur. J.* **2017**, 23, 11294-11300.

(14) Ercole, F.; Whittaker, M. R.; Halls, M. L.; Boyd, B. J.; Davis, T. P.; Quinn, J. F. Garlic-inspired trisulfide linkers for thiol-stimulated $H_2S$ release. *Chem. Commun.* **2017**, 53, 8030-8033.

(15) Foster, J.C.; Radzinski, S. C.; Zou, X.; Finkielstein, C. V.; Matson, J. B. $H_2S$-Releasing Polymer Micelles for Studying Selective Cell Toxicity. *Mol. Pharm*. **2017**, 14, 1300-1306.

(16) Feng, S.; Zhao, Y.; Xian, M.; Wang, Q. Biological thiols-triggered hydrogen sulfide releasing microfibers for tissue engineering applications. *Acta. Biomater*. **2015**, 27 205-213.

(17) Wu, J.; Li, Y.; He, C.; Kang, J.; Ye, J.; Xiao, Z.; Zhu, J.; Chen, A.; Feng, S.; Li, X.; Xiao, J.; Xian, M.; Wang, Q. Novel $H_2S$ Releasing Nanofibrous Coating for In Vivo Dermal Wound Regeneration. *ACS Appl. Mater. Interfaces* **2016**, 8, 27474-27481.

(18) Yang, C. T.; Chen, L.; Xu, S.; Day, J. J.; Li, X.; Xian, M. Recent Development of Hydrogen Sulfide Releasing/Stimulating Reagents and Their Potential Applications in Cancer and Glycometabolic Disorders. *Front. Pharmacol.* **2017**, 8, 664-677.

(19) Qian, Y.; Matson, J. B. Gasotransmitter delivery via self-assembling peptides: Treating diseases with natural signaling gases. *Adv. Drug Deliv. Rev*. **2017**, 110-111, 137-156.

(20) Wang, Y.; Cheetham, A. G.; Angacian, G.; Su, H.; Xie, L. S.; Cui, H. G. Peptide-drug conjugates as effective prodrug strategies for targeted delivery. *Adv. Drug Deliver. Rev.* **2017**, 110, 112-126.

(21) Kapadia, M. R.; Chow, L. W.; Tsihlis, N. D.; Ahanchi, S. S., Eng, J. W.; Murar, J.; Martinez, J.; Popowich, D. A.; Jiang, Q.; Hrabie, J. A.; Saavedra, J. E.; Keefer, L. K.; Hulvat, J.

F.; Stupp, S. I.; Kibbe, M. R. Nitric oxide and nanotechnology: a novel approach to inhibit neointimal hyperplasia. *J. Vasc. Surg.* **2008**, 47, 173-82.

(22) Carter, J. M.; Qian, Y.; Foster, J. C.; Matson, J. B. Peptide-based hydrogen sulphide-releasing gels. *Chem. Commun*. **2015**, 51, 13131-13134.

(23) Qian, Y., Kaur, K.; Foster, J. C.; Matson, J. B. Supramolecular Tuning of $H_2S$ Release from Aromatic Peptide Amphiphile Gels: Effect of Core Unit Substituents. *Biomacromolecules* **2019**, 20, 1077-1086.

(24) Foster, J. C.; Powell, C. R.; Radzinski, S. C.; Matson, J. B. *S*-aroylthiooximes: a facile route to hydrogen sulfide releasing compounds with structure-dependent release kinetics. *Org. Lett.*, **2014**, 16, 1558-1561.

(25) Dubuis, C.; May, L.; Alonso, F.; Luca, L.; Mylonaki, I.; Meda, P.; Delie, F.; Jordan, O.; Deglise, S.; Corpataux, J. M.; Saucy, F.; Haefliger, J. A. Atorvastatin-loaded hydrogel affects the smooth muscle cells of human veins. *J. Pharmacol. Exp. Ther.*, **2013**, 347, 574-581.

(26) Longchamp, A.; Alonso, F.; Dubuis, C.; Allagnat, F.; Berard, X.; Meda, P.; Saucy, F.; Corpataux, J. M.; Deglise, S.; Haefliger, J. A. The use of external mesh reinforcement to reduce intimal hyperplasia and preserve the structure of human saphenous veins. *Biomaterials*, **2014**, 35, 2588-2599.

(27) Allagnat, F.; Haefliger, J. A.; Lambelet, M.; Longchamp, A.; Berard, X.; Mazzolai, L.; Corpataux, J. M.; Deglise, S. Nitric Oxide Deficit Drives Intimal Hyperplasia in Mouse Models of Hypertension. *Eur. J. Vasc. Endovasc. Surg.*, **2016**, 51, 733-742.

(28) Lin, V. S.; Lippert, A. R.; Chang, C. J. Cell-trappable fluorescent probes for endogenous hydrogen sulfide signaling and imaging $H_2O_2$-dependent $H_2S$ production. *Proc. Natl. Acad. Sci. USA*, **2013**, 110, 7131-7135.

(29) Fleming, S.; Debnath, S.; Frederix, P. W.; Tuttle, T.; Ulijn, R. V. Aromatic peptide amphiphiles: significance of the Fmoc moiety. *Chem. Commun.*, **2013,** 49, 10587-10589.

(30) Fleming, S.; Ulijn, R. V. Design of nanostructures based on aromatic peptide amphiphiles. *Chem. Soc. Rev*., **2014**, 43, 8150-8177.

(31) Mart, R. J.; Osborne, R. D.; Stevens, M. M.; Ulijn, R. V. Peptide-based stimuli-responsive biomaterials. *Soft Matter,* **2006**, 2, 822-835.

(32) Smith, A. M.; Williams, R. J.; Tang, C.; Coppo, P.; Collins, R. F.; Turner, M. L.; Saiani, A.; Ulijn, R. V. Fmoc-Diphenylalanine Self Assembles to a Hydrogel via a Novel Architecture Based on π–π Interlocked β-Sheets. *Adv. Mater.*, **2008**, 20, 37-41.

(33) Matson, J. B.; Stupp, S. I. Self-assembling peptide scaffolds for regenerative medicine. *Chem. Commun.*, **2012**, 48, 26-33.

(34) Wang, Y.; Kaur, K.; Scannelli, S. J.; Bitton, R.; Matson, J. B. Self-Assembled Nanostructures Regulate $H_2S$ Release from Constitutionally Isomeric Peptides. *J. Am. Chem. Soc.*, **2018**, 140, 14945-14951.

(35) Stendahl, J. C.; Rao, M. S.; Guler, M. O.; Stupp, S. I. Intermolecular Forces in the Self-Assembly of Peptide Amphiphile Nanofibers. *Adv. Funct. Mater*., **2006**, 16, 499-508.

(36) Katsouda, A.; Bibli, S. I.; Pyriochou, A.; Szabo, C.; Papapetropoulos, A. Regulation and role of endogenously produced hydrogen sulfide in angiogenesis. *Pharmacol. Res.*, **2016**, 113, 175-185.

(37) Meng, Q. H.; Yang, G.; Yang, W.; Jiang, B.; Wu, L.; Wang, R. Protective effect of hydrogen sulfide on balloon injury-induced neointima hyperplasia in rat carotid arteries. *Am. J. Pathol.*, **2007**, 170, 1406-1414.

(38) Ma, B.; Liang, G.; Zhang, F.; Chen, Y.; Zhang, H. Effect of hydrogen sulfide on restenosis of peripheral arteries after angioplasty. *Mol. Med. Rep.*, **2012**, 5, 1497-1502.

(39) Yang, G.; Li, H.; Tang, G.; Wu, L.; Zhao, K.; Cao, Q.; Xu, C.; Wang, R. Increased neointimal formation in cystathionine gamma-lyase deficient mice: role of hydrogen sulfide in alpha5beta1-integrin and matrix metalloproteinase-2 expression in smooth muscle cells. *J. Mol. Cell. Cardiol.*, **2012**, 52, 677-688.

(40) Yang, G.; Wu, L.; Bryan, S.; Khaper, N.; Mani, S.; Wang, R. Cystathionine gamma-lyase deficiency and overproliferation of smooth muscle cells. *Cardiovasc. Res.*, **2010**, 86, 487-495.

(41) Owens, C. D.; Gasper, W. J.; Rahman, A. S.; Conte, M. S. Vein graft failure. *J. Vasc. Surg.*, **2015**, 61, 203-216.

(42) Mylonaki, I.; Allemann, E.; Saucy, F.; Haefliger, J. A.; Delie, F.; Jordan, O. Perivascular medical devices and drug delivery systems: Making the right choices. *Biomaterials*, **2017**, 128, 56-68.

(43) Potenza, D. M.; Guerra, G.; Avanzato, D.; Poletto, V.; Pareek, S.; Guido, D.; Gallanti, A.; Rosti, V.; Munaron, L.; Tanzi, F.; Moccia, F. Hydrogen sulphide triggers VEGF-induced intracellular Ca(2)(+) signals in human endothelial cells but not in their immature progenitors. *Cell Calcium*, **2014**, 56, 225-234.

(44) Longchamp, A.; Mirabella, T.; Arduini, A.; MacArthur, M. R.; Das, A.; Trevino-Villarreal, J. H.; Hine, C., Ben-Sahra, I.; Knudsen, N. H.; Brace, L. E.; Reynolds, J.; Mejia, P.; Tao, M.; Sharma, G.; Wang, R.; Corpataux, J. M.; Haefliger, J. A.; Ahn, K. H.; Lee, C. H.; Manning, B. D.; Sinclair, D. A.; Chen, C. S.; Ozaki, C. K.; Mitchell, J. R. Amino Acid

Restriction Triggers Angiogenesis via GCN2/ATF4 Regulation of VEGF and $H_2S$ Production. *Cell*, **2018**, 173, 117-129.

(45) Kanagy, N. L.; Szabo, C.; Papapetropoulos, A. Vascular biology of hydrogen sulfide, American journal of physiology. *Cell Physiol*., **2017**, 312, C537-C549.

(46) Papapetropoulos, A.; Pyriochou, A.; Altaany, Z.; Yang, G.; Marazioti, A.; Zhou, Z.; Jeschke, M. G.; Branski, L. K.; Herndon, D. N.; Wang, R.; Szabo, C. Hydrogen sulfide is an endogenous stimulator of angiogenesis. *Proc. Natl. Acad. Sci. USA*, **2009**, 106, 21972-21977.

(47) van den Berg, J. C. Drug-eluting balloons for treatment of SFA and popliteal disease - A review of current status. *Eur. J. Radiol*., **2017**, 91, 106-115.

(48) Ramakrishna, C. D.; Dave, B. A.; Kothavade, P. S.; Joshi, K. J.; Thakkar, A. S. Basic Concepts and Clinical Outcomes of Drug-Eluting Balloons for Treatment of Coronary Artery Disease: An Overview. *J. Clin. Diagn. Res*., **2017**, 11, OE01-OE04.

## Chapter 4. Linker-Regulated $H_2S$ Release from Aromatic Peptide Amphiphile Hydrogels

4.1 Authors

Kuljeet Kaur, Yin Wang, and John B. Matson

Department of Chemistry, Virginia Tech, Virginia Tech Center for Drug Discovery, Macromolecules Innovation Institute, Virginia Tech, Blacksburg, VA, 24061

### 4.2 Abstract

Controlled release is an essential requirement for delivery of hydrogen sulfide ($H_2S$) because of its reactive nature, short half-life in biological fluids, and toxicity at high concentrations. In this context, $H_2S$ delivery via hydrogels may be beneficial as they can deliver $H_2S$ locally at the site of interest. Herein, we employed hydrogels based on aromatic peptide amphiphiles (APAs) with tunable mechanical properties to modulate the rates of $H_2S$ release. The APAs contained an aromatic *S*-aroylthiooxime $H_2S$ donor attached with a linker to a short IAVEEE hexapeptide. Linker units included carbonyl, substituted *O*-methylenes, alkenyl, and alkyl segments, with the goal of evaluating the role of linker structure on self-assembly, capacity for hydrogelation, and $H_2S$ release rate. We studied each peptide by transmission electron miscroscopy, circular dichroism spectroscopy, and rheology, and we measured $H_2S$ release rates using an $H_2S$-selective electrode probe. We found that the rate of $H_2S$ release from the hydrogels correlated inversely with hydrogel storage modulus, with stiffer gels showing faster release. We attribute this relationship to the differential rate of diffusion of cysteine, the trigger for $H_2S$ release from SATOs, through hydrogels of varying stiffness.

## 4.3 Introduction

Supramolecular materials find extensive use in drug delivery, tissue engineering, 3-D cell culture, regenerative medicine, and several other fields of biomedical research.[1, 2] In particular, self-assembling amphiphilic peptides have garnered much attention due to their ease of synthesis, tunability, and biocompatibility in many contexts.[3-5] Aromatic peptide amphiphiles (APAs) belong to a class of self-assembling peptides that bear an N-terminal aromatic unit and a short peptide chain attached with a linker. APAs self-assemble in aqueous solution as a result of hydrophobic and aromatic stacking interactions combined with H-bonding in the peptide chain, creating supramolecular nanoassemblies including spheres, cylinders, filaments, ribbons, coils, and others.[6] Furthermore, the self-assembly and hydrogelation of APAs can be controlled by several factors, including pH, temperature, and concentration, with synergistic contributions from individual structural units (aromatic group, peptide chain, and linker).[7-12] Therefore, APAs allow fine tuning of macroscopic properties through design modifications and can be potentially useful as efficient drug delivery systems.

APA hydrogels have been used as carriers of drugs, antigens, proteins, and other therapeutics.[13, 14] However, their ability to regulate payload delivery via small structural modifications in the linker segment has not been widely explored. The linker segment controls the spatial orientation of the aromatic unit relative to the peptide chain. As a result, subtle alterations in linker length and flexibility can influence both molecular packing and the ability of APAs to form gels.[7, 15-18] Herein, we investigate the effect of various linker segments on the rheological properties and drug release rates from a specific type of APA designed to release therapeutic doses of hydrogen sulfide ($H_2S$).

$H_2S$ is a signalling gas (gasotransmitter) that regulates various (patho)physiological processes, including cardioprotection,[19] vasodilation,[20] neurotransmission,[21] inflammation,[22, 23] and others.[24] However, in order to study $H_2S$ biology and potentially use it therapeutically, delivery strategies are needed. Its acute toxicity at high concentrations and short *in vivo* half-life makes it crucial to precisely control and confine $H_2S$ release to the site of interest.[25-29] While several polymeric and supramolecular $H_2S$ donors show controllable $H_2S$ release, [30, 31] most lack the capacity for localized release. Supramolecular hydrogels enable localized drug release,[32] so it is beneficial to understand how small changes to APA chemical structures affect the macroscopic properties of $H_2S$-releasing peptide hydrogels.

$H_2S$-releasing APA hydrogels, first reported from our lab in 2015, consist of a small peptide chain (typically 2–7 amino acids) with an *S*-aroylthiooxime (SATO) covalently attached to the N-terminus via a linker segment.[33] SATOs are thiol-triggered aromatic $H_2S$ donors,[34] and in recent work, we have shown that substitution on the aromatic ring of $H_2S$-releasing APAs can affect the rate of release of $H_2S$ from these hydrogels.[26] Herein, we aimed to investigate how the chemical structure of the linker segment affects the self-assembly, rheological behavior, and $H_2S$-releasing capacity of a series of $H_2S$-releasing APA hydrogels. We reasoned that by controlling the diffusion of cysteine into the hydrogel network, we could control the rate and duration of $H_2S$ release from these hydrogels. We hypothesized that stiffer hydrogels with slow diffusion of cysteine would show more gradual $H_2S$ release compared to their more flexible counterparts.

## 4.4 Results and Discussion

### Peptide design and synthesis

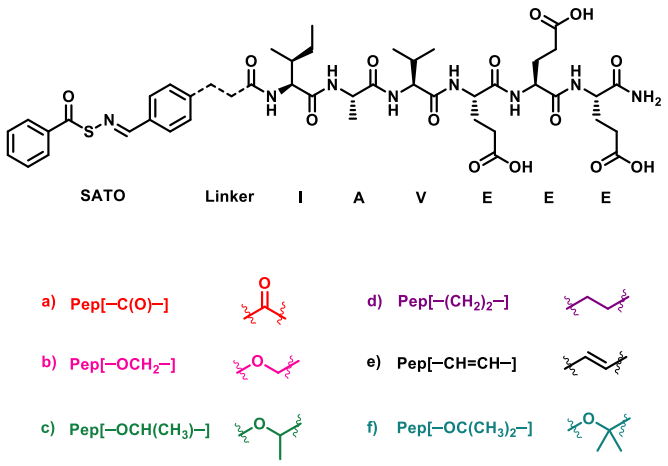


**Scheme 4.1.** Chemical structure of six APAs with different linker segments.

Previously, we reported an APA with a short carbonyl linker (Pep[–C(O)–]) that formed a robust hydrogel.[33] In order to investigate the effect of linker structure on self-assembly, hydrogelation, and $H_2S$ release profile, we synthesized five additional peptides with linkers *O*-methylene (Pep[–$OCH_2$–]), *O*-methyl-methylene (Pep[–$OCH(CH_3)$–]), ethyl (Pep[–$(CH_2)_2$–]), ethenyl (Pep[–CH=CH–]), and *O*-dimethyl-methylene (Pep [–$OC(CH_3)_2$–]) (Scheme 1). We speculated that the alkyl and *O*-methylene linkers would provide additional flexibility relative to the carbonyl linker, whereas the alkenyl linker would have restricted rotation compared with alkyl. We included *O*-methylene linkers with zero, one, or two pendant methyl groups to investigate the steric effects of methyl group substitution on the $CH_2$ carbon.

All six peptides were synthesized via solid-phase peptide synthesis as described in our previous work.[35] *S*-Benzylthiohydroxylamine (SBTHA) was covalently attached to the peptide fragment IAVEEE via an aryl aldehyde group on each linker segment, generating the $H_2S$-releasing SATO functional group and yielding the $H_2S$-releasing APAs. The nomenclature of each peptide consists of two parts: the first part depicts the physical state of the peptide (Pep or Gel), and the

second part depicts the type of linker (e.g., the soluble form of the peptide with the $–OCH_2–$ linker is referred to as Pep[$–OCH_2–$], while its hydrogel is referred to as Gel[$–OCH_2–$]).

**Secondary structure of APAs**

The first step toward understanding the molecular packing of the APAs was the measurement of their critical aggregation concentration (CAC), a minimum concentration above which self-assembly occurs. CAC values for all APAs were in the range of 0.8-1.0 mg/mL (~1 mM) as measured by the Nile red assay (Figure S5). This range is consistent with CAC measurements for APAs with similar structures.[26]

Next, we utilized circular dichroism (CD) spectroscopy to investigate the secondary structures of the APAs. Below the CAC (0.25 mg/mL), all peptides showed a characteristic random coil spectrum with a minimum around 200 nm (Figure 1A). However, above the CAC (10 mg/mL), differences in secondary structures of the APAs were observed (Figure 1B). Because the peptide backbone for all APAs is the same, any differences in their secondary structures should be a result of the linker segment and the role it plays in directing secondary structure. Linker [–C(O)–] showed a β-sheet signature with a minimum around 219 nm, but it lacked the typical peak near 197 nm. Similarly, Pep[$–OCH_2–$] and Pep[$–OCH(CH_3)–$], formed what appeared to be twisted β-sheets, characterized by red-shifted minima and maxima around 222 nm and 206 nm, respectively. Pep[$–(CH_2)_2–$] also showed a minimum at 214 nm along with an additional small negative peak around 195 nm suggesting that the observed structure may have some random coil character mixed with β-sheet. Pep[$–OC(CH_3)_2–$], on the other hand, showed an even stronger minimum around 199 nm suggesting a higher degree of random coil character. Interestingly, Pep[–CH=CH–] showed a small minimum at 208 nm along with a strong negative peak at 225

nm, indicating some α-helical character. Although definitive interpretations of the CD data are difficult, in part due to SATO absorptions in the 190–240 nm region, the differences observed in the secondary structures of APA hydrogels highlight the importance of the linker segment in dictating the secondary structure of the APAs.

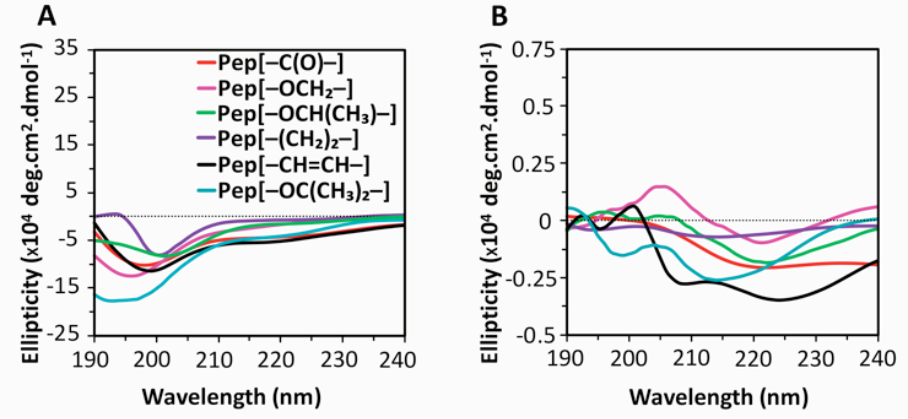


**Fig. 4.1.** Circular dichroism spectra of APA solutions at concentration of **A)** 0.25 mg/mL and **B)** 10 mg/mL in 1X phosphate buffer (PB).

## Morphology of APAs

To further understand the self-assembling behavior and to probe supramolecular structures formed by these APAs, we used transmission electron microscopy (TEM) (Figure 2). APA solutions well above their CAC (10 mg/mL) were aged overnight, diluted to 0.5 mg/mL, and quickly cast onto grids before staining with uranyl acetate. Pep[–C(O)–] formed long continuous fibrils, which were a few micrometres in length with average widths around 5 nm (Figure 2A). In the case of the *O*-methylene linkers, both Pep[–$OCH_2$–] and Pep[–$OCH(CH_3)$–] formed long and wide twisted nanoribbons with widths around 9 nm (Figure 2B and C), similar to literature reports on APAs containing similar linkers.[15-17] Pep[–$(CH_2)_2$–], on the other hand, formed short twisted nanoribbons with an average width of around 7 nm (Figure 2D). Several short fragments were also observed suggesting some disrupted packing, which is in agreement with the presence

of a substantial random coil peak in the CD spectrum for this peptide. Lastly, Pep[–CH=CH–] showed narrow, twisted nanoribbons with widths around 6 nm (Figure 2E). Although both [–CH=CH–] and [–C(O)–] are considered rigid, the observed differences in their morphologies may result from the hydrogen-bond accepting capability of the carbonyl in Pep[–C(O)–]. Furthermore, APAs with flexible linkers like Pep[–$OCH_2$–], Pep[–$(CH_2)_2$–], and Pep[–$OCH(CH_3)$–] formed twisted nanoribbons with fairly similar widths. However, there were notable differences in the pitch lengths of these three APAs, with values of 350 ± 50 nm, 220 ± 40 nm, and 100 ± 10 nm, respectively (Figure S6). The differences in the pitch lengths for Pep[–$OCH_2$–] and Pep[–$(CH_2)_2$–] may be due to the additional O atom in Pep[–$OCH_2$–], which may facilitate long range packing through additional H-bonding, as has been observed in related APAs.[16] On the other hand, the nanoribbons formed by Pep[–$OCH(CH_3)$–] showed smaller pitch lengths relative to Pep[–$OCH_2$–] and Pep[–$(CH_2)_2$–], possibly due to steric repulsions caused by the additional methyl group, which may drive the nanoribbons to twist at shorter intervals. This was further validated by examining the TEM image of Pep[–$OC(CH_3)_2$–] (Figure 2F); in this APA with two methyl groups on the linker carbon, no well-defined morphology was observed.

The differences in twisting pitch among the self-assembled structures of the APAs appears to be a result of how linker flexibility drives packing. Aggeli et al. determined in 2001 that in the case of long pitch length, β-sheets form closely packed assemblies and stack to form ribbons; in contrast, if the natural pitch length is small, then more loosely packed assemblies like fibrils are preferred.[36] More recently, Cui et al. observed similar effects in drug-conjugated peptides.[37] This is consistent with our observations that the flexible linkers, ([–$OCH_2$–], [–$OCH(CH_3)$–], and [–$(CH_2)_2$–]) formed less twisted and hence comparatively broader nanoribbons compared to rigid linkers ([–C(O)–] and [–CH=CH–]), which formed narrow, fibril-like structures. The observed

differences in the morphology of the APAs further confirms the role played by subtle alterations in the linker segment in controlling the self-assembly of APAs.

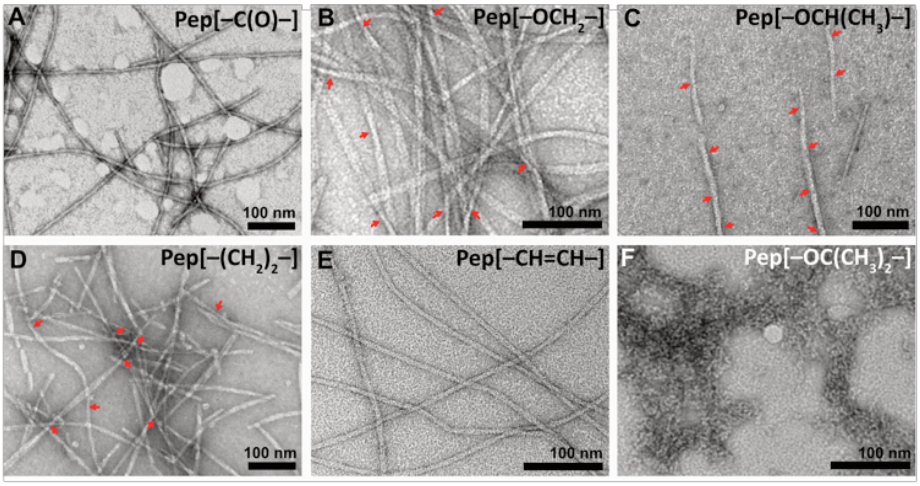


**Fig. 4.2.** TEM micrographs of self-assembling APAs. **A)** Pep [–C(O)–], **B)** Pep [–$OCH_2$–], **C)** Pep [–$OCH(CH_3)$–], **D)** Pep [–$(CH_2)_2$–), **E)** Pep [–(CH=CH)–], and **F)** Pep [–$OC(CH_3)_2$–]. The APAs were aged for 14 h in 1X PB (10 mM), diluted to 0.5 mM before casting onto grids, and stained with uranyl acetate. Twisted points in ribbons are indicated by red arrows.

## Gelation and rheological properties

As observed from the TEM micrographs, all APAs except Pep[–$OC(CH_3)_2$–] self-assembled into one dimensional nanostructures. We previously found that 10 mg/mL solutions of APAs at physiological pH formed hydrogels upon addition of 20 mM $CaCl_2$ via coordinate bridging of glutamic acid units in the peptide backbone.[26, 33] Similarly, in this work, we mixed APA solutions with $CaCl_2$ to initiate gelation. All APAs except Pep[–$OC(CH_3)_2$–] formed self-supporting hydrogels.

To evaluate the rheological properties of the APA hydrogels, all gels were prepared on a rheometer and allowed to sit for 10 min before applying oscillatory shear. Dynamic time sweep experiments under constant strain (0.5%) and frequency (1 Hz) showed that APA hydrogels were fairly stable to the applied force with storage moduli (G') higher than loss moduli (G") for all

hydrogels in the studied range (Figure S7A). This behaviour is typical of amphiphilic peptide hydrogels.[11, 38] Furthermore, after each time sweep, hydrogels were subjected to an oscillatory frequency sweep (Figure S7B). Nearly flat traces in the frequency sweep experiments in the low frequency regime (< 10 Hz) indicated frequency-independent rheological properties for all APA hydrogels.

Although all five APA hydrogels showed relatively constant rheological behavior, their storage moduli were affected by the linker unit (Figure 3). For example, Gel[–C(O)–] had a storage modulus of 250 ± 60 Pa, while Gel[–$OCH_2$–] formed a significantly stronger hydrogel with a storage modulus of 1400 ± 200 Pa. Furthermore, Gel[–$OCH(CH_3)$–] was also weaker than Gel[–$OCH_2$–] at 560 ± 50 Pa likely due to steric hinderance caused by the additional methyl group, which may hinder close packing of fibers essential for strong coordination with $Ca^{2+}$. The influence of steric effects on hydrogelation was further confirmed when Pep[–$OC(CH_3)_2$–] failed to form a hydrogel with $Ca^{2+}$, which we attribute to additional steric congestion caused by two methyl groups. Gel[–$(CH_2)_2$–] exhibited similar rheological behaviour to Gel[–$OCH(CH_3)$–] with G' at 570 ± 70 Pa. Gel[–CH=CH–] showed the lowest equilibrium storage modulus of all APA hydrogels tested at 40 ± 10 Pa.

Taken together, the TEM micrographs along with rheological data suggest that closely packed structures (twisted ribbons) formed stronger hydrogels with $Ca^{2+}$ relative to loosely packed structures (fibrils). This observation is consistent with related materials in the literature.[11, 14, 38] Additionally, the observed differences in the widths of the ribbons can be correlated to the hydrogel storage moduli, with wider nanoribbons forming stiffer hydrogels relative to their counterparts. This observation is likely due to strong matrices formed by inter-fibre calcium

coordination as observed previously.[11, 36] Collectively, these results support our hypothesis that the linker segment affects both self-assembly and gelation behaviour of APAs by controlling the orientation of the aromatic component relative to the peptide chain.

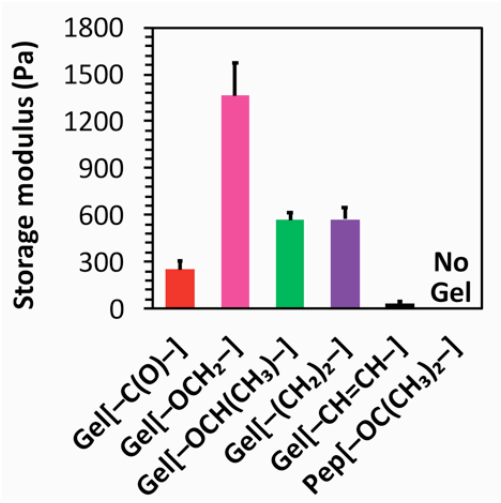


**Fig. 4.3.** Storage moduli of 10 mg/mL APA hydrogels at 1 Hz frequency and 0.5% strain with 20 mM $CaCl_2$ at physiological pH at 25 $^{o}$C.

Next, we explored whether the observed differences in molecular packing and viscoelastic properties of these APA hydrogels influenced their $H_2S$ release behavior. $H_2S$ release from APA hydrogels was triggered by cysteine, which led to decomposition of the SATO group with $H_2S$ release. $H_2S$ release from 10 mg/mL hydrogels at pH 7.4 was measured by an $H_2S$- sensitive electrochemical probe and a specially designed vial.[12, 26] The vial contained an inner well, which was loaded with APA hydrogel, onto which was added a solution of cysteine. $H_2S$, formed by the reaction of cysteine with SATO, percolated through a gas-permeable membrane into a trapping solution and was measured as an output current. We compared the peaking times of APA

hydrogels, which is the time required to reach a maximum $H_2S$ concentration from the time of addition of cysteine.

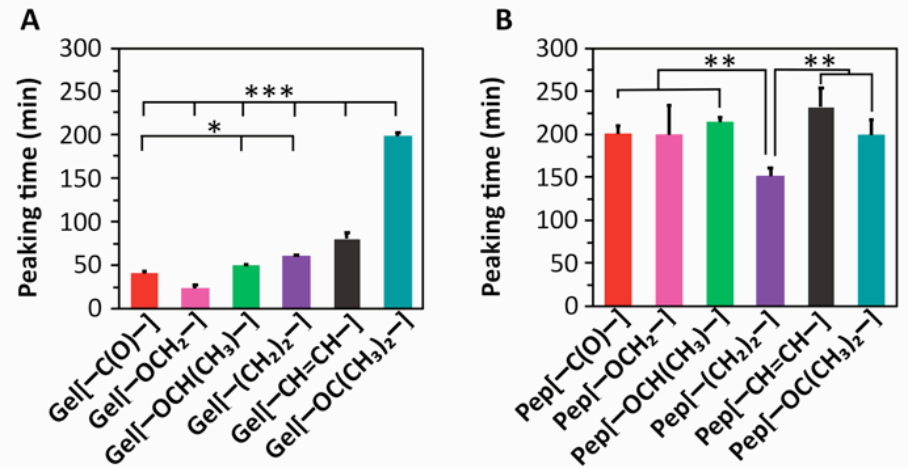


**Fig. 4.4**: $H_2S$ release from A) 10 mg/mL APA hydrogels and B) APA solutions at 10 mg/mL concentration, both in 1X PB with 2 equiv cysteine added to trigger $H_2S$ release. * indicates $p<0.05$, ** indicates $p<0.01$, and *** indicates $p<0.001$ for comparisons among the groups indicated, as determined by a one-way analysis of variance (ANOVA) with a Student-Newman-Keuls comparison posthoc test (n=3).

We expected that stiffer gels would retard the diffusion of cysteine through the hydrogel network and release $H_2S$ more slowly than weaker gels. However, $H_2S$ release peaking times, as measured by the $H_2S$ probe, showed the opposite trend (Figure 4A and S8A). The observed $H_2S$ release peaking times were shorter for stiff Gel[–$OCH_2$–] (22 ± 4 min) and longer for weaker Gel[–CH=CH–] (80 ± 6 min), with gels of intermediate stiffness falling in between. Moreover, Pep[–$OC(CH_3)_2$–], which formed a viscous solution upon addition of $CaCl_2$, showed longest $H_2S$ release profile with a peaking time above 200 min (Figure S8A).

This inverse correlation between stiffness and $H_2S$ release rate may be explained based on a reaction-diffusion mechanism that has been observed for other degradable hydrogel systems.[39-41] As cysteine passes through the hydrogel network, it reacts with SATOs to release $H_2S$, resulting

in hydrogel degradation (APAs without SATOs do not form gels). Therefore, a competition exists between cysteine diffusion within the hydrogel network and its reaction with the hydrogel SATO groups to release $H_2S$. When cysteine diffusion dominates, as is the case for weak hydrogels, cysteine navigates easily through the hydrogel network, creating a constant concentration immediately available around all SATOs (Figure 5, weak gel). Alternatively, for stiff hydrogels, cysteine cannot freely diffuse through the hydrogel network and is restricted to the top layer of hydrogel, increasing local cysteine concentration available to react with SATO groups near the gel surface (Figure 5, stiff gel). As a result, the output signal, which corresponds only to the degradation of the top layer, reaches a maximum rapidly. Put another way, $H_2S$ release in a weaker hydrogel is associated with bulk degradation, whereas a surface erosion-type mechanism exists for stiffer hydrogels.

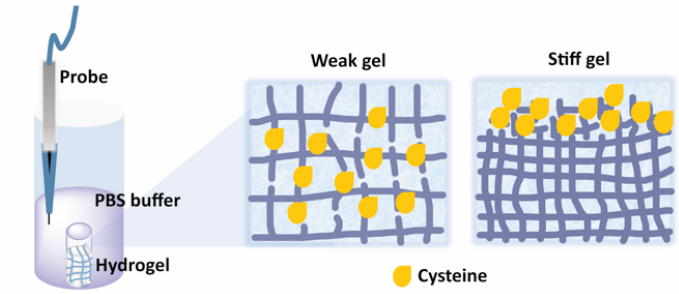


**Fig. 4.5.** Representation of cysteine diffusion in weak and strong hydrogel.

To further validate this conclusion, we measured $H_2S$ release from APA solutions under similar conditions but without $Ca^{2+}$ (Figure 4B and S8B). In the absence of $Ca^{2+}$, the inter-chain coordinate bridges cannot be formed, and $H_2S$ release depends on APA morphology instead of network topology. As expected, very similar $H_2S$ release peaking times were observed for all APA solutions except Pep[–$(CH_2)_2$–]. The shorter peaking time observed for Pep[–$(CH_2)_2$–] is consistent with the short nanoribbons and several small fragments observed by TEM.

Interestingly, peaking times observed for Pep[–OC($CH_3$)$_2$–] both in the presence and absence of $CaCl_2$ were very close, suggesting that $Ca^{2+}$ fails to form strong coordinate bonds to create a network and hence shows very similar cysteine diffusion behavior. These results suggest that the observed $H_2S$ release trends for APA hydrogels may be attributed to the network stiffness of each gel, which is controlled by the choice of linker.

Finally, we evaluated gel degradation over time visually after cysteine addition (Figure S10). As mentioned earlier, $H_2S$ release from hydrogels in the presence of cysteine results in hydrogel dissolution because the peptide aldehyde cannot form a hydrogel. As expected, we observed that the strongest hydrogel, Gel[–O$CH_2$–], took several minutes for any degradation to become visible, and even after 7 h, translucent structures could still be seen. In contrast, a weak hydrogel, Gel[–C(O)–], began to degrade within the first 30 min. These results suggest that stiff APA hydrogels may release $H_2S$ for longer periods of time by shielding SATOs inside their stiffer network. Due to baseline fluctuations in the electrode probe, measuring $H_2S$ release beyond a few hours is difficult, but strong Gel[–O$CH_2$–] appears to be a suitable candidate for localized $H_2S$ release over hours to days.

**4.5 Conclusion**

Self-assembling peptide hydrogels may be versatile and powerful drug delivery vehicles, especially for therapeutics such as $H_2S$ where localized delivery is crucial. APA-based hydrogels allow tunability of $H_2S$ release through minimal structural modifications. We synthesized six APAs, five of which formed hydrogels with $Ca^{2+}$ ions at 10 mg/mL. The rheological behavior of the APA hydrogels varied depending on the flexibility of the linker. While peptides with flexible linkers formed stiffer hydrogels, peptides containing a relatively rigid linker formed weaker hydrogels. Furthermore, the APA hydrogels showed varying release of $H_2S$ regulated by the

diffusion of cysteine through the hydrogel network. The stiffer hydrogels showed overall longer release times compared to weaker hydrogels by retarding the diffusion of cysteine. These hydrogels may be applied in tissue engineering and regenerative medicine, where slow, sustained delivery of $H_2S$ could be beneficial to a number of disease states.

## 4.6 Experimental

*Materials*

Rink Amide MBHA resin and 9-fluorenylmethoxy carbonyl (Fmoc) protected L-amino acids were purchased from P3Biosystems and used as received. HBTU, *N*-methylpiperidine, DBU and other reagents for peptide synthesis were purchased from commercial vendors and used as received unless otherwise noted. The solvents employed for peptide synthesis were reagent grade. The linkers were either synthesized (see supplementary information) or purchased commercially.

*Peptide synthesis and purification*

Peptides were synthesized either manually or using a Liberty 1 microwave-assisted peptide synthesizer (CEM) using solid-phase peptide synthesis (SPPS) via standard Fmoc protocol as described previously.[35] Linkers were coupled to the N-terminus of the peptide on resin using HBTU and DIEA in DMF. After cleavage and isolation, peptides were dissolved in water containing 0.1% $NH_4OH$ and filtered through a 0.45 μm PTFE filter before purification. Purification by preparative-scale reverse phase-high performance liquid chromatography (RP-HPLC) was carried out on an Agilent Technologies 1260 Infinity HPLC system, eluting with a gradient of 2% ACN to 90% ACN in milliQ $H_2O$ over 33 min using an Agilent PLRP-S column (100Å particle size, 25 x 150 mm) and monitoring at 220 nm. To both mobile phases was added

0.1% $NH_4OH$ to aid in solubility. Fractions were analysed by mass spectrometry (Advion ExpressIon Compact Mass Spectrometer), and product-containing fractions were combined, rotovapped to remove ACN, and lyophilized (LabConco).

The lyophilized peptide was dissolved in dry DMSO and reacted with *S*-benzoylthiohydroxylamine (SBTHA) in the presence of catalytic TFA to afford the final SATO-containing APAs. Peptides were dissolved in a mixture of phosphate buffer (100 mM at pH 7.4) and acetonitrile (5:2 v/v) and filtered through a 0.45 μm PTFE filter before purification. Purification was carried out using RP-HPLC, eluting with a gradient of 2% ACN to 90% ACN in milliQ $H_2O$ without any additives. The protocol for analysing and recovering the peptides was the same as described above. The final peptides were dissolved in milliQ water and distributed into aliquots (100 μg each). Aliquots were frozen, lyophilized, and stored at -20 $^oC$.

*Critical aggregation concentration (CAC) measurements*

Nile red stock solution in acetone (1 mg/mL) was diluted in PB (1X) to a concentration of 0.01 mg/mL and was used to make all peptide solutions. A peptide stock solution was prepared at 4 mg/mL in the Nile red stock solution and was further diluted to the concentration of 3 mg/mL, 2 mg/mL, 1 mg/mL, 0.5 mg/mL, 0.25 mg/mL, 0.1 mg/mL, 0.01 mg/mL, 0.001 mg/mL, and 0.0001 mg/mL. All peptide dilutions were vortexed for a few seconds, then 300 μL of each was transferred to a 96-well plate, and the plate was allowed to sit in the dark for 15–20 min. Fluorescence spectra were recorded using a Varian Cary Eclipse fluorescence spectrophotometer (FL1105M003) with an excitation wavelength of 550 nm. Fluorescence intensity measured at 628 nm was plotted against log[concentration], and the final CAC values were estimated to be the point of intersection between the linear fits of high and low concentration regime.

*Circular Dichroism (CD) Spectroscopy*

CD spectra were measured at room temperature using a Jasco J-815 CD spectrometer (Jasco Inc.) with a pre-set $N_2$ flow at 120 mL/min. The range of wavelengths employed was 190 to 250 nm (50 nm/min) with a response time of 8 s. Samples for both APA solutions were freshly prepared at 0.25 and 10 mM (20 μL) in 1X PB (pH 7.4) and were analysed using a quartz cuvette with a path length of 1 mm with 3 iterations for each sample. Similarly, CD spectra for freshly prepared hydrogels (20 μL) were recorded using a dismountable cuvette with a path length of 0.2 mm. Raw spectra were converted to mean residual ellipticity for comparison.

*Hydrogelation*

All APAs except Pep[–OC$(CH_3)_2$–] formed hydrogels in 1X PB at physiological pH upon addition of 10 μL of $CaCl_2$ solution (200 mM in water) to 90 μL of peptide solution (10 mM in 1X PB). The final concentration of $CaCl_2$ in the hydrogels was 20 mM. Hydrogels were allowed to sit for 10 min before any further analysis.

*Morphological analyses*

Peptide solutions (10 mM in 0.05 M phosphate buffer at pH 7.4) were prepared and allowed to age overnight, then diluted with water to 500 μM. Next, 10 μL of peptide solution was deposited on a carbon-coated copper TEM grid (300 mesh, Electron Microscopy Sciences), allowed to sit for 5–6 min, and then gently blotted with filter paper. The grid was then washed by adding a drop of MilliQ water, allowed it to stand for 1 min, and then blotted with filter paper. Samples were stained with 10 μL of a 2% uranyl acetate aqueous solution for 5–6 min, blotted with filter paper, and allowed to dry in air before TEM observation. Images were taken on a Philips EM420 TEM with a slow scan CCD camera.

*Rheology*

Rheological experiments were done on an AR-2000 (TA instruments) using a 25 mm parallel plate geometry. Buffered peptide solutions (225 µL, 10 mg/mL peptide, ~10 mM) were prepared for each peptide in 1X PB (pH 7.4) and quickly transferred to the rheometer's bottom geometry. Gelation was initiated upon addition of 25 µL $CaCl_2$ solution (200 mM in water) and the resulting solution was mixed thoroughly with a pipet tip to ensure homogeneity. After allowing the solution to gel for 10 min, the upper geometry was lowered to a pre-set gap of 500 µm, and a dynamic time sweep was performed at a frequency of 1 Hz and 0.5% strain to measure storage (G') and loss (G") moduli. Each time sweep was followed by a dynamic frequency sweep (0.010-100 Hz at 0.5% strain) and a strain sweep (1 Hz at 0.5-100% strain).

*$H_2S$ release measurement*

$H_2S$ release from peptide gels and solutions was measured amperometrically using an electrode probe [8]. A solution of APA (90 µL of 10 mM solution in 1X PB) was placed in an inner well inside a specially designed glass vial equipped with a stir bar. 10 µL of $CaCl_2$ was added to the inner well and mixed thoroughly with a pipette tip to form hydrogel. After 10 min, 4 µL of cysteine solution (200 mM in water) was gently deposited on the top layer of the hydrogel. The final concentrations in the inner well were 10 mM in peptide and 20 mM (2 equiv) in cysteine. The well was immediately covered with the gas-permeable membrane (Breathe easier, Diversified Bioteck), and phosphate buffer at pH 7.4 (4.95 mL) mixed with 50 µL of diethylenetriaminepentaacetic acid (DTPA) solution (10 mM in water) was added into the vial, covering the inner well. The $H_2S$-selective microelectrode was then immersed in the phosphate buffer solution, and the output signal was recorded. Similarly, $H_2S$ release from APA solutions was measured by mixing 90 µL of peptide solution (10 mM) with 10 µL of $CaCl_2$ in the inner

well to form a hydrogel. 4 μL (2 equiv) cysteine solution (200 mM in water) was added, the well was covered with the membrane, and output signal was measured as above. Calibration was carried out as previously reported.[42]

**4.7 References**

(1) Aida, T.; Meijer, E. W.; Stupp, S. I. Functional Supramolecular Polymers *Science.* **2012**, 335, 813–817.

(2) Webber, M. J.; Appel, E. A.; Meijer, E. W.; Langer, R. Supramolecular Biomaterials. *Nat. Mater.,* **2016**, 15, 13–26.

(3) Acar, H.; Srivastava, S.; Chung, E. J.; Schnorenberg, M. R.; Barrett, J. C.; LaBelle, J. L.; Tirrell, M. Self-assembling Peptide-Based Building Blocks in Medical Applications. *Adv. Drug. Deliv. Rev.,* **2017**, 110–111, 65–79.

(4) Cavalli, S.; Albericio, F.; Kros, A. Amphiphilic Peptides and their Cross-Disciplinary Role as Building Blocks for Nanoscience. *Chem. Soc. Rev.,* **2010**, 39, 241–263.

(5) Sato, K.; Hendricks, M. P.; Palmer, L. C.; Stupp, S. I. Peptide Supramolecular Materials for Therapeutics. *Chem. Soc. Rev.,* **2018**, 47, 7539–7551.

(6) Fleming, S.; Ulijn, R. V. Design of Nanostructures Based on Aromatic Peptide Amphiphiles. *Chem. Soc. Rev.,* **2014**, 43, 8150–8177.

(7) Bowerman, C. J.; Liyanage, W.; Federation, A. J.; Nilsson, B. L. Tuning beta-sheet Peptide Self-assembly and Hydrogelation Behavior by Modification of Sequence Hydrophobicity and Aromaticity. *Biomacromolecules,* **2011**, 12, 2735–2745.

(8) Castelletto, V.; Moulton, C. M.; Cheng, G.; Hamley, I. W.; Hicks, M. R.; Rodger, A.; López-Pérez, D. E.; Revilla-López, G.; Alemán, C. Self-assembly of Fmoc-Tetrapeptides Based on the RGDS Cell Adhesion Motif. *Soft Matter,* **2011**, 7, 11405–11415.

(9) Sahoo, J. K.; Nazareth, C.; VandenBerg, M. A.; Webber, M. J. Self-assembly of Amphiphilic Tripeptides with Sequence-Dependent Nanostructure. *Biomater. Sci.,* **2017**, 5, 1526–1530.

(10) Sahoo, J. K.; Nazareth, C.; VandenBerg, M. A.; Webber, M. J. Aromatic Identity, Electronic Substitution, and Sequence in Amphiphilic Tripeptide Self-assembly. *Soft Matter,* **2018**, 14, 9168–9174.

(11) Shi, J.; Gao, Y.; Zhang, Y.; Pan, Y.; Xu, B. Calcium ions to cross-link supramolecular nanofibers to tune the elasticity of hydrogels over orders of magnitude. *Langmuir,* **2011**, 27, 14425–14431.

(12) Wang, Y.; Kaur, K.; Scannelli, S. J.; Bitton, R.; Matson, J. B. Self-Assembled Nanostructures Regulate $H_2S$ Release from Constitutionally Isomeric Peptides. *J. Am. Chem. Soc.,* **2018**, 140, 14945–14951.

(13) Singh, N.; Kumar, M.; Miravet, J. F.; Ulijn, R. V.; Escuder, B. Peptide-Based Molecular Hydrogels as Supramolecular Protein Mimics. *Chemistry,* **2017**, 23, 981–993.

(14) Chakroun, R. W.; Wang, F.; Lin, R.; Wang, Y.; Su, H.; Pompa, D.; Cui, H. Fine-Tuning the Linear Release Rate of Paclitaxel-Bearing Supramolecular Filament Hydrogels through Molecular Engineering. *ACS Nano,* **2019**, 13, 7780–7790.

(15) Fleming, S.; Debnath, S.; Frederix, P. W.; Tuttle, T.; Ulijn, R. V. Aromatic peptide amphiphiles: significance of the Fmoc moiety. *Chem. Commun.,* **2013**, 49, 10587–10589.

(16) Yang, Z.; Liang, G.; Ma, M.; Gao, Y.; Xu, B. Conjugates of naphthalene and dipeptides produce molecular hydrogelators with high efficiency of hydrogelation and superhelical nanofibers. *J. Mater. Chem.,* **2007**, 17, 850–854.

(17) Yang, Z.; Liang, G.; Xu, B. Supramolecular hydrogels based on beta-amino acid derivatives. *Chem. Commun.,* **2006**, 7, 738–740.

(18) Chen, L.; Revel, S.; Morris, K.; L, C. S.; Adams, D. J. Effect of molecular structure on the properties of naphthalene-dipeptide hydrogelators. *Langmuir,* **2010**, 26, 13466–13471.

(19) Barr, L. A.; Calvert, J. W. Discoveries of hydrogen sulfide as a novel cardiovascular therapeutic. *Circ. J.,* **2014**, 78, 2111–2118.

(20) Zhao, W. Z., J Lu, Y. Wang, R. The vasorelaxant effect of H2S as a novel endogenous gaseous KATP channel opener. *EMBO J.,* **2001**, 20, 6008–6016.

(21) Zhang, X.; Bian, J. S. Hydrogen sulfide: a neuromodulator and neuroprotectant in the central nervous system. *ACS Chem. Neurosci.,* **2014**, 5, 876–883.

(22) Bhatia, M. $H_2S$ and Inflammation: An Overview. *Handb. Exp. Pharmacol.,* **2015**, 230, 165–180.

(23) Whiteman, M.; Winyard, P. G. Hydrogen sulfide and inflammation: the good, the bad, the ugly and the promising. *Expert. Rev. Clin. Pharmacol.,* **2011**, 4, 13–32.

(24) Wang, R. Physiological implications of hydrogen sulfide: a whiff exploration that blossomed. *Physiol. Rev.,* **2012**, 92, 791–896.

(25) Longchamp, A.; Kaur, K.; Macabrey, D.; Dubuis, C.; Corpataux, J. M.; Deglise, S.; Matson, J. B.; Allagnat, F. Hydrogen sulfide-releasing peptide hydrogel limits the development of intimal hyperplasia in human vein segments. *Acta. Biomater.,* **2019**, 97, 374–384.

(26) Qian, Y.; Kaur, K.; Foster, J. C.; Matson, J. B. Supramolecular Tuning of $H_2S$ Release from Aromatic Peptide Amphiphile Gels: Effect of Core Unit Substituents. *Biomacromolecules,* **2019**, 20, 1077–1086.

(27) Qian, Y.; Matson, J. B. Gasotransmitter delivery via self-assembling peptides: Treating diseases with natural signaling gases. *Adv. Drug Deliv. Rev.,* **2017**, 110–111, 137–156.

(28) Connal, L. A. The benefits of macromolecular hydrogen sulfide prodrugs. *J. Mater. Chem. B,* **2018**, 6, 7122–7128.

(29) Urquhart, M. C.; Ercole, F.; Whittaker, M. R.; Boyd, B. J.; Davis, T. P.; Quinn, J. F. Recent advances in the delivery of hydrogen sulfide via a macromolecular approach. *Polym. Chem.,* **2018**, 9, 4431–4439.

(30) Foster, J. C.; Carrazzone, R. J.; Spear, N. J.; Radzinski, S. C.; Arrington, K. J.; Matson, J. B. Tuning $H_2S$ Release by Controlling Mobility in a Micelle Core. *Macromolecules,* **2019**, 52, 1104–1111.

(31) Hasegawa, U.; van der Vlies, A. J. Polymeric micelles for hydrogen sulfide delivery. *MedChemCommun,* **2015**, 6, 273–276.

(32) Fan, D. Y.; Tian, Y.; Liu, Z. J. Injectable Hydrogels for Localized Cancer Therapy. *Front. Chem.,* **2019**, 7, 675–685.

(33) Carter, J. M.; Qian, Y.; Foster, J. C.; Matson, J. B. Peptide-based hydrogen sulphide-releasing gels. *Chem. Commun.,* **2015**, 51, 13131–13134.

(34) Foster, J. C.; Powell, C. R.; Radzinski, S. C.; Matson, J. B. S-aroylthiooximes: a facile route to hydrogen sulfide releasing compounds with structure-dependent release kinetics. *Org. Lett.,* **2014**, 16, 1558–1561.

(35) Kaur, K.; Qian, Y.; Gandour, R. D.; Matson, J. B. Hydrolytic Decomposition of *S*-Aroylthiooximes: Effect of pH and N-Arylidene Substitution on Reaction Rate. *J. Org. Chem.,* **2018**, 83, 13363–13369.

(36) Aggeli, A.; Nyrkova, I. A.; Bell, M.; Harding, R.; Carrick, L.; McLeish, T. C.; Semenov, A. N.; Boden, N. Hierarchical self-assembly of chiral rod-like molecules as a model for peptide beta -sheet tapes, ribbons, fibrils, and fibers. *Proc. Natl. Acad. Sci. U. S. A.,* **2001**, 98, 11857–11862.

(37) Hu, Y.; Lin, R.; Zhang, P.; Fern, J.; Cheetham, A. G.; Patel, K.; Schulman, R.; Kan, C.; Cui, H. Electrostatic-Driven Lamination and Untwisting of beta-Sheet Assemblies. *ACS Nano,* **2016**, 10, 880–888.

(38) Greenfield, M. A.; Hoffman, J. R.; de la Cruz, M. O.; Stupp, S. I. Tunable mechanics of peptide nanofiber gels. *Langmuir,* **2010**, 26, 3641–3647.

(39) Skaalure, S. C.; Akalp, U.; Vernerey, F. J.; Bryant, S. J. Tuning Reaction and Diffusion Mediated Degradation of Enzyme-Sensitive Hydrogels. *Adv. Healthc. Mater.,* **2016**, 5, 432–438.

(40) van Bommel, K. J.; Stuart, M. C.; Feringa, B. L.; van Esch, J. Two-stage enzyme mediated drug release from LMWG hydrogels. *Org. Biomol. Chem.,* **2005**, 3, 2917–2920.

(41) Branco, M. C.; Pochan, D. J.; Wagner, N. J.; Schneider, J. P. Macromolecular diffusion and release from self-assembled beta-hairpin peptide hydrogels. *Biomaterials,* **2009**, 30, 1339–1347.

(42) Powell, C. R.; Kaur, K.; Dillon, K. M.; Zhou, M.; Alaboalirat, M.; Matson, J. B. Functional *N*-Substituted *N*-Thiocarboxyanhydrides as Modular Tools for Constructing $H_2S$ Donor Conjugates. *ACS Chem. Biol.,* **2019**, 14, 1129–1134.

## Appendix B

## Synthesis of linkers

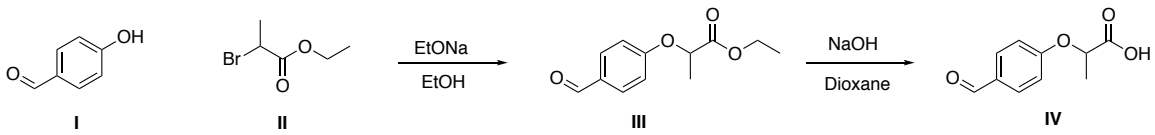


**Scheme 4.S1**: Synthesis of 2-(4-formylphenoxy)propanoic acid

To a solution of 4-hydroxybenzaldehyde **(I)** (3.0 g, 1.0 equiv) in ethanol (30 mL) in a single-neck round bottom flask, sodium ethoxide (4.0 g, 2.5 equiv) was added in portions followed by the addition of 2-methyl bromoacetate **(II)** (1.8 mL, 1.5 equiv) via syringe. The reaction mixture was refluxed overnight, and the reaction progress was monitored by TLC (developed in 50 % EtOAc in hexanes; visualized via long-wavelength UV light). After complete disappearance of 4-hydrobenzaldehyde, the reaction mixture was allowed to cool to rt and diluted with EtOAc (50 mL) and $H_2O$ (50 mL). The organic layer was isolated using a separatory funnel, dried over $Na_2SO_4$, and concentrated to yield a yellow oil. Product **(III)** was purified by silica gel chromatography, eluting in 10% ethyl acetate-hexanes.

The recovered product (2.0 g, 1.0 equiv) was dissolved in 1,4-dioxane (10 mL) in a single-neck round bottom flask, followed by the addition of 1 N NaOH solution (10 mL). The reaction mixture was allowed to stir at rt for 4 h. The reaction progress was monitored via TLC (developed in pure ethyl acetate and visualized via long-wavelength UV light). After completion, the reaction mixture was concentrated by rotary evaporation, and the resulting mixture was diluted with water and washed with $CH_2Cl_2$ (1 X 30 mL). The pH of the aqueous layer was adjusted to 1 using 1 N HCl, and the product was extracted with $CH_2Cl_2$. The organic layer was washed several times with ice cold water to remove residual dioxanes. The resulting product was

isolated as a white solid (1.6 g, 80% yield), dried under vacuum, and used without further purification.

$^{1}$H-NMR (DMSO-d6): δ ppm 1.5 (s, 3H); 5.00-5.06 (q, 1H); 7.04-7.07 (dd, 2H); 7.85-7.87 (dd, 2H); 9.86 (s, 1H), and 13.20 (s, 1H). $^{13}$C-NMR (DMSO-d6): δ ppm 18.14, 71.69, 115.20, 129.90, 131.77, 162.40, 172.47, 191.33.

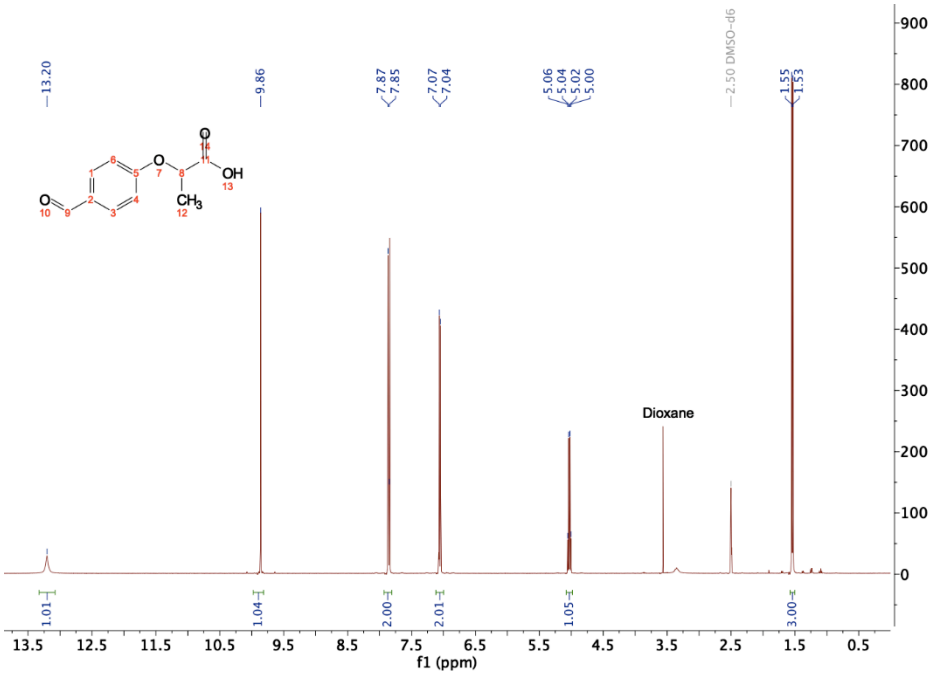


**Fig. 4.S1:** $^{1}$H-NMR spectrum of *2-(4-formylphenoxy)propanoic acid*

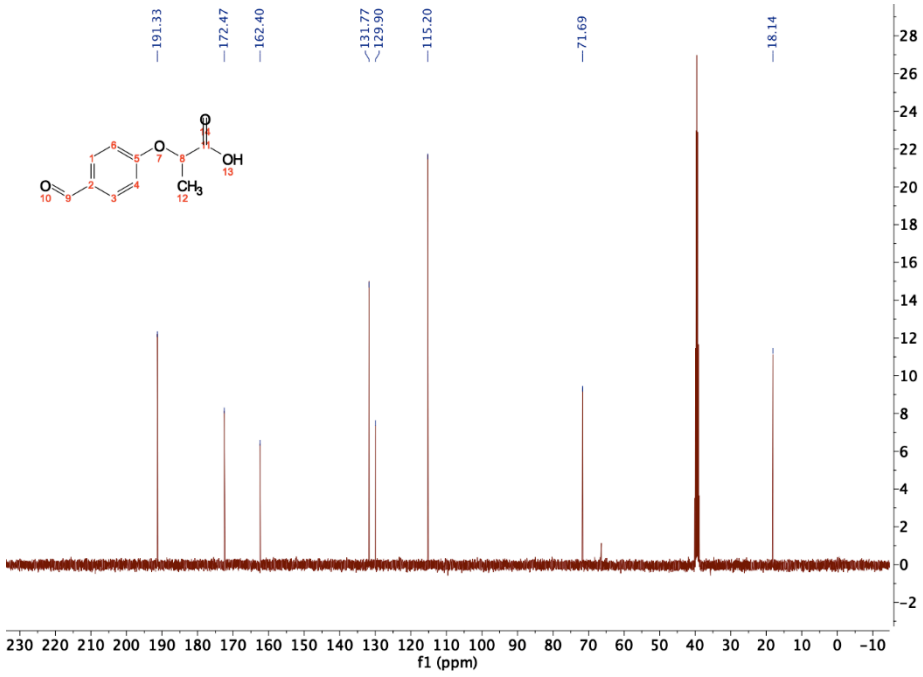


**Fig. 4.S2:** $^{13}$C-NMR spectrum of *2-(4-formylphenoxy)propanoic acid*

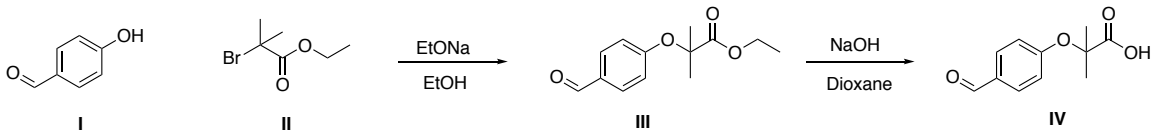


**Scheme 4.S2**: Synthesis of 2-(4-formylphenoxy)-2-methylpropanoic acid

2-(4-formylphenoxy)-2-methylpropanoic acid was synthesized following a similar procedure as described above for the synthesis of 2-(4-formylphenoxy)propanoic acid, replacing of 2-methyl bromoacetate with 2,2-dimethylbromoacetate. The product was recovered as a white solid in 77% yield.

$^{1}$H-NMR (DMSO-d6): δ ppm 1.59 (s, 6H); 6.93-6.96 (dd, 2H); 7.83-7.85 (dd, 2H); 9.85 (s, 1H), and 13.33 (s, 1H). $^{13}$C-NMR (DMSO-d6): δ ppm 25.10, 79.01, 117.39, 129.74, 131.51, 160.63, 174.37, 191.34. The NMR chemical shifts were consistent with those reported in the literature.[1]

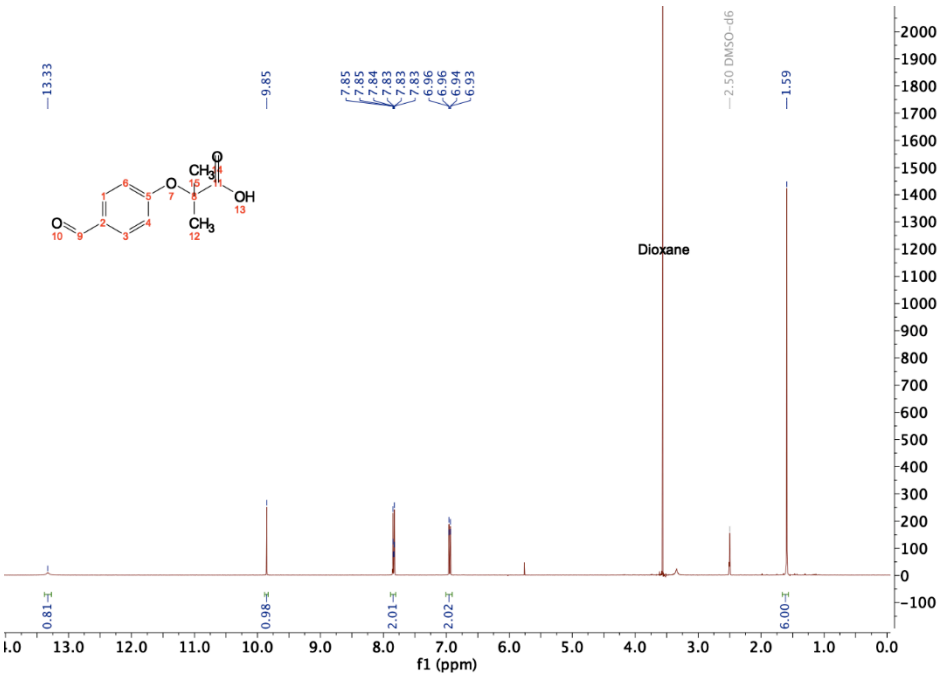


**Fig. 4.S3:** $^{1}$H-NMR spectrum of *2-(4-formylphenoxy)-2-methylpropanoic acid*

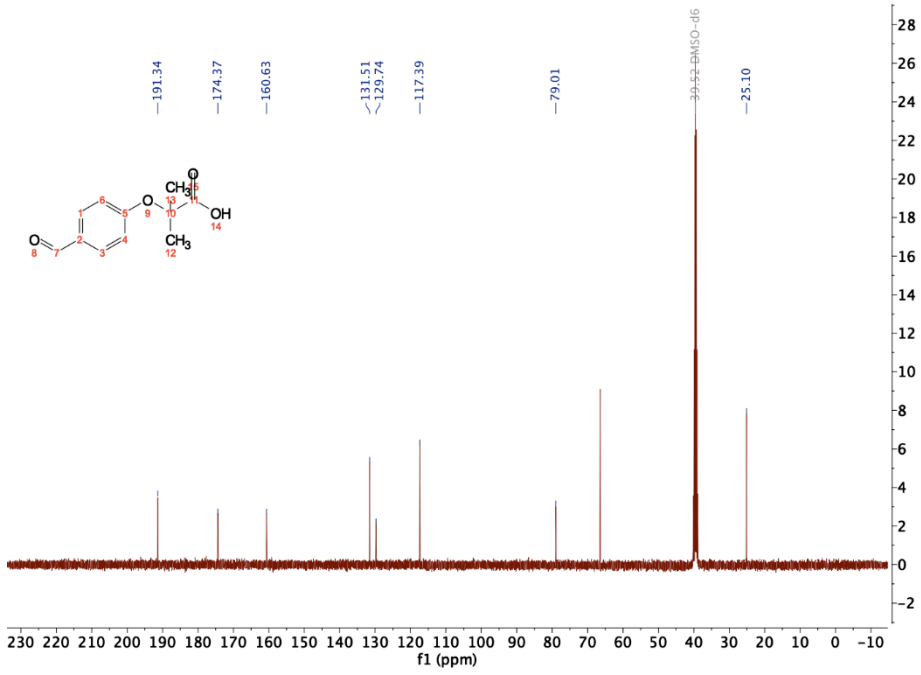


**Fig. 4.S4:** $^{13}$C-NMR spectrum of *2-(4-formylphenoxy)-2-methylpropanoic acid*

## Critical aggregation concentration

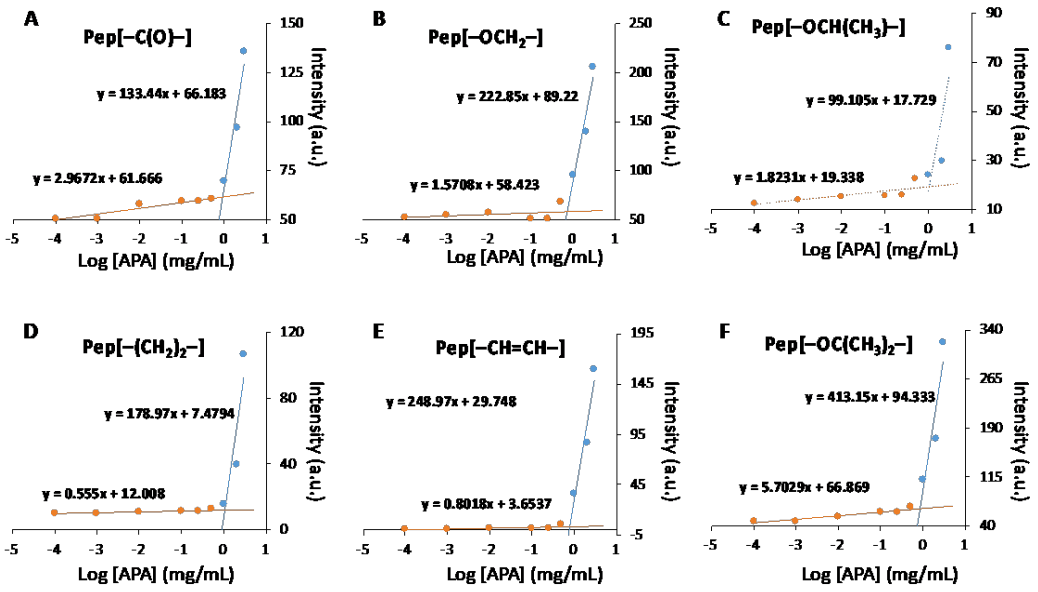


**Fig. 4.S5**: Critical aggregation concentration (CAC) measurements via Nile Red fluorescence assay. Fluorescence intensity versus concentration plots of **A)** Pep[–C(O)–], **B)** Pep[–$OCH_2$–], **C)** Pep[–$OCH(CH_3)$–], **D)** Pep[–$(CH_2)_2$–), **E)** Pep[–(CH=CH)–], and **F)** Pep[–$OC(CH_3)_2$–] in 10 mM PB. The CACs calculated for **Pep[–C(O)–]**, **Pep[–$OCH_2$–]**, **Pep[–$OCH(CH_3)$–]**, **Pep[–$(CH_2)_2$–)**, **Pep[–(CH=CH)–]**, and **Pep[–$OC(CH_3)_2$–]** were 0.9, 0.8, 1.0, 1.0 , 0.8, and 0.9 mg/mL, respectively.

## Pitch Length

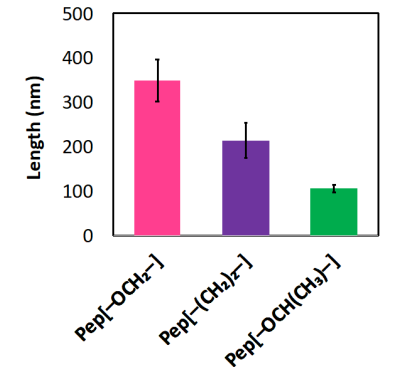


**Fig. 4.S6:** Pitch length of APAs with different linker segments measured using ImageJ and averaged over 40 different measurements from several images.

## Rheological measurements of APA hydrogels

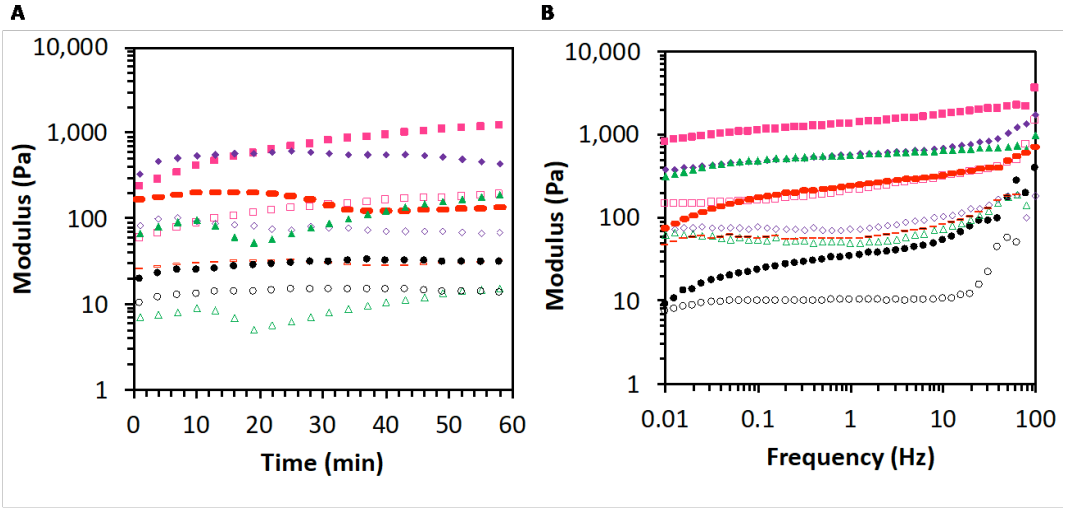


**Fig. 4.S7:** Graphical representation of **A)** Dynamic time sweep and B) Dynamic frequency sweep measurements for 10 mg/mL APA hydrogels with 20 mM $Ca^{2+}$ at physiological pH and 25 $^{o}$C. Solid markers indicate storage moduli (G') and the open markers indicate loss moduli (G''). (Gel[-$OCH_2$-], ■; Gel[-$(CH_2)_2$-], ▯; Gel[-$OCH(CH_3)$-], ▲, Gel[-C(O)-], –; Gel[-CH=CH-]: ●)

## $H_2S$ release curves

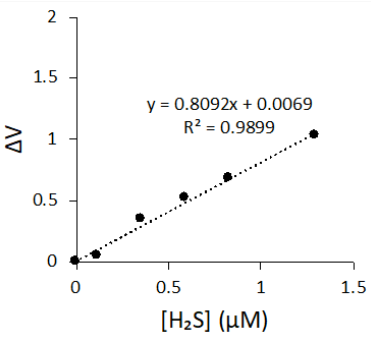


**Fig. 4.S9**: Calibration curve for $H_2S$ selective electrochemical probe. The change in voltage (y-axis), measured after successive additions of $Na_2S$ is plotted against concentration of $Na_2S$ (x-axis) solution in 10 mM PBS buffer at pH 7.4. Concentration of $H_2S$ is calculated via equation

$$[H_2S] = [Na_2S]/\{1 + \frac{K_a^1}{[H^+]} + \frac{K_a^1 K_a^2}{[H^+]}\}$$ where $pK_a^1$ = 6.89 and $pK_a^2$ = 19.

## Hydrogel degradation in the presence of cysteine

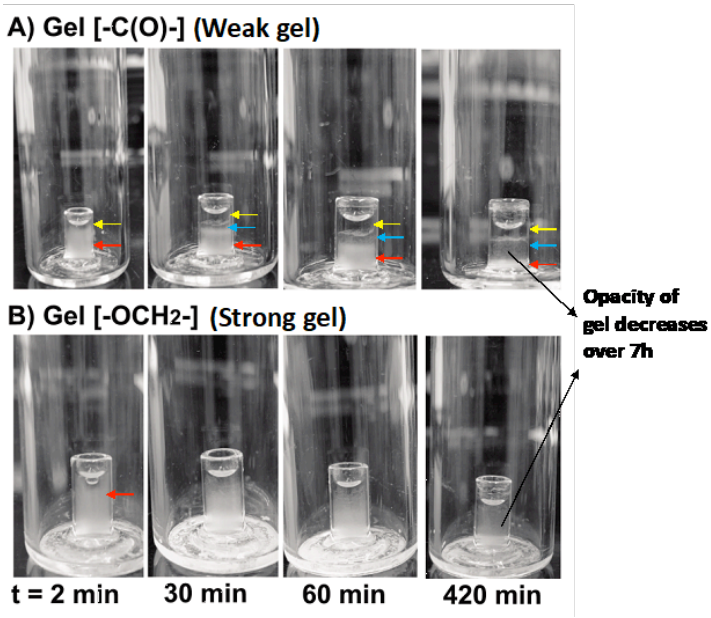


**Fig. 4.S10.** Degradation of APA hydrogels with 2 equiv. of cysteine. The opacity of each hydrogel decreases over time due to degradation. Panel A shows the degradation of weak Gel[–C(O)–] over 7 h, highlighting a clear separation of the degraded layer [clear bands (yellow arrows) and translucent bands (blue arrows)] and intact layer [opaque band (red arrows)]. Panel B shows the degradation of strong Gel[–$OCH_2$–]. Distinct degraded and intact layers were not observed in the degradation profile of strong gel, only a decrease in opacity was observed over time.

## References

(1) Park, M. H.; Park, J. Y.; Lee, H. J.; Kim, D. H.; Park, D.; Jeong, H. O.; Park, C. H.; Chun, P.; Moon H. R.; Chung, H. Y. *PLoS One*, 2013, **8**, e78815.

## Chapter 5. Conclusion and Future work

$H_2S$ is a biologically relevant signaling gas which plays several physiological roles. Exogenous delivery of $H_2S$ may be beneficial as a potential treatment for various conditions. We have worked to develop $H_2S$-releasing materials and study their properties. We were particularly interested in exploring the hydrolytic stability and self-assembling behavior of $H_2S$-releasing materials to improve their potential applicability.

### Chapter 2

We did a detailed study of SATO-peptides over a range of pH (6.0–10.9) to understand its hydrolytic stability under physiologically relevant conditions. We found that the stability of peptides is dependent on the pH of the solution as well as the chemical makeup of the $H_2S$ donor attached to the peptides. The electron-donating substituents were less stable relative to electron-withdrawing substituents at physiological pH. However, electron-donating substituents were more stable at basic pH values. We learned that several different mechanisms were involved in the hydrolysis of SATO-peptides.

For future work, we would like to study the effect of solvent on the hydrolysis mechanism for SATO-peptides. In preliminary work we found that including various organic solvents with phosphate buffer slowed down the hydrolysis reaction considerably. Although this study might not be relevant from physiological perspective, it will provide an insight into behavior of SATO-peptides under co-solvent conditions. This may help in improving the yield of these peptides during THA conjugation reactions.

**Chapter 3**

Here we used SATO-peptide to study the effectiveness of $H_2S$ as potential treatment for intimal hyperplasia. We synthesized $H_2S$-releaing SATO-FBA-IAVEE and a control peptide, both of which formed a hydrogel with a low $Ca^{2+}$ concentration. The slow $H_2S$ releasing Pep-$H_2S$ was more effective in inhibiting VSMC proliferation relative to fast releasing NaSH salt. Further, it selectively promoted *in vitro* proliferation of HUVEC.

In the future, we are interested in applying $H_2S$-releasing hydrogels to the animal models to understand their *in vivo* behavior. This may need a hydrogel with robust rheological properties. The current hydrogels are weak and need to be reapplied after a couple of hours. We envision an $H_2S$-releasing hydrogel that is capable of releasing $H_2S$ over the time frame of days to months. This would be beneficial as intimal hyperplasia takes about 30 days to develop after the vascular surgery and a long releasing $H_2S$ hydrogel will prevent repeated surgical interventions. We further speculate that polymer hydrogels might work better in that context and need to further explored.

**Chapter 4**

We report a series of peptide hydrogels based on aromatic peptide amphiphiles (APA), which differ only by a linker segment. The APAs self-assembled in aqueous buffer to form nanoscale assemblies ranging from fibrils to ribbons. These peptides formed hydrogels with $Ca^{2+}$ exhibiting significantly different rheological behavior. We found that flexible linkers formed stronger hydrogels compared to relatively rigid linkers. More interestingly, hydrogels showed different $H_2S$ release behavior based on their stiffness. We found that strong hydrogels can release $H_2S$

over longer periods of time by retarding the diffusion of thiol trigger compared to weak hydrogels which undergo bulk degradation as they release $H_2S$.

For future work, we would like to explore the network structure of the hydrogels with SEM. From our present work, it was clear that peptide solutions had very similar $H_2S$ release profiles even though they form different self-assembled structures. So the observed difference in the release behavior from hydrogels is believed to be due to differences in the network topologies. We need further work to study diffusion from the hydrogels using fluorimetry in order to devise a mathematical model that can explain the $H_2S$ release behavior. As an alternative, we can look into the methods to measure kinetics of $H_2S$ release from hydrogels. Our preliminary work showed that available methods like, methylene blue, MBB, fluorescent probes cannot work very well mostly due to interference from cysteine.

## Appendix C

### *COS releasing small molecule donors for $H_2S$ delivery*

COS is a most abundant component of the natural sulfur cycle and one of the prominent sulfur-containing gas in the earth's atmosphere. COS is a toxic gas due to its rapid conversion into $H_2S$ under the action of enzyme carbonic anhydrase (CA). However, it's still unclear whether the observed toxicity of COS originates from the action of gas itself or from its conversion into $H_2S$. Furthermore, its presence in tissues, cell permeability, and moderate water solubility, suggests that COS may have a significant role in mammalian cell biology much like accepted gasotransmitters, $H_2S$. Therefore, there is a need for COS donors, which can help in understanding of physiological role of COS.

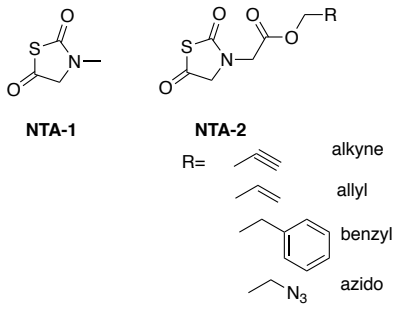


**Fig B1.** Structure of NTA-1 and series of NTA-2 with various R groups

*N*-thiocarboxyanhydrides (NTAs) are COS/$H_2S$ donors that release COS by nucleophile mediated ring opening reaction. We previously reported an N-substituted NTA-1 and a series of NTA-2 with the short $H_2S$ release half-lives (Fig B1). For the current work, we speculated that substitution at C-3 carbon of the NTA ring might impede the nucleophilic attack and slower the NTA ring opening reaction. In order to test our hypothesis, we synthesized a total of nine different NTAs from naturally occurring L-amino acids as well as synthetic amino acids. This included a set of seven NTAs derived from amino acids alanine, valine, leucine, isoleucine, and

phenylalanine with alkyl side chains like methyl, isopropyl, butyl, isobutyl, and benzyl respectively at C-3 carbon and one NTA derived from artificial amino 2-aminoisobutyric acid yielding a dimethyl group at the C-3 carbon (Fig B2). In order to study the effect of strained ring on the ring-opening of NTA, another 5-membered NTA was synthesized from proline. Since six membered rings are typically less strained than five membered rings, we also synthesized a six membered NTA from β-alanine in order to understand the role of ring size on the nucleophilic ring opening reaction.

**Synthesis of NTA-3 library**

All the NTAs were synthesized in a two-step reaction. The amino acid was reacted with xanthate to yeild corresponding thiocarbamate, which undergo ring closing catalysed by $PBr_3$ to yeild NTA. The NTAs were named after the amino acid they are synthesized from.

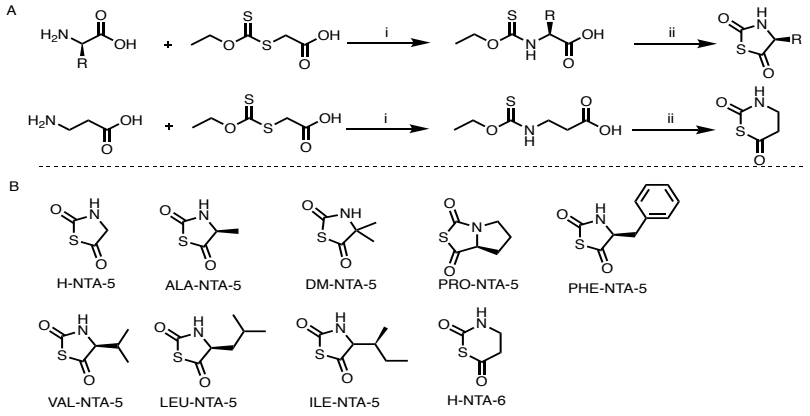


**Fig. B2. A)** General scheme for synthesis of 5-membered NTAs and 6-membered NTA; i) NaOH, methanol/$H_2O$ ii) $PBr_3$, DCM. **B)** Chemical structure of nine NTAs.

## $H_2S$ release kinetics

Next we were curious to test our hypothesis that the substitution at C-3 carbon effects the rate of $H_2S$ release by decelerating the rate of nucleophilic ring opening of the NTA ring. We started by measuring the $H_2S$ release from the NTAs using an $H_2S$ sensitive electrochemical probe. The release curves indicated the differences in the peaking times. Gly-NTA had a shorter peaking time, whereas NTAs with bulky side group e.g. Val-NTA and Ile-NTA showed long peaking times. Surprisingly, β-Ala-NTA, which is a six-membered ring showed a comparable $H_2S$ release curve to Gly-NTA. Next, in order to quantify the $H_2S$ release from the NTAs, we ran methylene blue assays. The calculated half-lives followed almost similar trends to the $H_2S$ release curves as measured by the electrochemical probe. The $H_2S$ release half-lives varied from around 1 h for β-Ala-NTA and Gly-NTA to about 20 h for Val-NTA and Ile-NTA. The results indicate a trend between increase in half-life with increasing side group bulk at C-3 carbon of the NTA ring. This supported our hypothesis that the side chain substitution at C-3 carbon plays a role in slowing down the nucleophilic attack at the C-5 carbonyl.

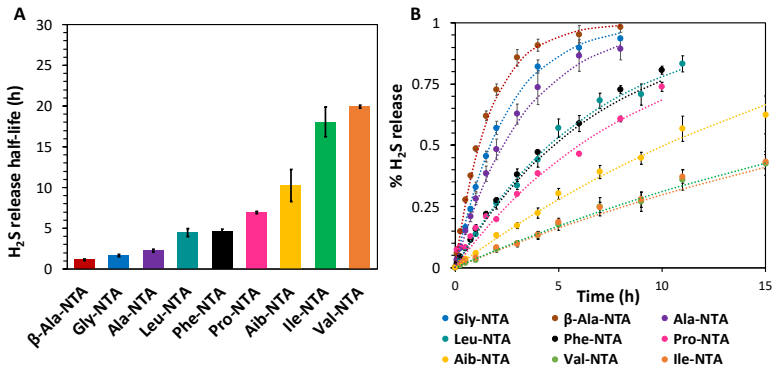


**Fig. B3: A)** $H_2S$ release half-lives for NTAs in 10X PBS solution with 5% DMSO estimated via methylene blue assay and **B)** representation of $H_2S$ release from NTAs as first-order reaction kinetics. The solid points are actual time points with dotted lines representing the respective first-order fits.

## Computational studies

In an attempt to understand the differences in the $H_2S$ released behavior of the series of NTAs, we calculated the transition state free energies for a few NTAs using B3LYP method with 6-311+G* basis sets, choosing water as a solvent. The observed results show a trend that can be correlated to the increasing steric bulk at the C-3 carbon, but the differences in the transition state energies were not as significant as that observed for $H_2S$ release half-lives. This warrants for an improved theoretical parameters and advanced level of theory to be utilized for better understanding of the role of NTA ring structure on the $H_2S$ release kinetics.

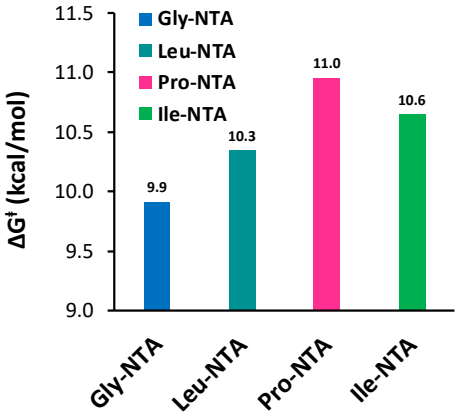


**Fig B4.** Energy of activation of NTAs calculated using B3LYP theory with 6-311+G* basis set with water as solvent.

## Appendix D

### *COS releasing materials for $H_2S$ delivery*

### COS releasing peptide-based materials

We utilized click chemistry to generate NTA-functionalized peptides. Typically, an azide functionalized lysine is synthesized and conjugated within a desired peptide chain (using standard solid phase peptide synthesis protocols) to yeild an azide functionalized peptide. On the other hand, the NTA ring is modified with an alkyne handle and clicked onto the azido-peptide. The click reaction conditions and were optimized through several trials (Table B2).

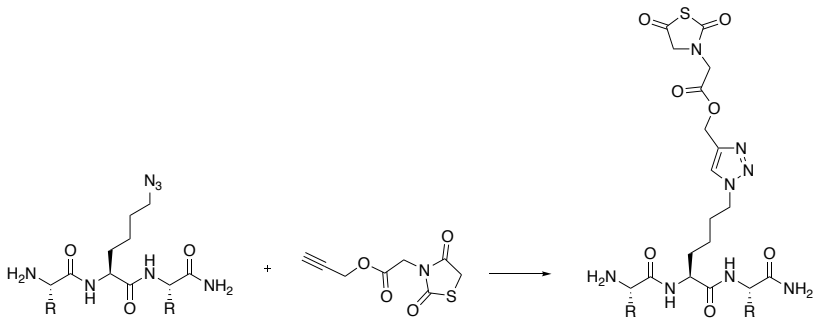

**Scheme C1.** General synthetic scheme of click reaction between azide-functionalized peptide and alkyne NTA (NTA-2).

| Trials | Catalyst | Ligand/ reducing agent | Solvents | Results |
|---|---|---|---|---|
| 1. KK-642 | CuI (0.001 eq) | PMDETA (0.003 eq.), Ascorbic acid (20 eq.) | THF/t-BuOH (1:1) | No product |
| 2. KK-657 | $CuSO_4.5H_2O$ (0.01 eq) | Ascorbic acid (0.1 eq) | t-ButOH/$H_2O$ (1:1) | No product |
| 3. KK-658 | $CuSO_4.5H_2O$ (0.25 eq) | TCEP (0.25 eq), PMDETA (2 eq) | t-ButOH/$H_2O$ (1:1) | No product |
| 4. KK-667 | $CuSO_4.5H_2O$ (2 eq), | Ascorbic acid (20 eq) | 0.1 M phosphate buffer (pH 7.4) | Peak at P-44 formed within 1 hr |
| 5. KK-668 | $CuSO_4.5H_2O$ (2 eq) | Ascorbic acid (20 eq) | t-ButOH/$H_2O$ (1:1) | **Reaction successful Workup after 1 hour** |

**Table C1.** Optimization of click reaction conditions

## General procedure for synthesis of NTA-peptide

Azide functionalized peptide (1 equiv) and alkyne NTA (1.2 equiv) were charged in a 20 mL scintillation vial along with 1:1 mixture of t-BuOH and water (10 mL). The reaction mixture was vortexed to afford a clear solution followed by addition of $CuSO_4.5H_2O$ (2 equiv) and ascorbic acid (20 equiv). The reaction mixture was sonicated for 20 min to dissolve all copper sulfate resulting in a clear bright yellow solution. After 1h reaction completion was checked via mass spec and showed full conversion of SATO to SATA. Crude product was filtered using PTFE filter (0.45 μm) and purified via RP-HPLC eluting with a gradient of 2% ACN to 90% ACN in water. Purified fractions were checked via mass spec and desired fractions were combined and lyophilized to obtain white solid as NTA-peptide.

## Self-assembly and hydrogelation of NTA-peptides

Among several NTA-peptides which were tested, only four peptides self-assembled in aqueous buffer solutions (Figure C1). Further, hydrogelation was tested for 20 mM solution of C12-FEFEK-NTA and C8-O-Phe-VEVEEK-NTA 2% DMSO-PBS (1X) with 6 μL and 8 μL CaCl2 solution (200 mM). Both peptides formed weak hydrogels, confirmed by the inverted vial method. Addition of more $CaCl_2$ to the peptide solution lead to precipitation and disruption of the hydrogel, suggesting that there is a delicate balance between hydrophobic, hydrophilic, and the charged segment of the peptide.

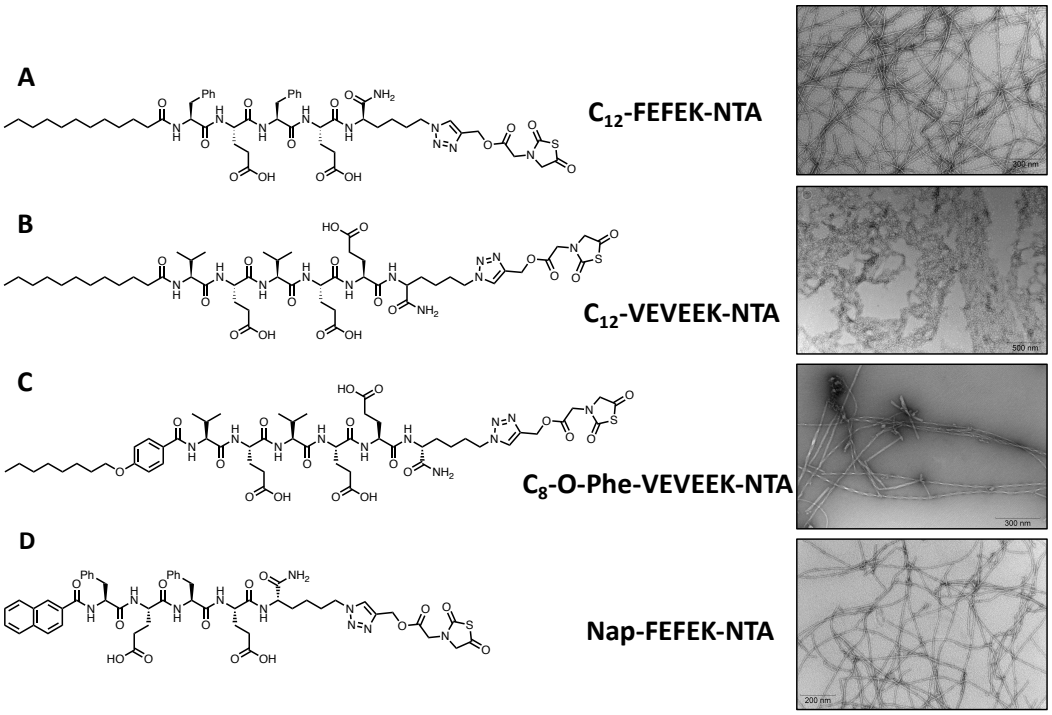


**Fig C1.** Structures and TEM micrographs of 4 NTA peptides. Peptides Self-assembled at 1 wt. % in 2% DMSO-PB buffer (10 mM), aged overnight, and diluted to 500 mM before casting onto grids

## $H_2S$ release from NTA-peptides

$H_2S$ release curves for the NTA-peptide solution as well as hydrogel showed that peaking time in both cases were around 150 min. This indicates that incorporation of NTA within a peptide scaffold slows down the $H_2S$ release relative to small molecule NTA (peaking time of alkyne-NTA is 35-40 min) by shielding the NTA within its hydrophobic core.

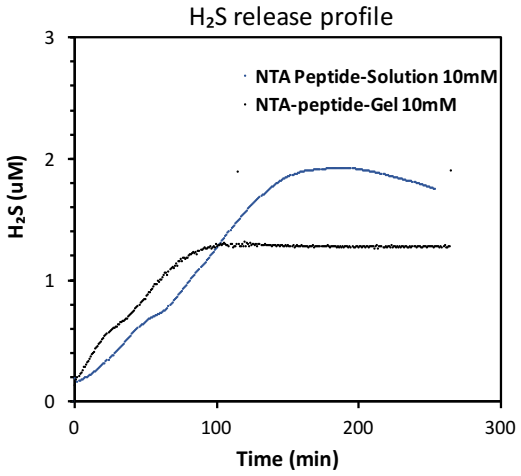


**Fig C2.** Comparison of $H_2S$ release profiles of NTA-peptide solution (blue trace) and NTA-peptide hydrogel (black trace)

## Future directions

Although NTA-peptides reported here are the first ever COS releasing peptides, but these peptide form very soft hydrogels. Further, the hydrogels do not show an increase in hydrogel stiffness depending on the $Ca^{2+}$ concentration. We envision a robust hydrogel system that is easy to handle and shows a sustained release for up to days and months.

## Appendix E

### Journal copyright permissions

Chapter 1 of this dissertation has appeared in the Antioxidants and Redox Signaling, which belongs to the publishing company Mary Ann Liebert, Inc. According to the copyright policies of Mary Ann Liebert Inc., authors retain rights to use their contributions, in full or in part, for inclusion in a theses or dissertation. Therefore, the permission to include this paper in this dissertation is granted. The published article can be found at: https://www.liebertpub.com/doi/abs/10.1089/ars.2019.7864

Chapter 2 of this dissertation has appeared in The Journal of Organic Chemistry, which belongs to the American Chemical Society. According to the copyright policies of American Chemical society, the authors retain the right to reproduce the article in whole or in part in a thesis or dissertation, provided appropriate citation of the published work is made. An acknowledgment to the original published article has been prominently placed at the beginning of chapter 2. Detailed information on the copyright policy of American Chemical society can be found on https://pubs.acs.org/page/copyright/permissions_otherpub.html. The published article is available at: http://dx.doi.org/10.1007/s10659-018-9673-6.

Chapter 3 of this dissertation has appeared in Acta Biomaterialia, which belongs to the publishing company Elsevier. According to the copyright policies of Elsevier, the authors can use their articles, in whole or in part, for inclusion in a thesis or dissertation (provided that it is not published commercially). Detailed information on the copyright policy of Elsevier can be found on https://www.elsevier.com/about/policies/copyright/permissions. The published article

is available at: https://www.sciencedirect.com/science/article/pii/S1742706119305318

Chapter 4 of this dissertation has not yet appeared in any journal, and therefore, no permissions are required.